U.S. Department
of Transportation
**Federal Railroad
Administration**

Estimation of Elastic and Residual Stresses in Railroad Rails Subject to Service Loading

Working Paper
DOT-VNTSC-RR728-WP-96-2
November 1996

Approved for Distribution:

Andrew Kish for HW

Division Chief

Research and Special Programs
Administration
John A. Volpe National
Transportation Systems Center
Cambridge, MA 02142-1093

TABLE OF CONTENTS

LIST OF ILLUSTRATIONS

LIST OF ILLUSTRATIONS (continued)

LIST OF ILLUSTRATIONS (continued)

LIST OF ILLUSTRATIONS (continued)

1. INTRODUCTION

The subject of this report is the analysis of elastic and residual stresses in railroad rails working in service conditions. The report consists of two parts.

The first part (section 2) covers the development of an elastic model for the analysis of contact stresses in railroad rails. The main goal of the work was to develop a reliable method of analysis of such stresses in rails subject to both normal and tangent surface tractions. It has been assumed that both the stress-strain and strain-displacement relations are linear, and consequently, the minimum total potential energy principle has been chosen as the mechanical model for the problem under consideration. Such assumptions, usually considered to be very restrictive in analysis of contact stresses, are consistent with the assumptions underlying the model for analysis of residual stresses where the elastic stresses constitute the main input data. The numerical model applied to the analysis of elastic stresses is the displacement model of the finite element method. It has been assumed that the external loads can be described by means of Fourier series, and the analysis can be performed by superimposing the responses due to symmetric and antisymmetric load contributions. This way the problem can be reduced to a selected cross section of the rail. An appropriate two-dimensional finite element has been derived and applied to the analysis. Both the mechanical and numerical models have been implemented in two computer programs. These programs have verified using an example problem formulated for a simply supported beam subject to contact loading varying along the longitudinal axis and constant along the width of the beam. Finally, the approach has been applied to analysis of contact stresses in a real railroad rail working in service conditions.

The second part of the report deals with the modification of the existing software for the evaluation of residual stresses in railroad rails subject to cyclic loads. Significant changes have been made with regard to the types of loads that can be considered. A new finite element has been formulated and the program flow logic has been expanded so that not only normal but also tangent surface traction can be considered. Additionally, a new algorithm that allows the inclusion of thermal loads has been implemented in the computer programs. The mechanical and numerical models, the computer programs, and their validation are described in section 3 of this report.

2. ELASTIC MODEL FOR ANALYSIS OF CONTACT STRESSES

This section covers all the matters associated with the development of an elastic model for analysis of contact stresses in railroad rails. Section 2.1 contains some introductory remarks dealing with possible approaches to such analyses. Sections 2.2 and 2.3 describe the mechanical and numerical models, respectively. The above models have been implemented in two computer programs described in section 2.4. The approach has been validated by means of test problems formulated for a simply supported beam subject to contact loads. The results and discussion of these tests are presented in section 2.5. Finally, the model has been applied to the evaluation of elastic contact stresses in a railroad rail subject to both normal and tangent tractions (section 2.6).

2.1 INTRODUCTION

The subject of this section is the analysis of elastic stresses in a selected class of prismatic bodies subject to contact loading. The purpose of the work is to formulate a reliable method of analysis of such stresses in railroad rails under normal and tangent tractions.

In general, there are two approaches to the problem of analysis of elastic contact stresses. The first one is mainly based on analytical formulae and certain experimental observations. The second approach takes advantage of numerical methods, especially of the finite element method.

As far as the first approach is concerned, the engineering design of rail and wheel profiles is traditionally based on the simplified application of the Hertz contact theory [7]. Both the rail and the wheel are modeled as circular cylinders crossing at right angles. The cylinder radii are defined as the design crown radius of the rail and the design nominal rolling radius of the wheel, respectively. The normal load pressing the cylinders together is defined as equal to the design static load supported by the wheel. The contact area is an ellipse with semi-major axis A and semi-minor axis B computed by means of the Hertz formulae. The normal pressure distribution over the contact zone is given by

$$p(X,Y) = p_0\sqrt{1-\left(\frac{X}{A}\right)^2-\left(\frac{Y}{B}\right)^2} \tag{2.1}$$

with respect to tangent-plane coordinates (X,Y) and with the origin at the center of the contact zone. The peak pressure p_0 is also computed using the Hertz formulae. The main task in the next step of this approach is to compute the corresponding stresses. This is usually done by means of integration of the classical Boussinesq influence functions [7] for stresses due to a unit normal force acting at a surface point on an unbounded half space. In this case, the pressure distribution determined from the Hertz formulae plays the role of a weighting function. A similar approach may be applied in case of a tangent load using the classical Cerruti influence functions [7] for stresses due to a unit tangent force acting at a surface point on an unbounded half space.

The main disadvantages of this approach are the quite restrictive assumptions concerning the shape of the surfaces in contact. As for the shape of the contact zone and the distribution of the

surface tractions, they can be modified quite easily to take into account real conditions, e.g., to deal with offset contacts (by introducing local radii, including the third radius representing the wheel profile curvature) or to comply with experimental observations. On the contrary, the application of simplified formulae for stress distributions may result in significant violation of the equilibrium equations and the static boundary conditions.

Regarding the second approach, numerical methods seem to be the most powerful mehtods for analysis of contact problems. They not only allow taking into account the real geometry of the bodies in contact and their material properties but also modeling the contact phenomenon including all accompanying effects. The problem could be solved using one of the commercial finite element analysis programs. However, their practical application in the case under consideration is limited, especially when one takes into account the fact that the problem is fully three-dimensional, the shapes of the wheel and rail are quite complex, and the size of the contact zone is very small. It implies application of meshes that consist of a huge number of finite elements. The analysis becomes extremely memory- and time-consuming, not to mention all the problems connected with mesh generation.

In this work, the main purpose of the elastic analysis of contact stresses is to provide essential input data for the elastic-plastic analysis of residual stresses. The elastic analysis usually has to be performed repeatedly, especially when multiple loading paths are considered. For this reason it has been decided to apply a simplified approach to the problem. Both the shape and size of the contact zone, as well as the surface tractions, are treated as known data, usually but not necessarily obtained by means of the Hertz formulae. The approach also allows one to eliminate the wheel from the analysis and to take advantage of the prismatic shape of the rail. The key point in this approach is that the external loads can be expanded in the Fourier series and the complete analysis can be performed by superimposing the response due to the symmetric and antisymmetric load contributions. The problem is still three-dimensional but only a selected cross section has to be discretized. This allows one to reduce significantly the total number of unknown variables and consequently the required amount of computer memory, unfortunately at the expense of central processor time. This approach is described in section 2.3.

2.2 MECHANICAL MODEL

Let a body be in a state of static equilibrium under the action of body forces $\overline{F}_i(\mathbf{x})$ in V, surface tractions $\overline{T}_i(\mathbf{x})$ on ∂V_σ, and displacements $\overline{u}_i(\mathbf{x})$ on ∂V_u, where V is the volume occupied by the body, ∂V_σ and ∂V_u are parts of the boundary surface ∂V, $\mathbf{x}$ represents a point of the body, and $i = 1, 2, 3$.

It has been assumed that both the stress-strain and strain-displacement relations are linear. These assumptions, usually considered to be very restrictive in the analysis of contact stresses, are consistent with the assumptions underlying the model for analysis of residual stresses (section 3) where elastic stresses are used as input data.

Thus, the analysis of the elastic stresses is the classical boundary value problem of linear elasticity and may be solved using the minimum total potential energy principle [8]. This principle may be stated in the form of the following optimization problem:

Find the minimum of the total potential energy functional

$$\Pi = \int_V \frac{1}{2} \varepsilon_{ij} E_{ijkl} \varepsilon_{kl} \, dV - \int_V u_i \overline{F}_i \, dV - \int_{\partial V_\sigma} u_i \overline{T}_i \, dS \tag{2.2}$$

with respect to the displacement field $u_i(\mathbf{x})$ *satisfying the kinematical boundary conditions*

$$u_i = \overline{u}_i \quad on \ \partial V_u, \tag{2.3}$$

where $\varepsilon_{ij}(\mathbf{x})$ is the strain field related to the displacement field $u_i(\mathbf{x})$ by

$$\varepsilon_{ij} = \frac{1}{2}\left(\frac{\partial u_i}{\partial x_j} + \frac{\partial u_j}{\partial x_i} \right) \tag{2.4}$$

and E_{ijkl} is the tensor of elasticity coefficients that relates the stress field $\sigma_{ij}(\mathbf{x})$ to the strain field $\varepsilon_{ij}(\mathbf{x})$ in generalized Hooke's law

$$\sigma_{ij} = E_{ijkl} \varepsilon_{kl}. \tag{2.5}$$

For proof of the minimum total potential energy principle, the reader is referred to [8].

2.3 NUMERICAL MODEL

This section describes the numerical model applied to the analysis of elastic stresses. It has been divided into three parts. The first part presents some basics of the finite element method, its concepts and notation. The second and third parts deal with the detailed description of the finite element that has been implemented in the computer programs developed for the problem under consideration.

2.3.1 Finite-Element Formulation

The numerical model applied to the analysis of elastic stresses is the displacement model of the finite element method. It may be derived from the minimum total potential energy principle (see the previous section). The region of the body V is divided into a finite number N_e of disjoint subregions V_n (finite elements) and the functional (2.2) is written (using matrix notation) in the form

$$\Pi = \sum_{n=1}^{Ne} \pi_n \tag{2.6}$$

in which

$$\pi_n = \int_{V_n} \frac{1}{2} \boldsymbol{\varepsilon}^T \mathbf{E} \boldsymbol{\varepsilon} \, dV - \int_{V_n} \mathbf{u}^T \overline{\mathbf{F}} \, dV - \int_{(\partial V_\sigma)_n} \mathbf{u}^T \overline{\mathbf{T}} \, dS, \tag{2.7}$$

where $(\partial V_\sigma)_n$ denotes the part of ∂V_σ that belongs to the nth element.

For each finite element, the displacements $\mathbf{u}$ are represented in the following form

$$\mathbf{u} = \mathbf{N}\mathbf{q}_n \tag{2.8}$$

where $\mathbf{N} = \mathbf{N}(\mathbf{x})$ is the displacement interpolation matrix and $\mathbf{q}_n$ is the vector of generalized displacements defined at a finite number of nodal points of the element. The corresponding strains $\boldsymbol{\varepsilon}$, related to the displacements $\mathbf{u}$ by (2.4), and stresses $\boldsymbol{\sigma}$, related to the strains $\boldsymbol{\varepsilon}$ by (2.5), can also be expressed in terms of the generalized displacements $\mathbf{q}_n$, that is

$$\boldsymbol{\varepsilon} = \mathbf{L}\mathbf{u} = \mathbf{L}\mathbf{N}\mathbf{q}_n = \mathbf{B}\mathbf{q}_n, \tag{2.9}$$

$$\boldsymbol{\sigma} = \mathbf{E}\boldsymbol{\varepsilon} = \mathbf{E}\mathbf{B}\mathbf{q}_n \tag{2.10}$$

where $\mathbf{L}$ is the matrix of differential operators and $\mathbf{B}$ is the strain interpolation matrix.

The substitution of (2.8) and (2.9) into (2.7) results in

$$\pi_n = \frac{1}{2} \mathbf{q}_n^T \mathbf{k}_n \mathbf{q}_n - \mathbf{q}_n^T \mathbf{Q}_n \tag{2.11}$$

in which

$$\mathbf{k}_n = \int_{V_n} \mathbf{B}^T \mathbf{E} \mathbf{B} \, dV \tag{2.12}$$

and

$$\mathbf{Q}_n = \int_{V_n} \mathbf{N}^T \overline{\mathbf{F}} \, dV + \int_{(\partial V_\sigma)_n} \mathbf{N}^T \overline{\mathbf{T}} \, dS \tag{2.13}$$

are, respectively, the element stiffness matrix and the vector of generalized forces due to loads acting on the element.

Finally, the substitution of (2.11) into (2.6) yields

$$\Pi = \sum_{n=1}^{N_e} \left(\frac{1}{2} \mathbf{q}_n^T \mathbf{k}_n \mathbf{q}_n - \mathbf{q}_n^T \mathbf{Q}_n \right) \tag{2.14}$$

which may be written in the following short form

$$\Pi = \frac{1}{2} \mathbf{q}^T \mathbf{K} \mathbf{q} - \mathbf{q}^T \mathbf{Q}, \tag{2.15}$$

where $\mathbf{K}$ is the stiffness matrix of the whole domain, $\mathbf{q}$ is the vector of total generalized displacements, and $\mathbf{Q}$ is the vector of total generalized forces. The total generalized displacements $\mathbf{q}$ can be found as such values that satisfy the kinematical boundary conditions (2.3) and minimized the total potential energy of the body (2.15). After they have been determined, the corresponding strains ε and stresses σ can be evaluated using formulae (2.9) and (2.10). For a more extensive description of the finite element method and its techniques, the reader is referred to [9], [10], [11].

2.3.2 Prismatic Finite Element

The subject of the analysis is a prismatic body subject to external loads that can be represented by means of Fourier series. Taking into account the well-known orthogonality properties of these series and assuming that the material of the body is linear elastic, uncoupling of the Fourier modes occurs and the analysis can be performed by superimposing the response of the body due to the symmetric and antisymmetric load contributions. Thus, the description of the finite element can be simplified significantly [9], [11].

In the case under consideration, it is convenient to describe the problem in a system of rectangular cartesian coordinates (x, y, z). Some of the relations just presented can be rewritten almost automatically and will be done without any extensive comment. The other relations, especially those connected with the strain interpolation matrix and element stiffness matrix, will be discussed in detail to provide assistance in case the computer programs have to be modified.

The first goal of the analysis is to describe the external loads and their Fourier representation. The vector of surface tractions $\overline{\mathbf{T}}$ can be written in the following form

$$\overline{\mathbf{T}}^T(z,l) = \left\{ \overline{T}_x(z,l) \quad \overline{T}_y(z,l) \quad \overline{T}_z(z,l) \right\} \tag{2.16}$$

in which

$$\overline{T}_x(z,l) = \sum_{n=0}^{N} \left[\overline{T}_{xn}^s(l) \sin \beta_n z + \overline{T}_{xn}^a(l) \cos \beta_n z \right],$$

$$\overline{T}_y(z,l)=\sum_{n=0}^{N}\left[\overline{T}_{yn}^{s}(l)\sin\beta_n z+\overline{T}_{yn}^{a}(l)\cos\beta_n z\right], \tag{2.17}$$

$$\overline{T}_z(z,l)=\sum_{n=0}^{N}\left[\overline{T}_{zn}^{s}(l)\cos\beta_n z+\overline{T}_{zn}^{a}(l)\sin\beta_n z\right]$$

where the indices s and a denote the symmetric and antisymmetric load contributions, respectively. Almost identical expansions can also be written for body forces, boundary conditions, etc. The parameter $\beta_n = n\Pi/L$, where L denotes the length of the body, has been introduced in order to simplify further notation. The coordinate z is defined in the longitudinal direction of the body. The coordinate l represents any local coordinate that allows one to describe the surface tractions uniquely for all points of the boundary surface. Usually, it is identified with the vertical coordinate y except for flat parts of the boundary surface where the horizontal coordinate x is used instead.

In order to simplify the notation, further considerations will be restricted to the symmetric load contributions and only the nth Fourier mode will be taken into account (consequently, the indices s, a, and n will be omitted). For the antisymmetric loading, the sine function should be replaced by the cosine function and vice versa. When derivatives are calculated (matrix $\mathbf{B}$), such replacement is sometimes accompanied by a change in sign.

The vector of displacements $\mathbf{u}$, the vector of generalized displacements $\mathbf{q}_n$, and the displacement interpolation matrix $\mathbf{N}$ defined in (2.9) can be written in the system of rectangular cartesian coordinates as follows

$$\mathbf{u}^T(x,y,z)=\left\{u_x(x,y,z) \quad u_y(x,y,z) \quad u_z(x,y,z)\right\}, \tag{2.18}$$

$$\mathbf{q}_n^T=\left\{\mathbf{q}_1^T \quad \ldots \quad \mathbf{q}_k^T\right\}, \tag{2.19}$$

$$\mathbf{N}(x,y,z)=\left[\mathbf{N}_1(x,y,z) \quad \ldots \quad \mathbf{N}_k(x,y,z)\right] \tag{2.20}$$

in which

$$\mathbf{q}_i^T=\left\{q_{xi} \quad q_{yi} \quad q_{zi}\right\}, \qquad i=1,\ldots,k, \tag{2.21}$$

$$\mathbf{N}_i(x,y,z)=\begin{bmatrix} N_i(x,y)\sin\beta_n z & 0 & 0 \\ 0 & N_i(x,y)\sin\beta_n z & 0 \\ 0 & 0 & N_i(x,y)\cos\beta_n z \end{bmatrix} \tag{2.22}$$

where k is equal to the number of nodal points of the element, $\mathbf{q}_i$ is the vector of generalized nodal displacements at the ith node of the element, and N_i is the shape function associated with this node. The assemblage of different parameters associated with nodal points of finite elements

will be used quite frequently, since it corresponds to the structure of the computer programs. There also exists an opposite approach where the information of the same type is grouped for the whole element or even for the whole structure. In spite of the fact that this usually allows one to describe the problem much more concisely, it is rarely implemented in computer codes.

Further analysis requires the relations (2.9) and (2.10) also to be specified in the system of rectangular cartesian coordinates. The stress σ and strain ε vectors, and the matrix of differential operators $\mathbf{L}$ can be written as follows

$$\varepsilon^T = \{\varepsilon_{xx}\ \varepsilon_{yy}\ \varepsilon_{zz}\ \gamma_{xy}\ \gamma_{yz}\ \gamma_{xz}\}, \tag{2.23}$$

$$\sigma^T = \{\sigma_{xx}\ \sigma_{yy}\ \sigma_{zz}\ \tau_{xy}\ \tau_{yz}\ \tau_{xz}\}, \tag{2.24}$$

$$\mathbf{L} = \begin{bmatrix} \frac{\partial}{\partial x} & 0 & 0 \\ 0 & \frac{\partial}{\partial y} & 0 \\ 0 & 0 & \frac{\partial}{\partial z} \\ \frac{\partial}{\partial y} & \frac{\partial}{\partial x} & 0 \\ 0 & \frac{\partial}{\partial z} & \frac{\partial}{\partial y} \\ \frac{\partial}{\partial z} & 0 & \frac{\partial}{\partial x} \end{bmatrix}. \tag{2.25}$$

The form of the matrix of elasticity coefficients $\mathbf{E}$ does not depend on the system of coordinates, that is

$$\mathbf{E} = \frac{E}{(1+\nu)(1-2\nu)} \begin{bmatrix} 1-\nu & \nu & \nu & 0 & 0 & 0 \\ & 1-\nu & \nu & 0 & 0 & 0 \\ & & 1-\nu & 0 & 0 & 0 \\ & & & \frac{1-2\nu}{2} & 0 & 0 \\ & \text{sym} & & & \frac{1-2\nu}{2} & 0 \\ & & & & & \frac{1-2\nu}{2} \end{bmatrix} \tag{2.26}$$

where E is Young's modulus and ν is Poisson's ratio.

Before the strain interpolation matrix $\mathbf{B}$ is derived, it is convenient, as it was done in (2.19) and (2.20), to divide it into submatrices that are associated with the nodal points of the element

$$\mathbf{B} = [\mathbf{B}_1 \ \ldots \ \mathbf{B}_k]. \tag{2.27}$$

The substitution of (2.27), (2.25), (2.20), and (2.22) into (2.9) results in

$$\mathbf{B}_i = \begin{bmatrix} \frac{\partial N_i}{\partial x}\sin\beta_n z & 0 & 0 \\ 0 & \frac{\partial N_i}{\partial y}\sin\beta_n z & 0 \\ 0 & 0 & -N_i\beta_n \sin\beta_n z \\ \frac{\partial N_i}{\partial y}\sin\beta_n z & \frac{\partial N_i}{\partial x}\sin\beta_n z & 0 \\ 0 & N_i\beta_n \cos\beta_n z & \frac{\partial N_i}{\partial y}\cos\beta_n z \\ N_i\beta_n \cos\beta_n z & 0 & \frac{\partial N_i}{\partial x}\cos\beta_n z \end{bmatrix}. \tag{2.28}$$

Consequently, before the element stiffness matrix $\mathbf{k}_n$ is computed, the integrand in (2.12) should be decomposed, to yield

$$\mathbf{B}^T\mathbf{E}\mathbf{B} = \begin{bmatrix} \mathbf{B}_1^T \\ \vdots \\ \mathbf{B}_k^T \end{bmatrix} \mathbf{E}\begin{bmatrix} \mathbf{B}_1 & \dots & \mathbf{B}_k \end{bmatrix} = \begin{bmatrix} \mathbf{B}_1^T\mathbf{E}\mathbf{B}_1 & \dots & \mathbf{B}_1^T\mathbf{E}\mathbf{B}_k \\ & \ddots & \vdots \\ \text{sym} & & \mathbf{B}_k^T\mathbf{E}\mathbf{B}_k \end{bmatrix} \tag{2.29}$$

in which

$$\mathbf{B}_i^T\mathbf{E}\mathbf{B}_j = \frac{E}{(1+\nu)(1-2\nu)} \begin{bmatrix} k_{11} & k_{12} & k_{13} \\ & k_{22} & k_{23} \\ **\text{sym}** & & k_{33} \end{bmatrix}. \tag{2.30}$$

It should be stressed that the matrix in (2.30) is not symmetric. The abbreviation **sym** is used to point out that the componenets of the lower triangular part of the matrix may be computed using the expressions for the corresponding symmetric components of the upper part, but at the same time the indices i and j have to be exchanged, i.e.,

$$k_{mn}(i,j) = k_{nm}(j,i). \tag{2.31}$$

The substitution of (2.28) with the appropriate indices and (2.26) into the left-hand side of (2.30) results in the following expressions for the components of the matrix on the right-hand side of (2.30)

$$k_{11} = (1-\nu)\frac{\partial N_i}{\partial x}\frac{\partial N_j}{\partial x}\sin^2\beta_n z + \frac{1-2\nu}{2}\frac{\partial N_i}{\partial y}\frac{\partial N_j}{\partial y}\sin^2\beta_n z + \frac{1-2\nu}{2}N_i N_j \beta_n^2 \cos^2\beta_n z, \tag{2.32a}$$

$$k_{12} = \nu \frac{\partial N_i}{\partial x}\frac{\partial N_j}{\partial y}\sin^2 \beta_n z + \frac{1-2\nu}{2}\frac{\partial N_i}{\partial y}\frac{\partial N_j}{\partial x}\sin^2 \beta_n z, \tag{2.32b}$$

$$k_{13} = -\nu \frac{\partial N_i}{\partial x} N_j \beta_n \sin^2 \beta_n z + \frac{1-2\nu}{2} N_i \frac{\partial N_j}{\partial x}\beta_n \cos^2 \beta_n z, \tag{2.32c}$$

$$k_{22} = (1-\nu)\frac{\partial N_i}{\partial y}\frac{\partial N_j}{\partial y}\sin^2 \beta_n z + \frac{1-2\nu}{2}\frac{\partial N_i}{\partial x}\frac{\partial N_j}{\partial x}\sin^2 \beta_n z + \frac{1-2\nu}{2} N_i N_j \beta_n^2 \cos^2 \beta_n z, \tag{2.32d}$$

$$k_{23} = -\nu \frac{\partial N_i}{\partial y} N_j \beta_n \sin^2 \beta_n z + \frac{1-2\nu}{2} N_i \frac{\partial N_j}{\partial y}\beta_n \cos^2 \beta_n z, \tag{2.32e}$$

$$k_{33} = (1-\nu) N_i N_j \beta_n^2 \sin^2 \beta_n z + \frac{1-2\nu}{2}\frac{\partial N_i}{\partial y}\frac{\partial N_j}{\partial y}\cos^2 \beta_n z + \frac{1-2\nu}{2}\frac{\partial N_i}{\partial x}\frac{\partial N_j}{\partial x}\cos^2 \beta_n z. \tag{2.32f}$$

Finally, the integrand in the second term of (2.13) should be found (in the case of body forces the procedure is identical). Using the same approach as above, it can be written as follows

$$\mathbf{N}^T\overline{\mathbf{T}} = \begin{bmatrix} \mathbf{N}_1^T \\ \vdots \\ \mathbf{N}_k^T \end{bmatrix} \overline{\mathbf{T}} = \begin{bmatrix} \mathbf{N}_1^T\overline{\mathbf{T}} \\ \vdots \\ \mathbf{N}_k^T\overline{\mathbf{T}} \end{bmatrix} \tag{2.33}$$

in which

$$\mathbf{N}_i^T\overline{\mathbf{T}} = \begin{Bmatrix} N_i\overline{T}_x \sin^2 \beta_n z \\ N_i\overline{T}_y \sin^2 \beta_n z \\ N_i\overline{T}_z \cos^2 \beta_n z \end{Bmatrix}. \tag{2.34}$$

At this point, the most important formulae that allow one to compute the element stiffness matrix $\mathbf{k}_n$ and the vector of the generalized forces $\mathbf{Q}_n$, defined respectively in (2.12) and (2.13), have been derived. After the displacement interpolation matrix $\mathbf{N}$ has been assumed, the appropriate integration (usually numerical) can be performed and both matrices can be assembled. The integration should be carried out in the system of rectangular cartesian coordinates, that is

$$\int_{V_n} f(x,y,z)\,dV = \int_0^L \int_{A_n} f(x,y,z)\,dx\,dy\,dz, \tag{2.35a}$$

$$\int_{(\partial V_o)_n} f(x,y,z)\,dS = \int_0^L \int_{s_n} f(x,y,z)\,ds\,dz \tag{2.35b}$$

where A_n is the area of the nth element, and s_n denotes the side of the element that belongs to $(\partial V_\sigma)_n$. In the above finite element formulae, the only functions that depend on z are the trigonometric functions, so the integration along the longitudinal direction may be carried out separately. Additionally, taking into account the following integrals,

$$\int_0^L \cos^2 \frac{n\Pi}{L} z\, dz = \begin{cases} L, & \text{if } n = 0 \\ L/2, & \text{if } n = 1, 2, \ldots \end{cases}, \tag{2.36a}$$

$$\int_0^L \sin^2 \frac{n\Pi}{L} z\, dz = \begin{cases} 0, & \text{if } n = 0 \\ L/2, & \text{if } n = 1, 2, \ldots \end{cases} \tag{2.36b}$$

the formulae can be simplified significantly.

2.3.3 Quadrilateral Finite Element

The finite element applied to the analysis of elastic stresses is the isoparametric four-node element with bilinear interpolation of the displacement field. It corresponds to the element that is used for the analysis of residual stresses in order to simplify the process of data preparation.

The elements are described in the global coordinate system (x, y) defined on a selected cross section. In general, they are irregular quadrilateral elements (figure 2.1a) and that is why it is convenient first to map them isoparametrically into squares (figure 2.1b) and then to construct the interpolation functions for one typical element. For the case under consideration, the transformation can be written as follows

$$\begin{aligned} x &= \sum_{i=1}^{4} f_i(\xi,\eta) x_i, \\ y &= \sum_{i=1}^{4} f_i(\xi,\eta) y_i \end{aligned} \tag{2.37}$$

in which

$$f_i(\xi,\eta) = \frac{1}{4}(1+\xi\xi_i)(1+\eta\eta_i) \tag{2.38}$$

where (x_i, y_i) and (ξ_i, η_i) are the coordinates of the nodes in the systems of global and local coordinates, respectively.

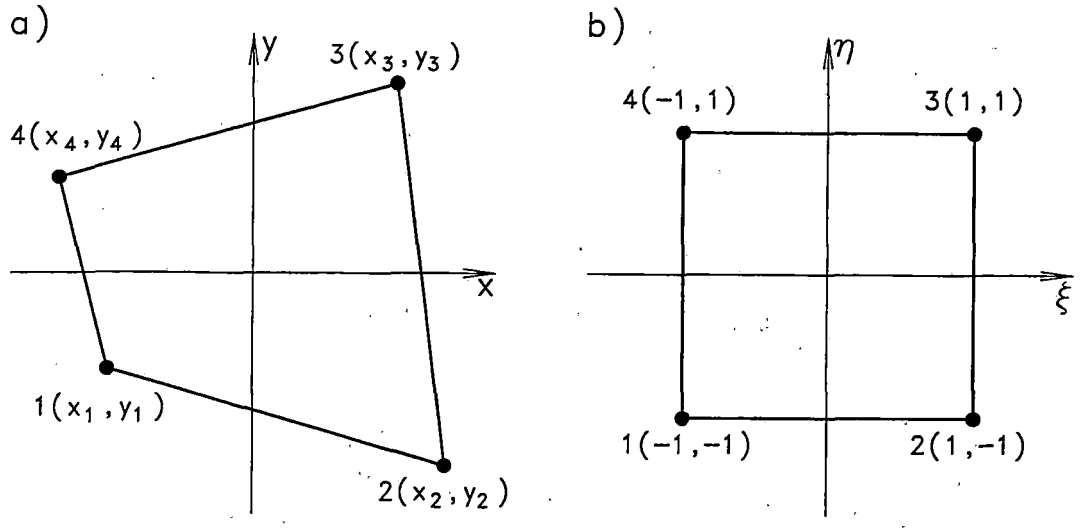

Figure 2.1 Quadrilateral Finite Element

The computation of the basic finite-element matrices requires the differentiation and integration in the system of global coordinates (x,y). However, both these operations can also be carried out in the system of local coordinates (ξ,η) using the following relations

$$\begin{Bmatrix} \dfrac{\partial}{\partial x} \\ \dfrac{\partial}{\partial y} \end{Bmatrix} = \mathbf{J}^{-1} \begin{Bmatrix} \dfrac{\partial}{\partial \xi} \\ \dfrac{\partial}{\partial \eta} \end{Bmatrix}, \tag{2.39}$$

$$\int_{A_n} g(x,y)\,dx\,dy = \int_{-1}^{1}\int_{-1}^{1} g(\xi,\eta)\,|\det \mathbf{J}|\,d\xi\,d\eta \tag{2.40}$$

where

$$\mathbf{J} \equiv \begin{bmatrix} \dfrac{\partial x}{\partial \xi} & \dfrac{\partial y}{\partial \xi} \\ \dfrac{\partial x}{\partial \eta} & \dfrac{\partial y}{\partial \eta} \end{bmatrix} \tag{2.41}$$

is the Jacobian matrix (operator) relating the global coordinate derivatives to the local coordinate derivatives and

$$\det \mathbf{J} \equiv \frac{\partial x}{\partial \xi}\frac{\partial y}{\partial \eta} - \frac{\partial x}{\partial \eta}\frac{\partial y}{\partial \xi} \tag{2.42}$$

is the determinant of the Jacobian matrix. The substitution of (2.37) and (2.38) into (2.41) and (2.42) results in

$$\mathbf{J}=\begin{bmatrix} a_1+a_3\eta & b_1+b_3\eta \\ a_2+a_3\xi & b_2+b_3\xi \end{bmatrix}, \tag{2.43}$$

$$\det\mathbf{J}=a_1b_2-a_2b_1+(a_1b_3-a_3b_1)\xi+(a_3b_2-a_2b_3)\eta \tag{2.44}$$

where

$$\begin{cases} a_1=\dfrac{1}{4}(-x_1+x_2+x_3-x_4) \\ a_2=\dfrac{1}{4}(-x_1-x_2+x_3+x_4) \\ a_3=\dfrac{1}{4}(x_1-x_2+x_3-x_4) \end{cases}, \qquad \begin{cases} b_1=\dfrac{1}{4}(-y_1+y_2+y_3-y_4) \\ b_2=\dfrac{1}{4}(-y_1-y_2+y_3+y_4). \\ b_3=\dfrac{1}{4}(y_1-y_2+y_3-y_4) \end{cases} \tag{2.45}$$

The shape functions N_i are assumed to have exactly the same form as the transformation functions (2.38), that is

$$N_i(\xi,\eta)=f_i(\xi,\eta). \tag{2.46}$$

2.4 COMPUTER PROGRAMS

The mechanical and numerical models described in the previous sections have been implemented in two computer programs called RAILE and FOURIER. Taking into account the goal of the work, both programs have been especially tailored for the analysis of elastic stresses in railroad rails subject to contact loads. However, their structures have been chosen so that they can be modified quite easily to include other types of loading. This section contains some basic information about the programs.

The program RAILE is a finite element code that allows one to analyze elastic stresses in a prismatic body subject to external loads represented by means of Fourier series. It is executed in batch mode, i.e., both the input and output data exist as external files and no interaction between the program and its user is required. The input data consist of six ASCII files, which contain the information about the topology of the finite element mesh, material properties, and loading. The loading information is prepared by means of the program FOURIER. The output data consist of three ASCII files that contain the solution to the problem, i.e., the stresses and displacements for the earlier user-specified cross sections.

The program FOURIER is an auxiliary program that computes the coefficients of the Fourier series for external loads. It has been assumed that a rail may be subject to any number of loads of contact type. In order to define each of the loads, the systems of global (x, y, z) and local (X, Y, Z) coordinates have to be established (figure 2.2). The system of global coordinates is a

rectangular cartesian system. The way the system of local coordinates is defined is very flexible. In the simplest case (figure 2.2), the origin C of the system coincides with the center of the contact zone, the X axis is normal to the plane (x, y) in the direction of the z axis, the Y axis directed along the x axis, and the Z axis is defined so that the system (X, Y, Z) is a right-handed, rectangular cartesian system. In the most general case (figure 2.3), the location of the origin does not have to coincide with the center of the contact zone and, additionally, the slope of the (X, Y) plane may be specified by giving the value of the angle α. In this case, the center of the contact zone C' is defined as the projection of the point C onto the rail surface in the Z direction.

The dimensions of the contact zone and the surface tractions are defined in the system of local coordinates. According to experimental observations, it has been assumed that the contact zone can be approximated by a rectangle with sides $2a$ and $2b$, which are parallel to the X and Y axes, respectively (figure 2.4), and the surface tractions can be described by means of bi-parabolic functions

$$t_i(X,Y) = t_{0i}\left[1-\left(\frac{X}{a}\right)^2\right]\left[1-\left(\frac{Y}{b}\right)^2\right], \qquad i = X, Y, Z \tag{2.47}$$

in which

$$t_{0i} = \frac{9}{16}\frac{T_i}{ab}, \qquad a = A\sqrt{\frac{3\pi}{8}}, \qquad b = B\sqrt{\frac{3\pi}{8}} \tag{2.48}$$

where t_i denotes the surface tractions caused by the force T_i acting in the ith local direction; the parameters A and B are the semi-major and semi-minor axes of the ellipse computed using the Hertz formulae. It should be stressed that such a definition does not correspond to the definition of the surface tractions in (2.16), where the system of global coordinates was used, but the appropriate transformation has been included in the program.

2.5 NUMERICAL TESTS

A wide variety of numerical tests has been carried out to validate the approach applied to the analysis of elastic stresses, as well as the computer programs described in the previous section. All of the tests performed can be divided into two groups.

The first one consists of relatively simple benchmark problems with known analytical solutions. Unfortunately, these tests are one-dimensional and they did not permit the drawing of conclusions that could be useful for real three-dimensional problems. These tests were performed in the initial stage of testing and their results are not presented here. There also exist more combined two- and three-dimensional problems with known analytical solutions, but the simplifying assumptions made to formulate them are so restrictive that their usefulness is also questionable.

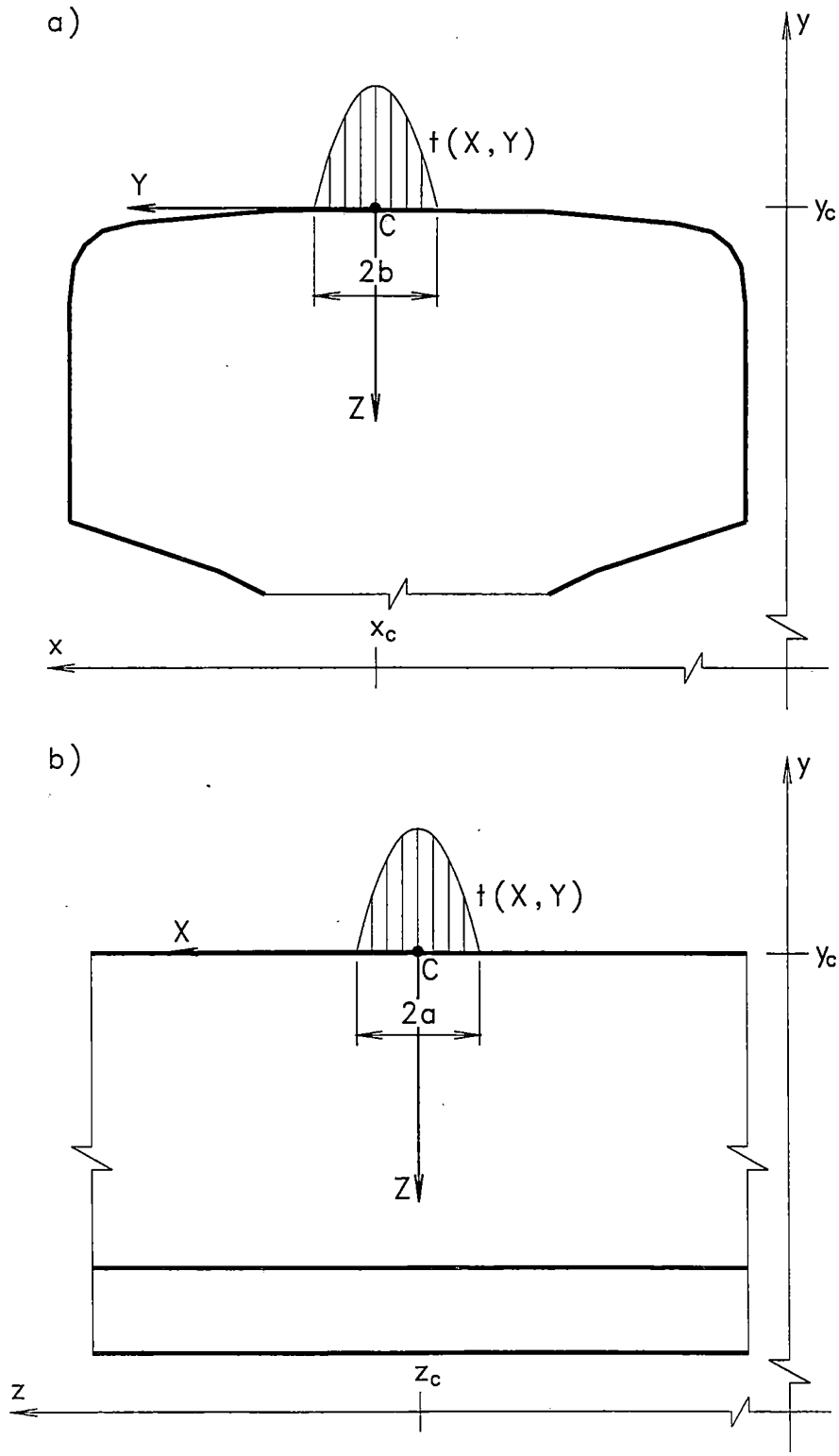

Figure 2.2 Conventions for the Global and Local Systems of Coordinates

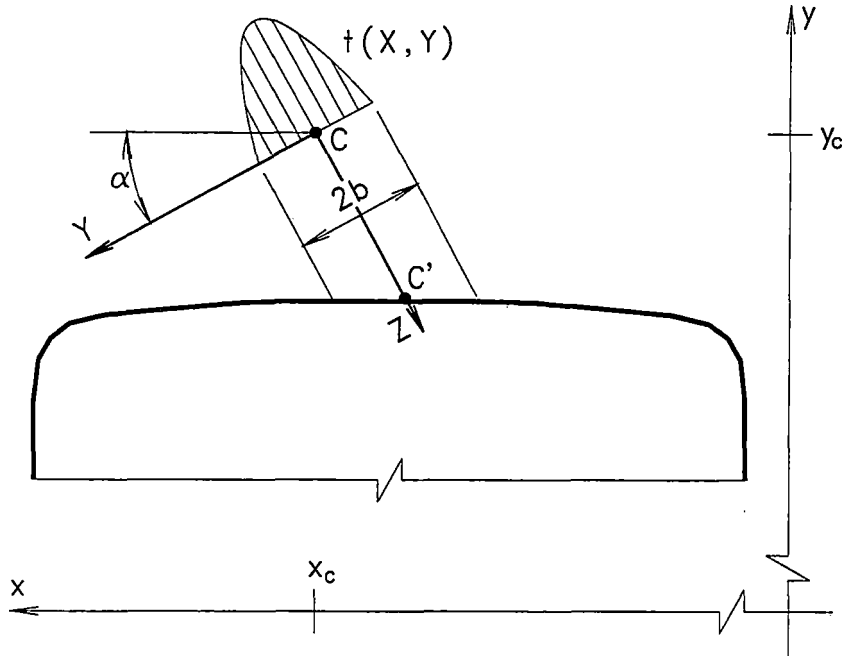

Figure 2.3 Conventions for the Local System of Coordinates – General Case

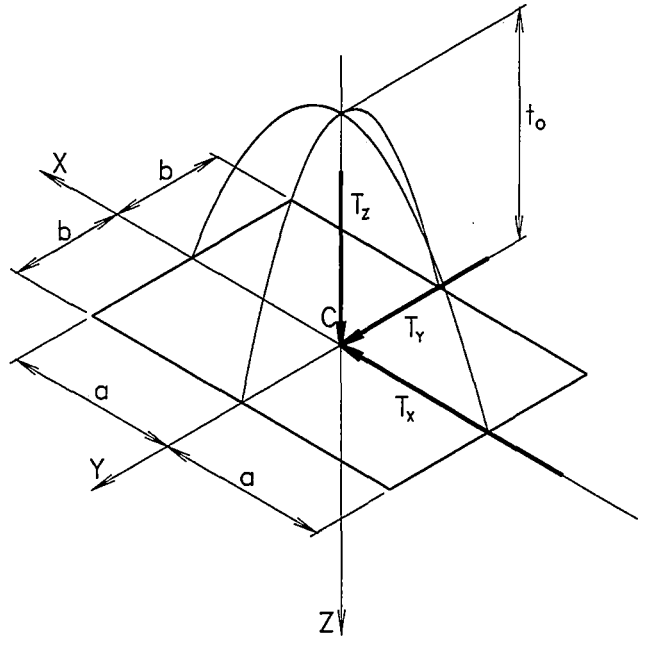

Figure 2.4 Conventions for a Rectangular Contact Zone with Bi-Parabolic Distribution of Surface Tractions

The second group of tests consists of more complex problems with unknown analytical solutions. The most important examples are those formulated for a simply supported beam subject to contact loading, varying along the longitudinal axis and constant along the width of the beam (figure 2.5). The solutions to these problems have been compared with solutions obtained by means of ABAQUS, v. 5.3-2 [12]. It should be stressed that such comparisons were possible because the problems were two-dimensional. If they had been formulated as three-dimensional problems, a special approach would have had to be applied while using ABAQUS. It could also have turned out that much more powerful computer equipment would have been necessary.

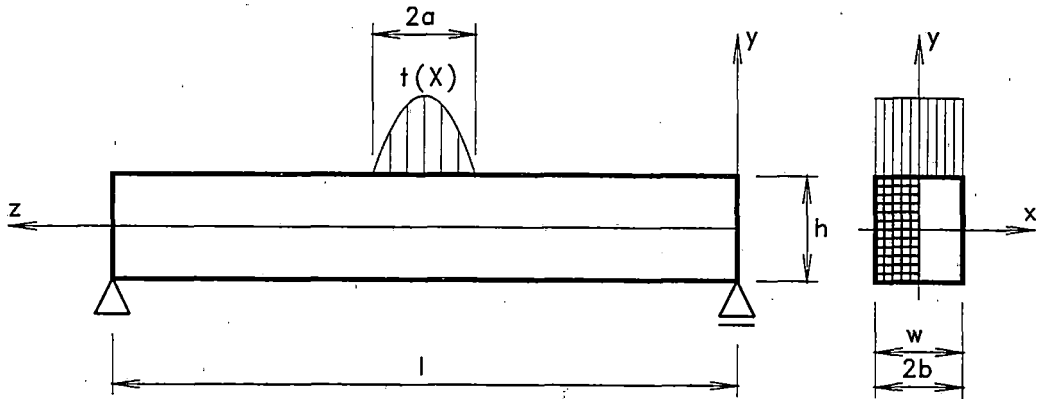

Figure 2.5 Simply Supported Beam under Concentrated Surface Tractions

Two cases of loading were considered, in which a simply supported beam of length l, height h, and width w was subject to concentrated vertical $t_z(X)$ and horizontal $t_x(X)$ surface tractions of parabolic distribution (figure 2.6). The corresponding Fourier series included only symmetric and antisymmetric modes.

Some selected results are shown in figures 2.7 through 2.18. They were obtained assuming the following non-dimensional data: length $l = 10$, height $h = 1$, width $w = 0.5$, Young's modulus $E = 1$, and Poisson's ratio $v = 0.3$. The intensity of the surface tractions (peak value) was equal to 1.0 and the width of the contact zone $2a = 0.5$ corresponded to the width of the beam. The number of Fourier modes (harmonics) was equal to 400 modes.

The problem was solved using three finite element meshes of square elements that consisted of 16, 32, and 64 elements in the vertical direction, and 8, 16, and 32 elements in the horizontal direction, respectively. For comparison, the problem was also solved using ABAQUS. In this case, it was treated as a two-dimensional plane stress problem.

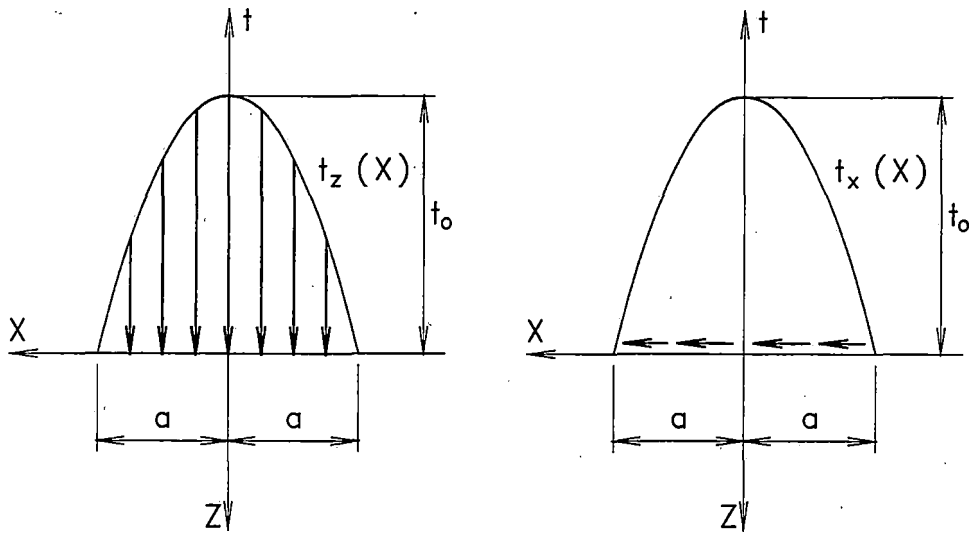

Figure 2.6 Vertical and Horizontal Surface Tractions in the Simply Supported Beam Problem

The convergence of the solution for the case of vertical loading is presented in figures 2.7 through 2.9. The vertical σ_{yy} and horizontal σ_{zz} normal stresses are plotted along the y axis for two selected cross sections that contain the center $(z = 5)$ and the end $(z = 4.75)$ of the contact zone, respectively. The shear stresses σ_{yz} are also plotted for two cross sections, but instead of the cross section $z = 5$, where these stresses are equal to zero, an additional cross section $z = 4.5$ was chosen. In figures 2.10 through 2.15, some selected stress tensor components are presented in the form of contour line plots.

The results for the case of horizontal loading are shown in figures 2.16 through 2.18. The stress tensor components are plotted for the same cross sections as before, i.e., containing the center of the contact zone and either the end point of the zone or the point of the coordinate $z = 4.5$, depending on where non-zero values exist.

In both cases of vertical and horizontal loads, high quality solutions have been obtained. The largest errors occur on both the top and bottom surfaces (a consequence of the bilinear interpolation of the displacement field). However, the values at the centroids of the elements, which are used in the analysis of residual stresses, are subject to much smaller errors, even in the vicinity of the contact zone. These results validate both of the programs developed for the analysis of elastic stresses.

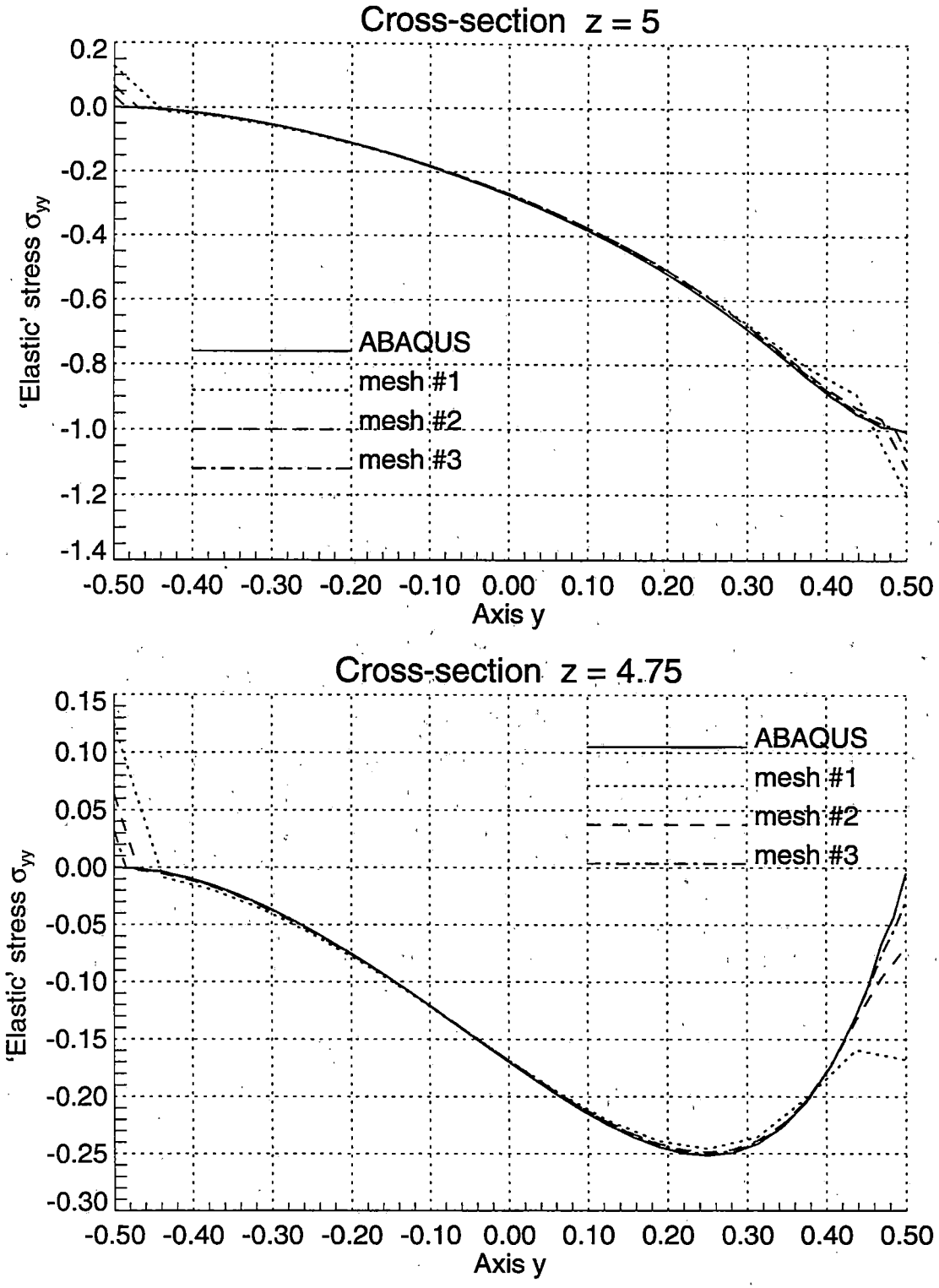

Figure 2.7 Normal 'Elastic' Stresses σ_{yy} in the Simply Supported Beam under Concentrated Vertical Surface Tractions

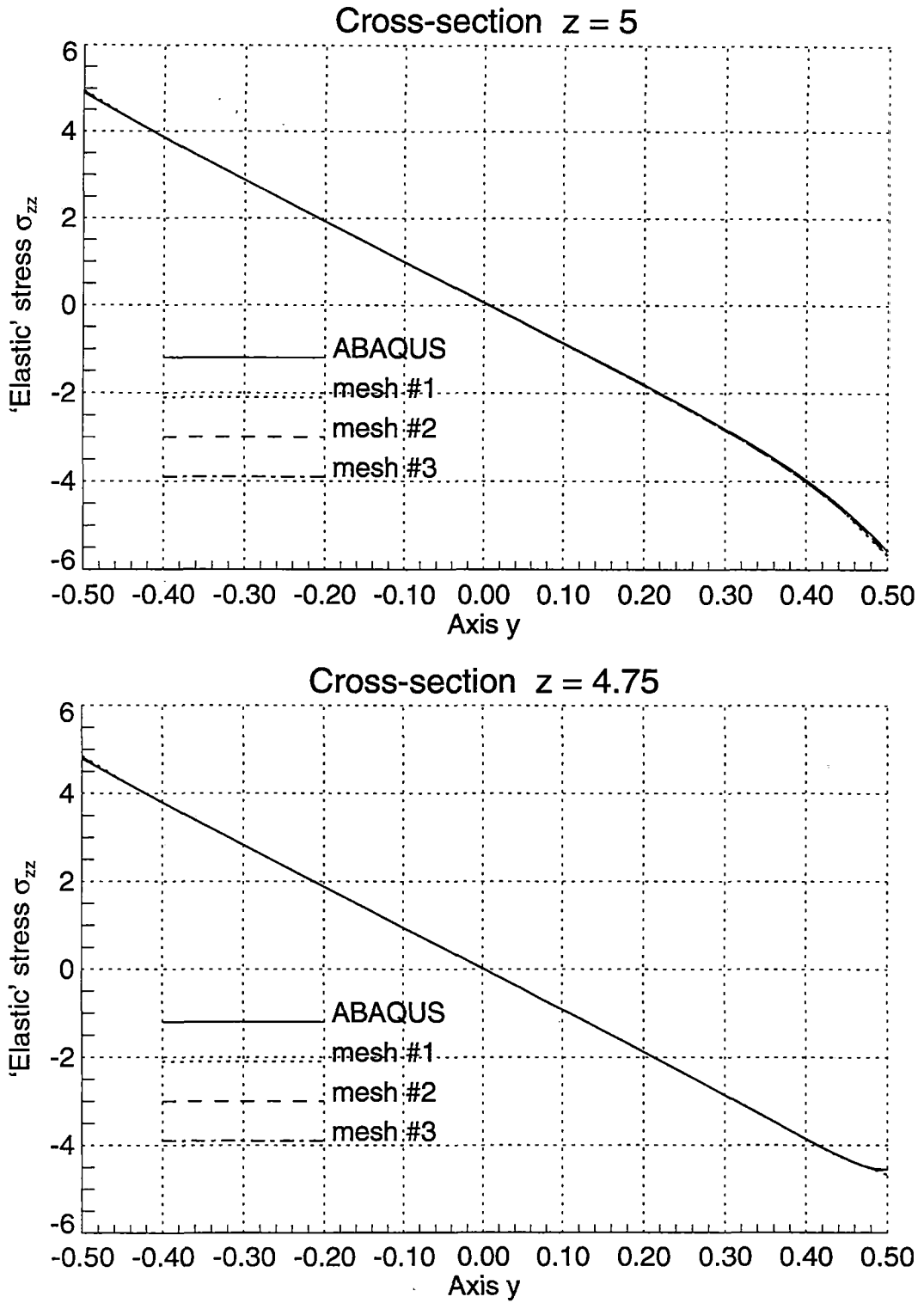

Figure 2.8 Normal 'Elastic' Stresses σ_{zz} in the Simply Supported Beam under Concentrated Vertical Surface Tractions

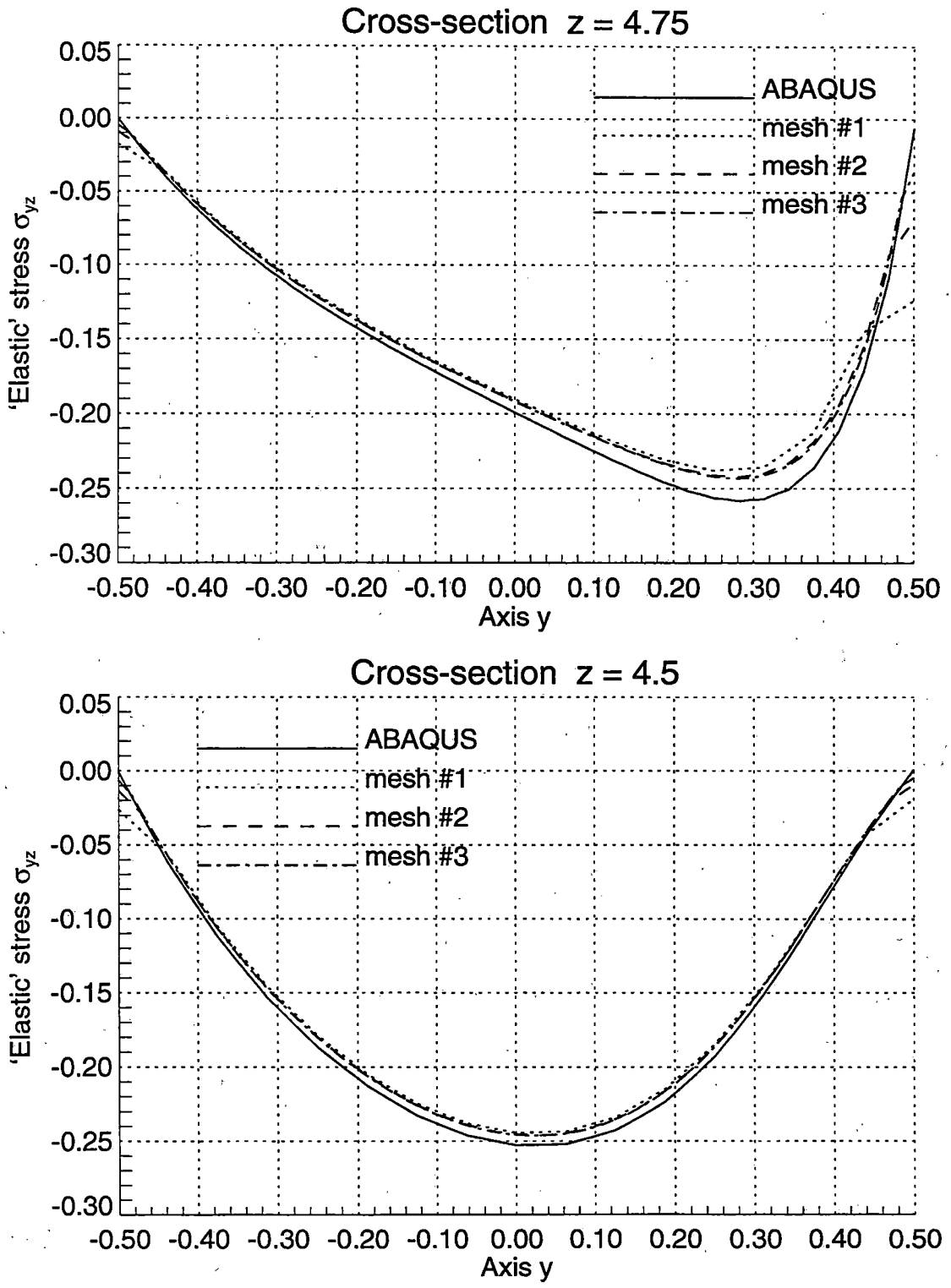

Figure 2.9 Shear 'Elastic' Stresses σ_{yz} in the Simply Supported Beam under Concentrated Vertical Surface Tractions

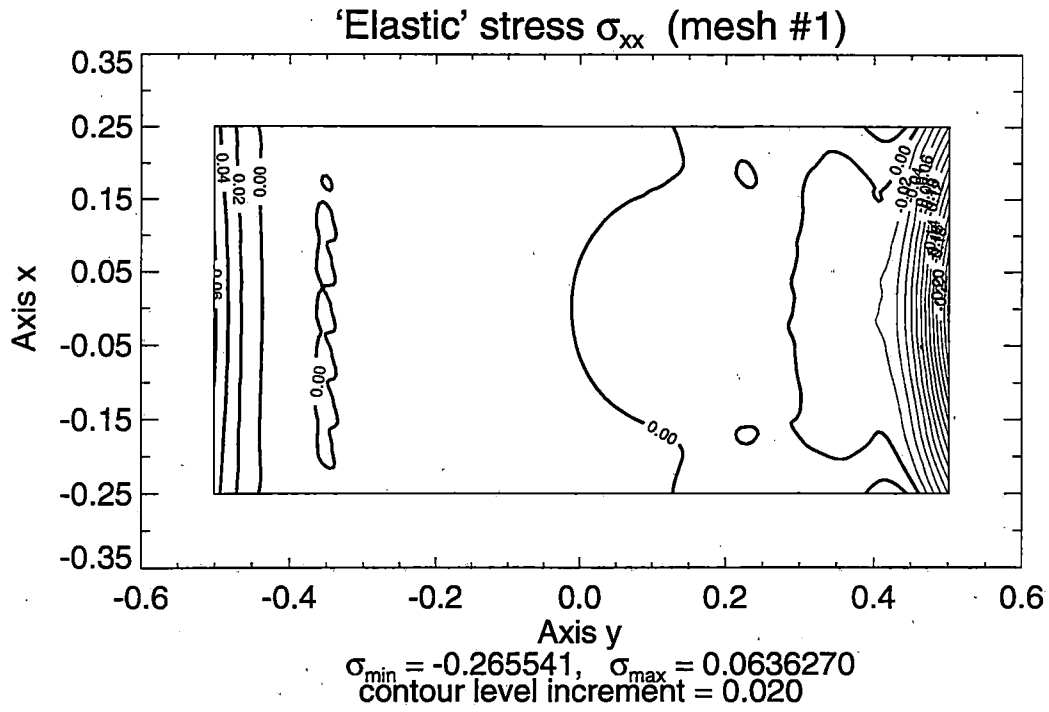

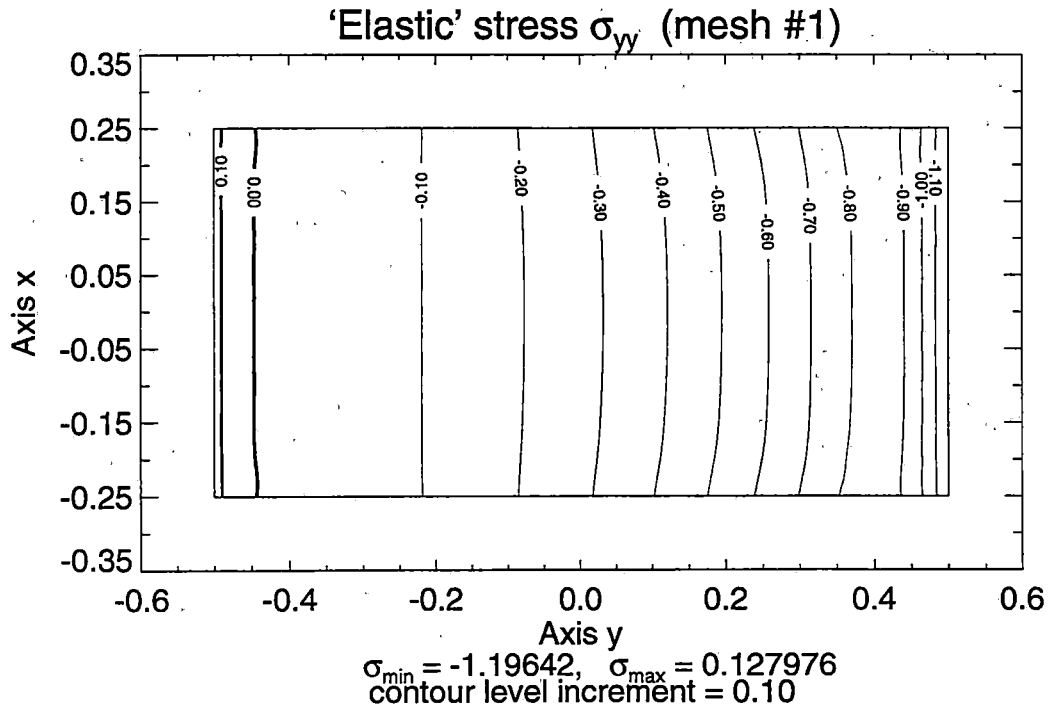

Figure 2.10 Contour Lines of Normal 'Elastic' Stresses σ_{xx} and σ_{yy} in the Simply Supported Beam under Vertical Surface Tractions – Solution for Mesh #1

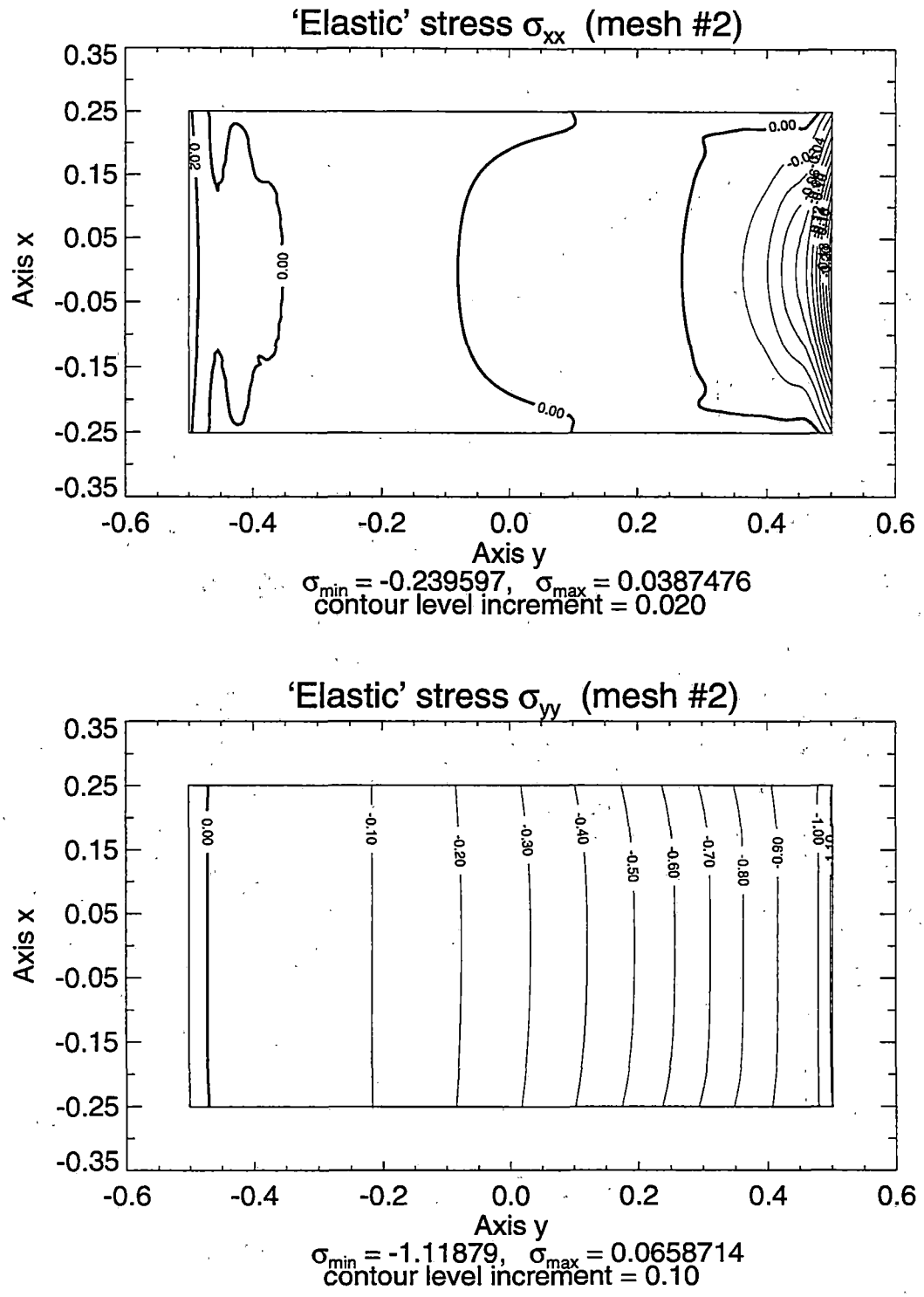

Figure 2.11 Contour Lines of Normal 'Elastic' Stresses σ_{xx} and σ_{yy} in the Simply Supported Beam under Vertical Surface Tractions – Solution for Mesh #2

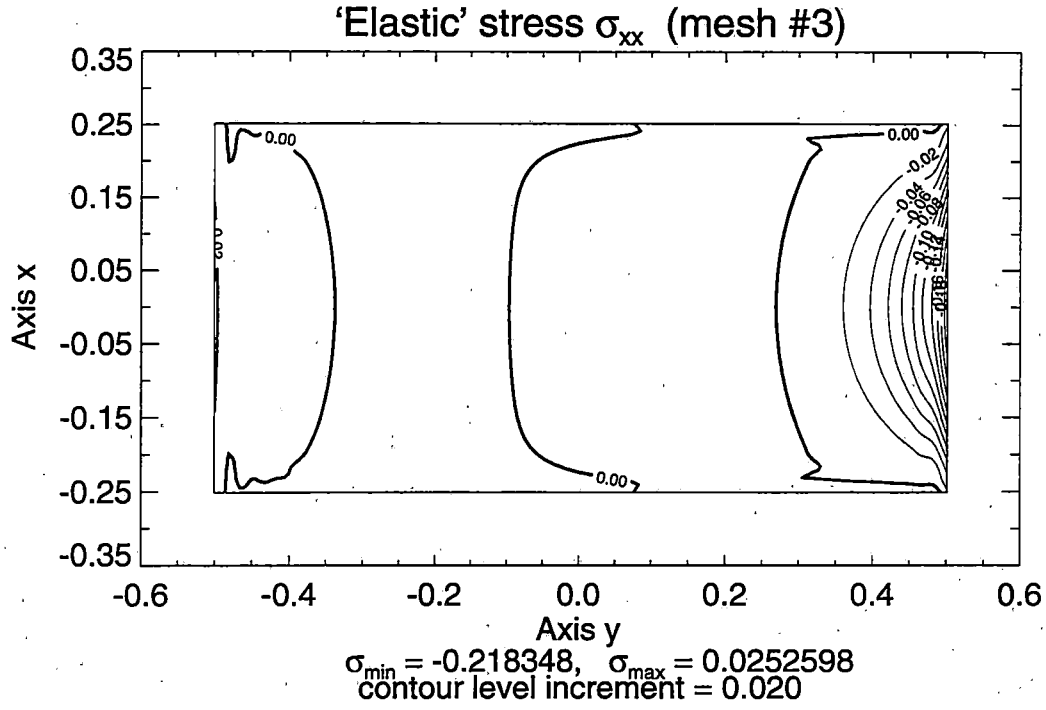

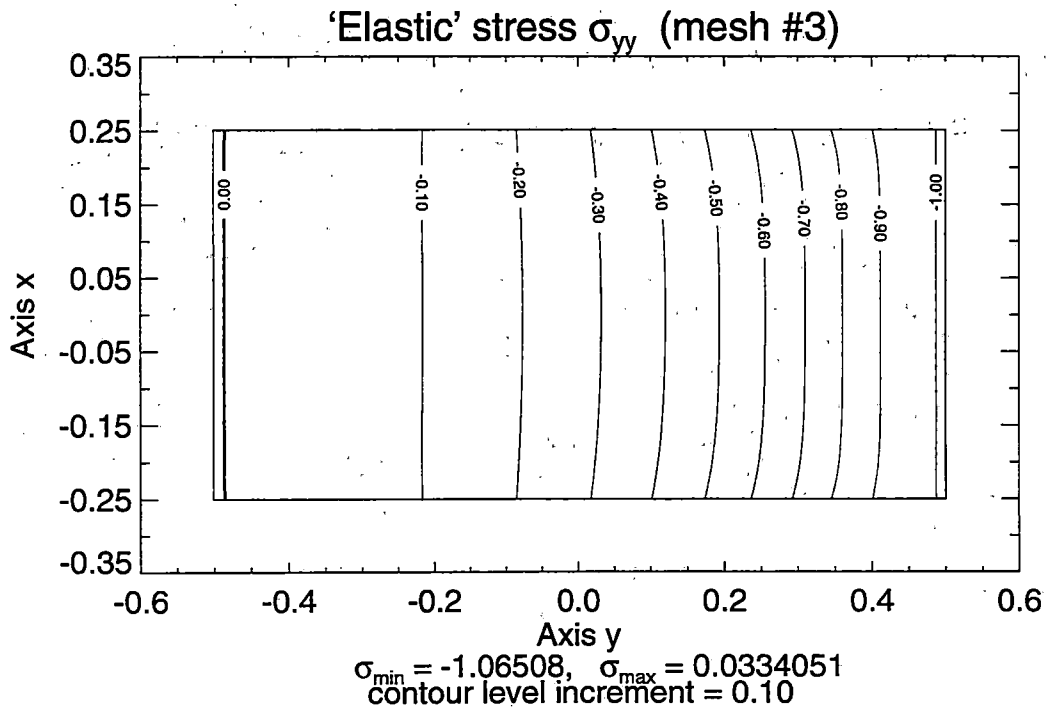

Figure 2.12 Contour Lines of Normal 'Elastic' Stresses σ_{xx} and σ_{yy} in the Simply Supported Beam under Vertical Surface Tractions – Solution for Mesh #3

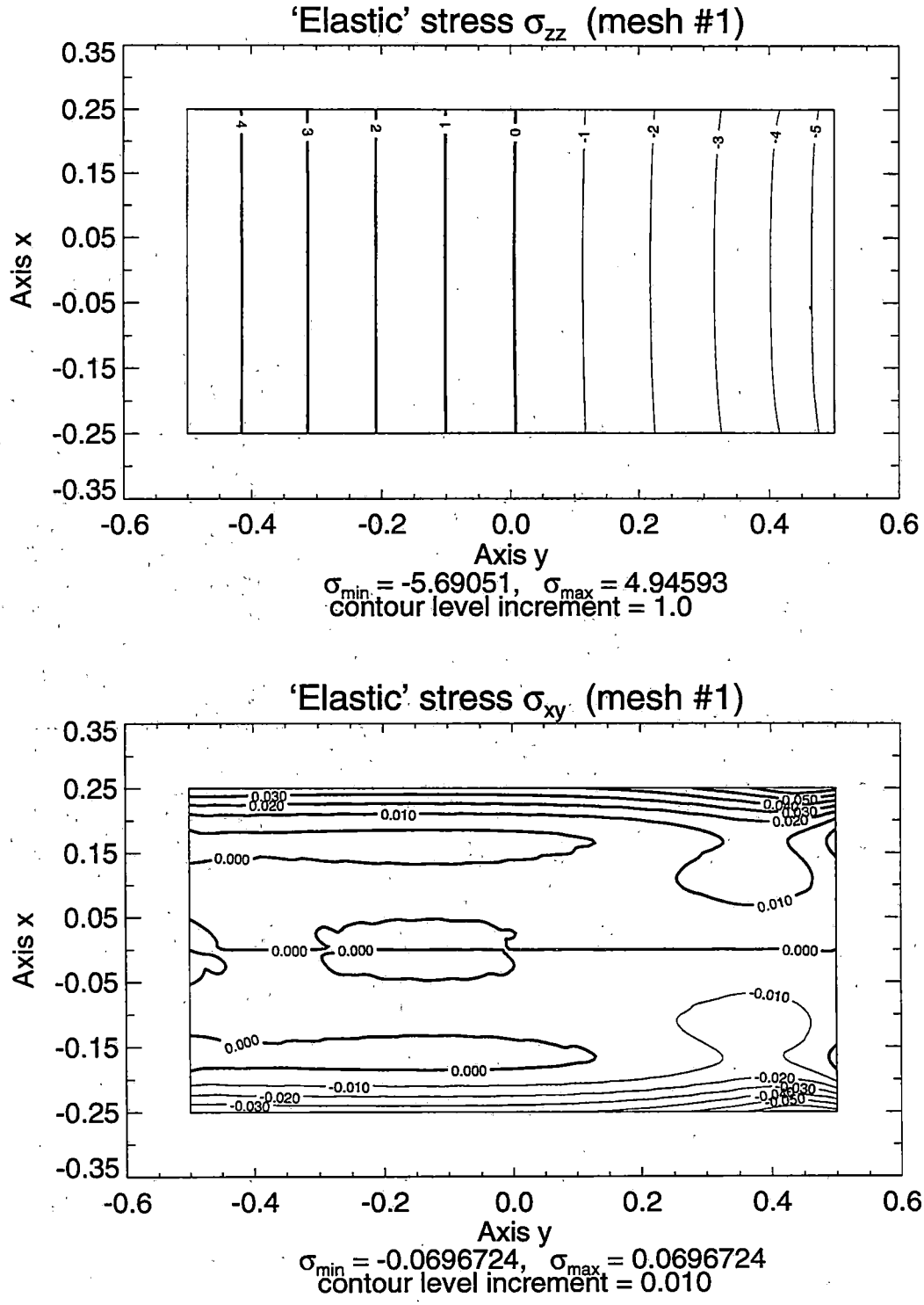

Figure 2.13 Contour Lines of Normal σ_{zz} and Shear σ_{xy} 'Elastic' Stresses in the Simply Supported Beam under Vertical Surface Tractions – Solution for Mesh #1

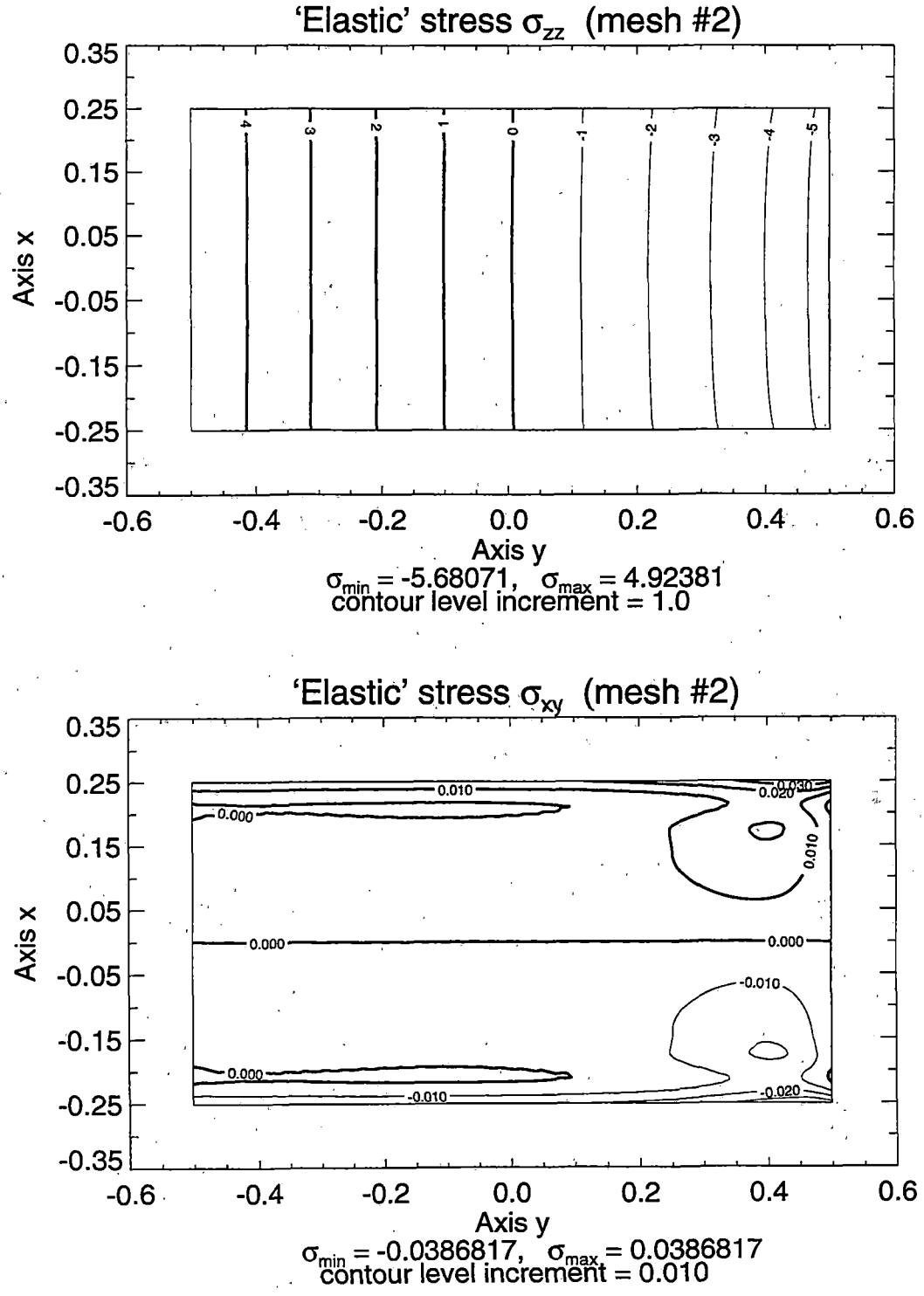

Figure 2.14 Contour Lines of Normal σ_{zz} and Shear σ_{xy} 'Elastic' Stresses in the Simply Supported Beam under Vertical Surface Tractions – Solution for Mesh #2

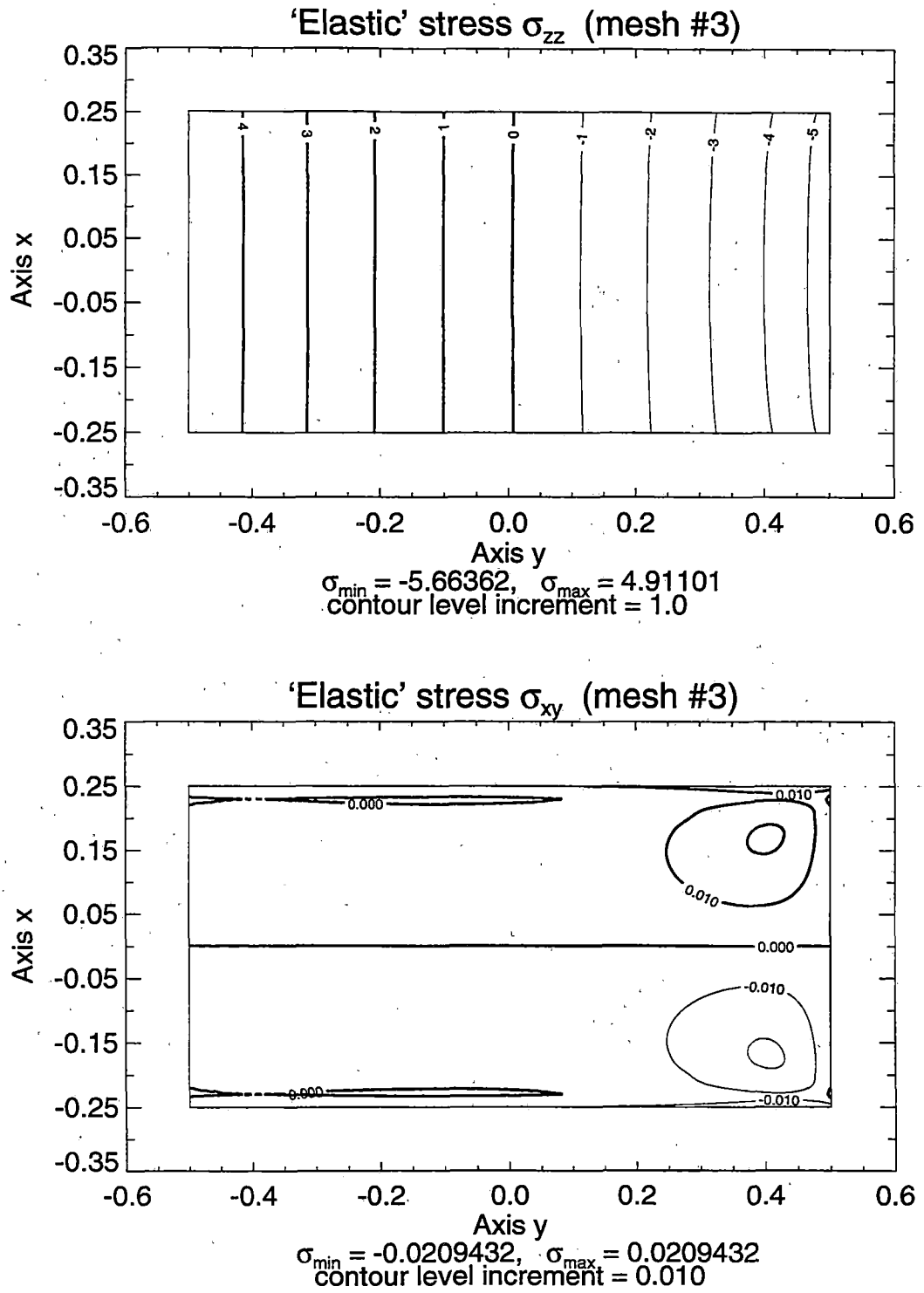

Figure 2.15 Contour Lines of Normal σ_{zz} and Shear σ_{xy} 'Elastic' Stresses in the Simply Supported Beam under Vertical Surface Tractions – Solution for Mesh #3

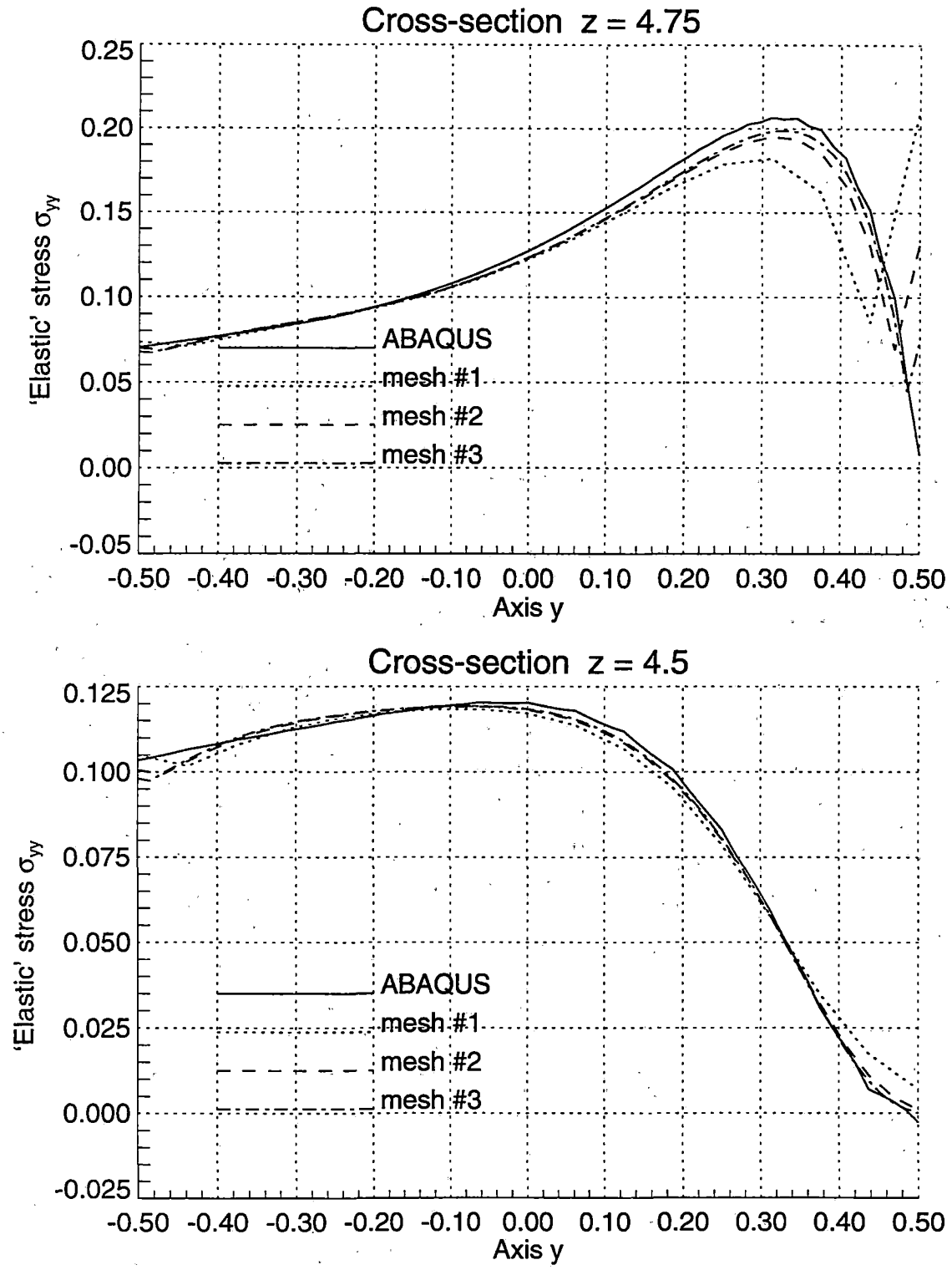

Figure 2.16 Normal 'Elastic' Stresses σ_{yy} in the Simply Supported Beam under Concentrated Horizontal Surface Tractions

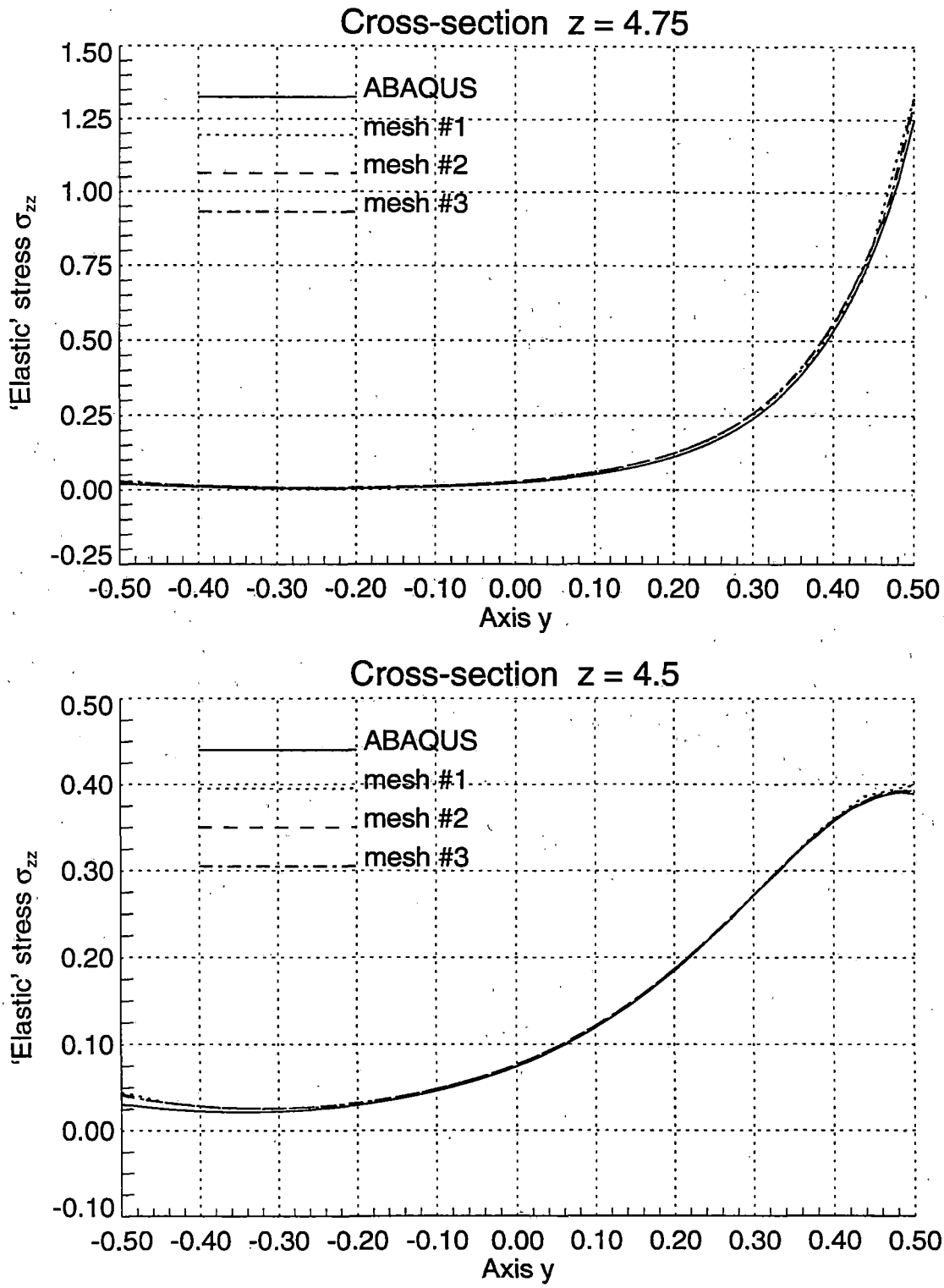

Figure 2.17 Normal 'Elastic' Stresses σ_{zz} in the Simply Supported Beam under Concentrated Horizontal Surface Tractions

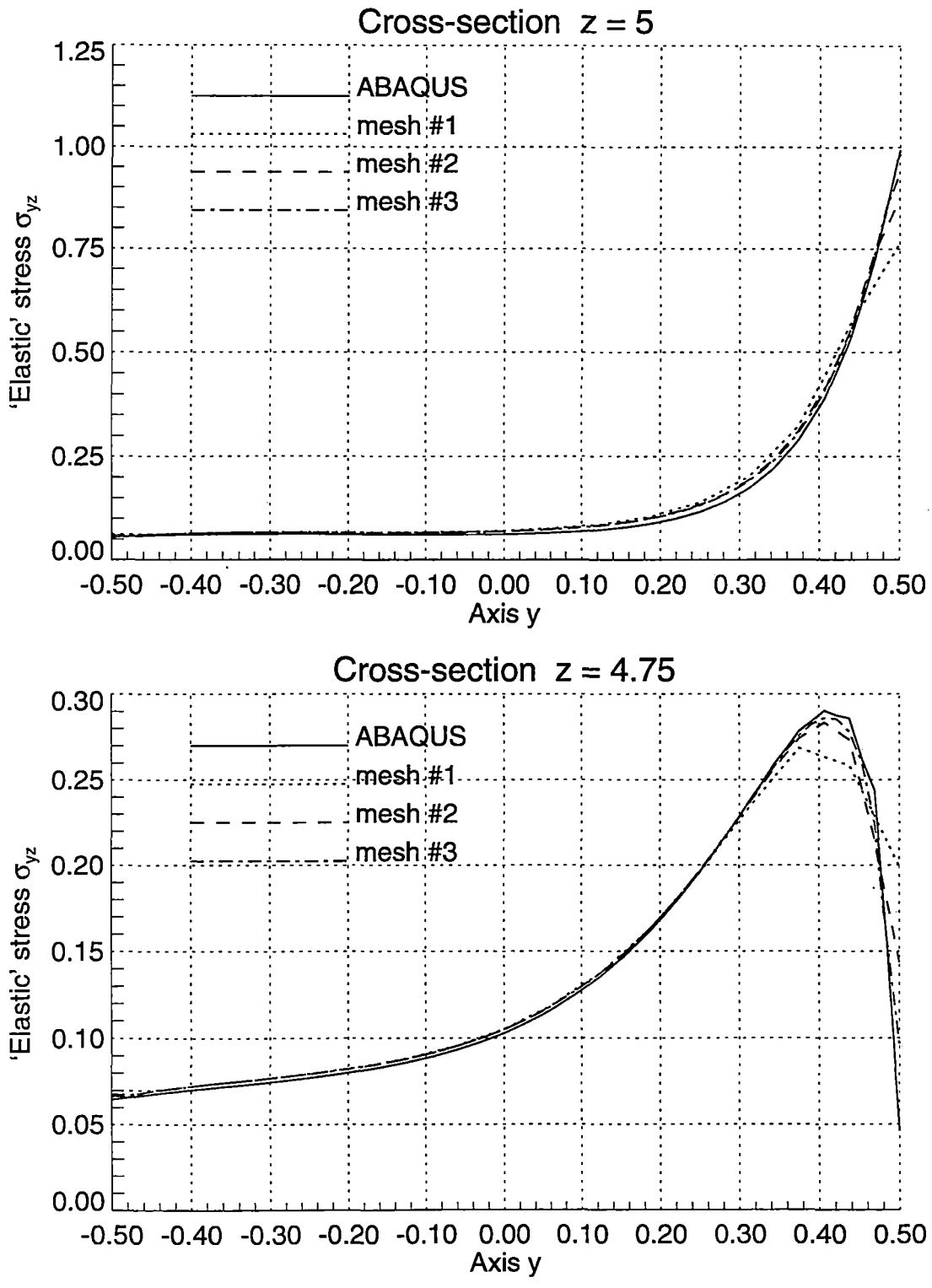

Figure 2.18 Shear 'Elastic' Stresses σ_{yz} in the Simply Supported Beam under Concentrated Horizontal Surface Tractions

2.6 EXAMPLE ANALYSES FOR A RAILROAD RAIL

After the computer programs had been successfully validated using the test problems described in the previous section, they were applied to the evaluation of elastic stresses in a 132 RE rail section subject to contact loading.

Two cases of loading were considered. In the first one, the rail was subject only to the vertical surface tractions $t_Z(X,Y)$ of intensity $t_{0Z} = 1239.98\,\text{MPa}$ acting over the rectangular contact area of dimensions $a = 6.947\,\text{mm}$ and $b = 5.083\,\text{mm}$, with the center C of coordinates $x = 0\,\text{m}$ and $y = 0.180086\,\text{m}$ and the slope $\alpha = 0^\circ$ (for the notation and conventions see section 2.4). The parameters t_{0Z}, a, and b were calculated using the formulae (2.48) where the vertical force T_Z was equal to 77.84 kN and the dimensions of the elliptical contact area, $A = 6.4\,\text{mm}$ and $B = 4.683\,\text{mm}$, were obtained by means of the Hertz formulae assuming the following data: radius of the wheel $R_2 = 0.4064\,\text{m}$, radius of the wheel profile $R_2' = \infty$, and radius of the rail profile $R_1 = 0.254\,\text{m}$; the rail was assumed to be flat in the longitudinal direction, i.e., $R_1' = \infty$.

In the second case of loading, the rail was subject to the horizontal surface tractions $t_X(X,Y)$ of intensity $t_{0X} = 0.3t_{0Z} = 371.994\,\text{MPa}$. For simplicity, the other data, including the dimensions of the contact zone, were assumed exactly the same as in the first case of loading.

The problem was solved for a rail section of length $l = 5.08\,\text{m}$ loaded in the middle of its span. The number of the Fourier modes (harmonics) was assumed to be equal to 1000 modes for both of the cases considered.

As far as the material properties are concerned, Young's modulus E and Poisson's ratio ν were assumed to be temperature-independent and equal to 206.832 GPa and 0.3, respectively. Additionally, the dimensions of the Hertz ellipse were calculated assuming that both the rail and the wheel were made of material with the same elastic constants.

The problem was solved using three finite element meshes that consisted of 340, 466, and 682 elements, respectively. The first mesh, shown in figures 2.19 and 2.20, is based on one of the meshes supplied by the Volpe National Transportation Systems Center. The original mesh was slightly modified, so that the generation of denser meshes could be performed partly automatically. The mesh refinement was restricted to the head where the highest concentration of stresses was expected, particularly to the area below the contact surface (figures 2.21 and 2.22).

The results for the case of vertical loading are shown in figures 2.23 through 2.36. The convergence of the solution with respect to the mesh density is presented in figures 2.23 through 2.28, where the stress tensor components are plotted along the lines $\alpha - \alpha$ and $\beta - \beta$ shown in figures 2.20 through 2.22. The normal stresses $\sigma_{xx}, \sigma_{yy}, \sigma_{zz}$, and shear stresses σ_{xy} are plotted for two selected cross sections, $z = 2.540\,\text{m}$ and $z = 2.547\,\text{m}$, that contain the center and the end point of the contact zone, respectively. The shear stresses σ_{yz} and σ_{xz} are also

plotted for two cross sections, but instead of the cross section $z = 2.540\,\mathrm{m}$, where these stresses are equal to zero, an additional cross section, $z = 2.554\,\mathrm{m}$, was chosen. These results indicate that the mesh #1 is definitely too coarse for the problem under consideration. It seems to be obvious when one takes into account the fact that the number of finite elements along the contact zone was equal to 4. The results obtained for the mesh #2 are good but the mesh is still too coarse to reflect the variation of stresses correctly. The mesh #3 may be recognized as appropriate for the problem considered.

The convergence of the solution with respect to the number of harmonics is presented in figures 2.29 and 2.30. Only one point of the rail — the center of the contact zone — was chosen to investigate this problem and that is why the shear stresses, which are equal to zero at this point, are not shown. The assumed number of harmonics seems to be appropriate for the problem under consideration. However, in real analyses some excess in this number is recommended, especially when the elastic stresses are used as input data for the analysis of residual stresses in which even small variations in the elastic stresses may result in different solutions.

Finally, in figures 2.31 through 2.36, the stress tensor components are shown in the form of contour line plots. Only the solutions obtained for the cross section $z = 2.540\,\mathrm{m}$ are presented.

The results for the case of horizontal loading are shown in figures 2.37 through 2.45. The convergence of the solution with respect to the mesh density is presented in figures 2.37 through 2.42. In figures 2.43 through 2.45, the stress tensor components are shown in the form of contour line plots. Only the plots for the shear stresses σ_{yz} and σ_{xz} are presented because these are the only stress tensor components strongly influenced by the horizontal loading.

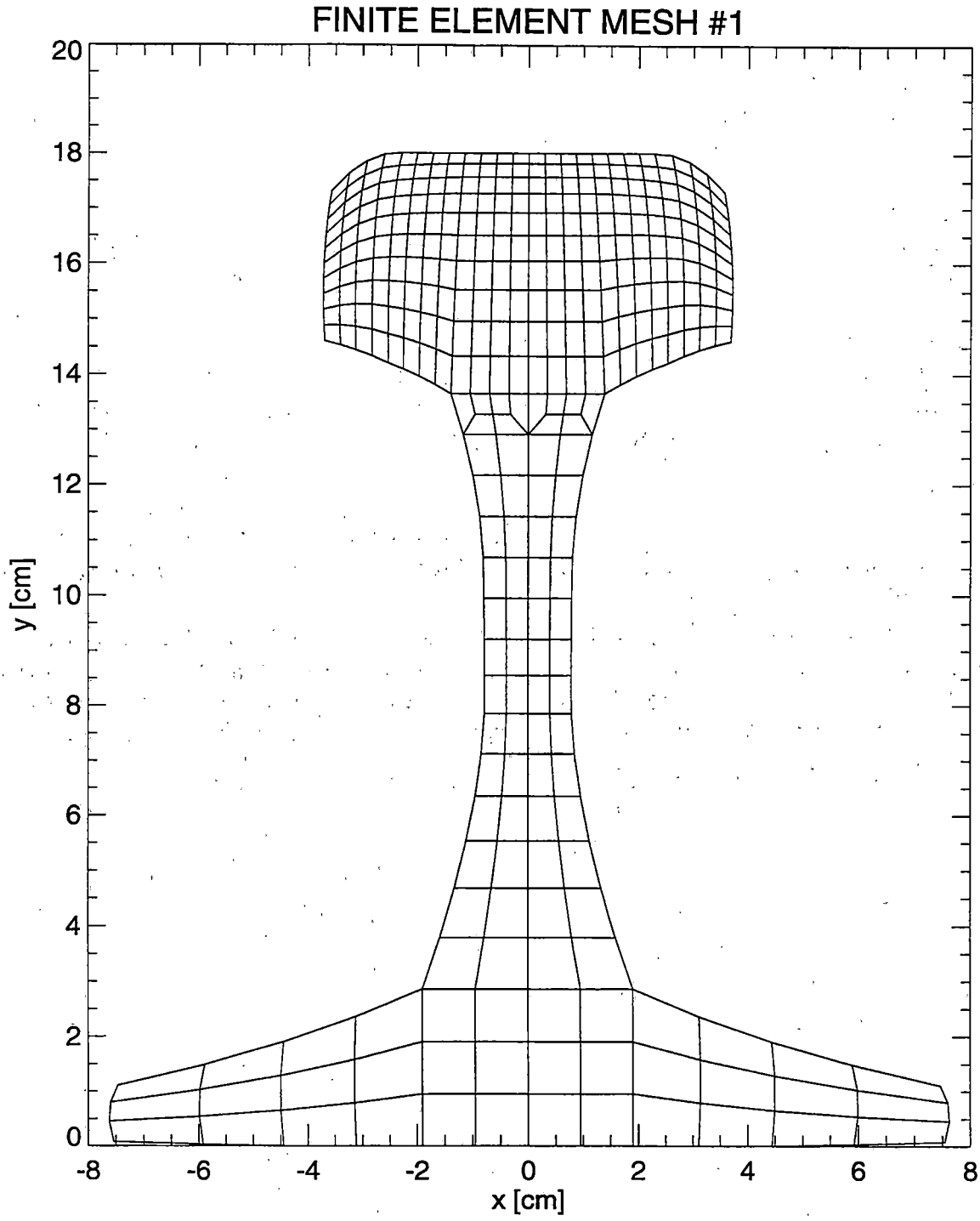

Figure 2.19 Finite Element Mesh #1 in the Problem of a Railroad Rail under Contact Loading

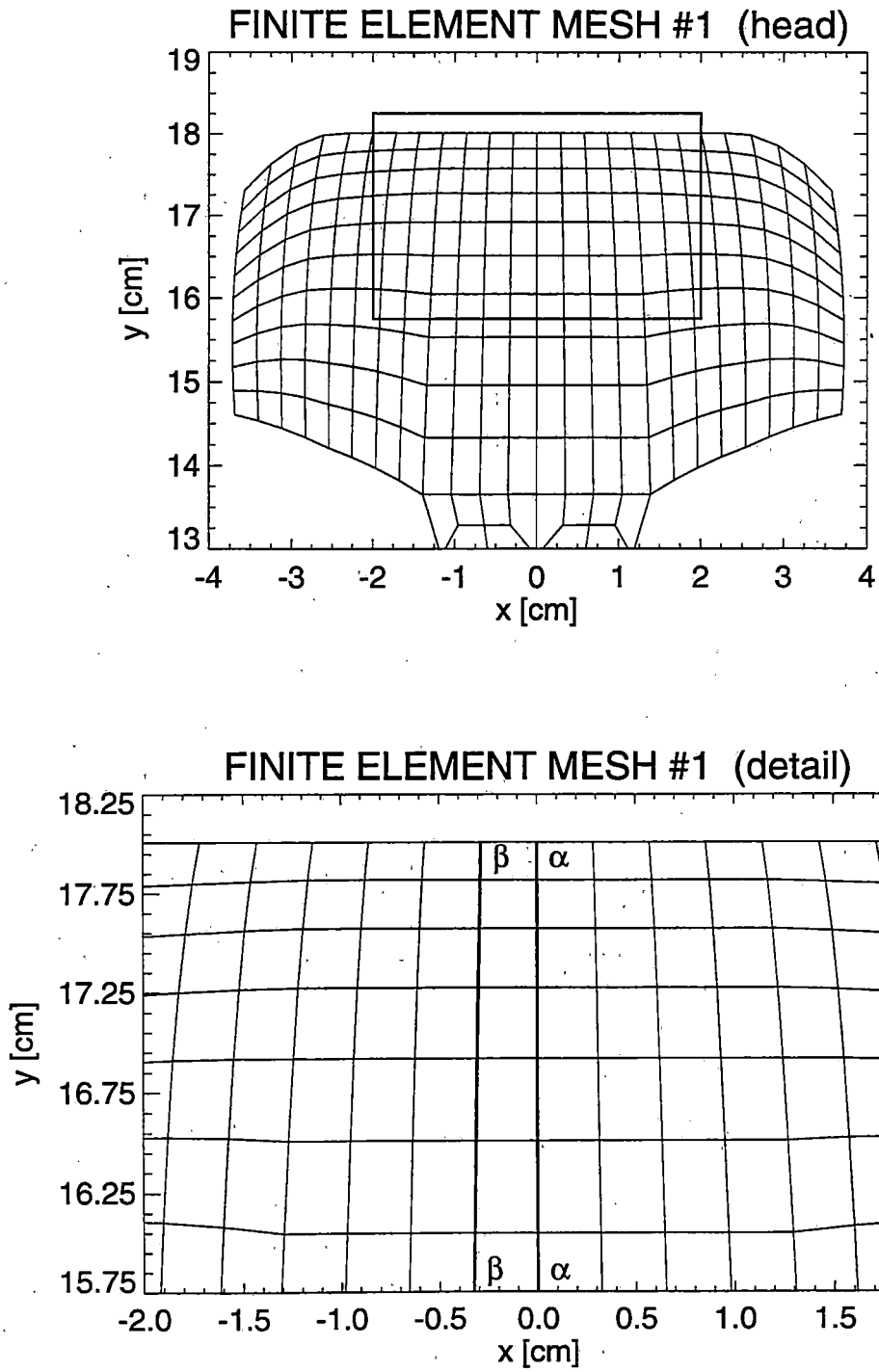

Figure 2.20 Finite Element Mesh #1 in the Problem of a Railroad Rail under Contact Loading – Head and Detail

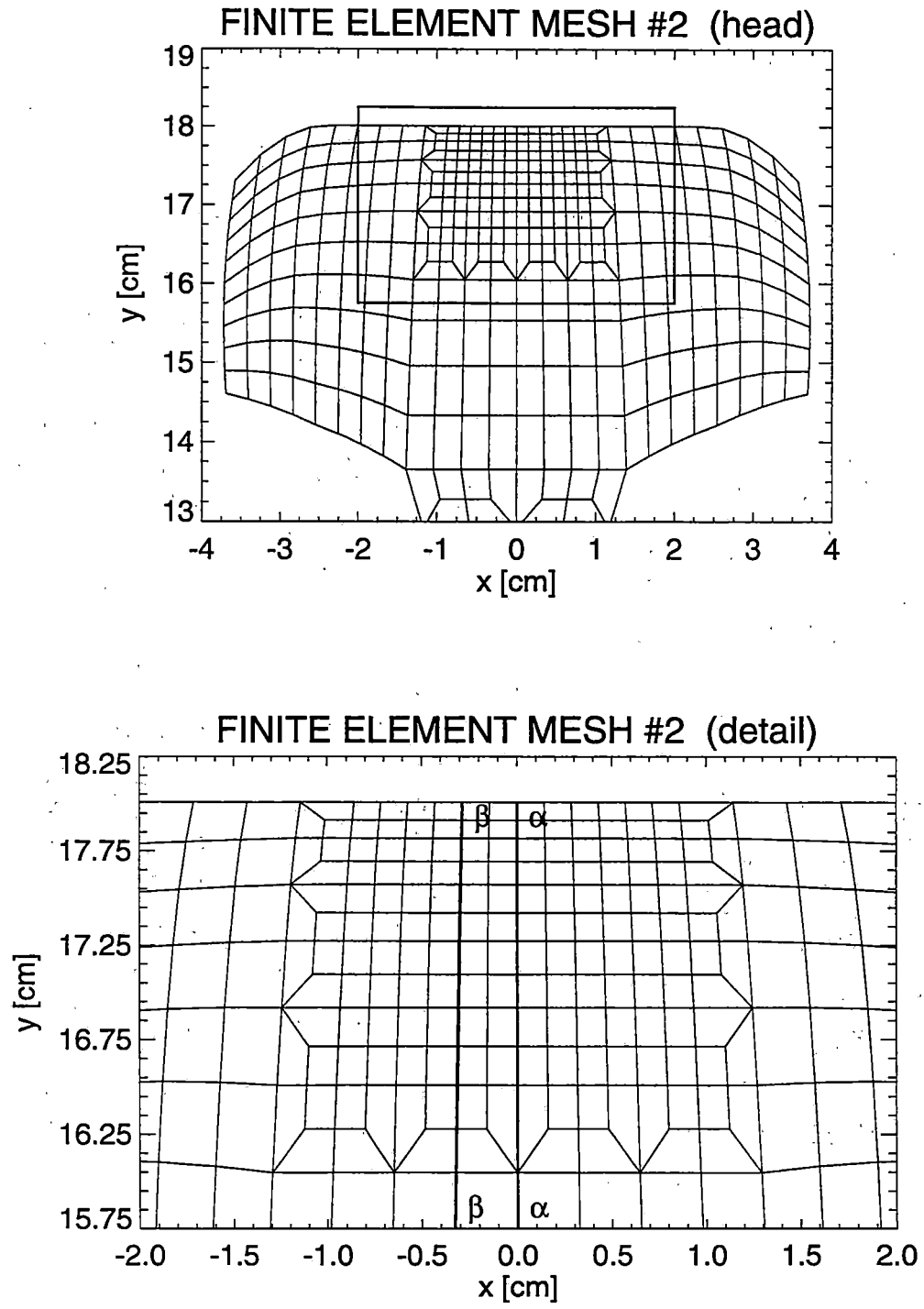

Figure 2.21 Finite Element Mesh #2 in the Problem of a Railroad Rail under Contact Loading – Head and Detail

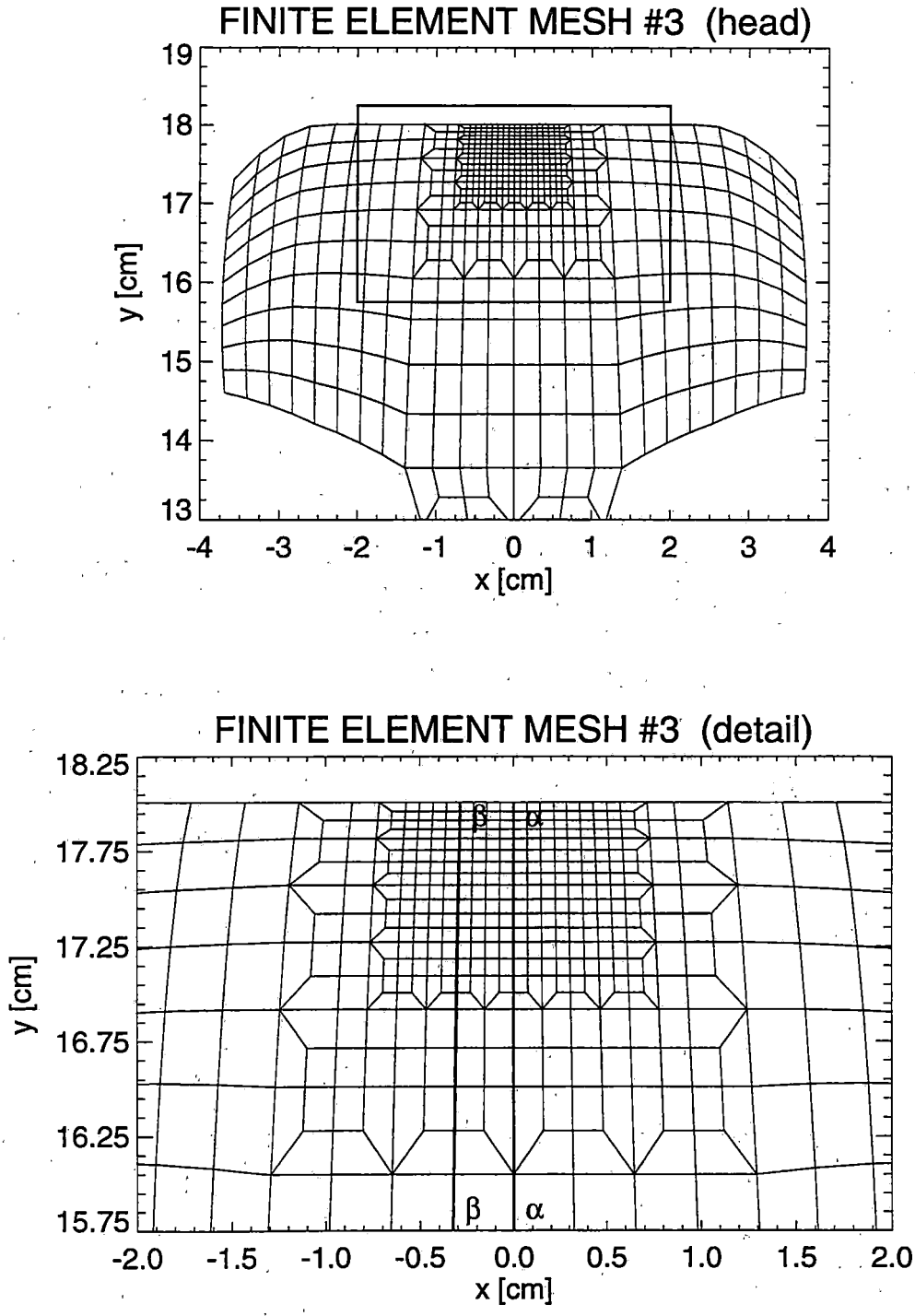

Figure 2.22 Finite Element Mesh #3 in the Problem of a Railroad Rail under Contact Loading – Head and Detail

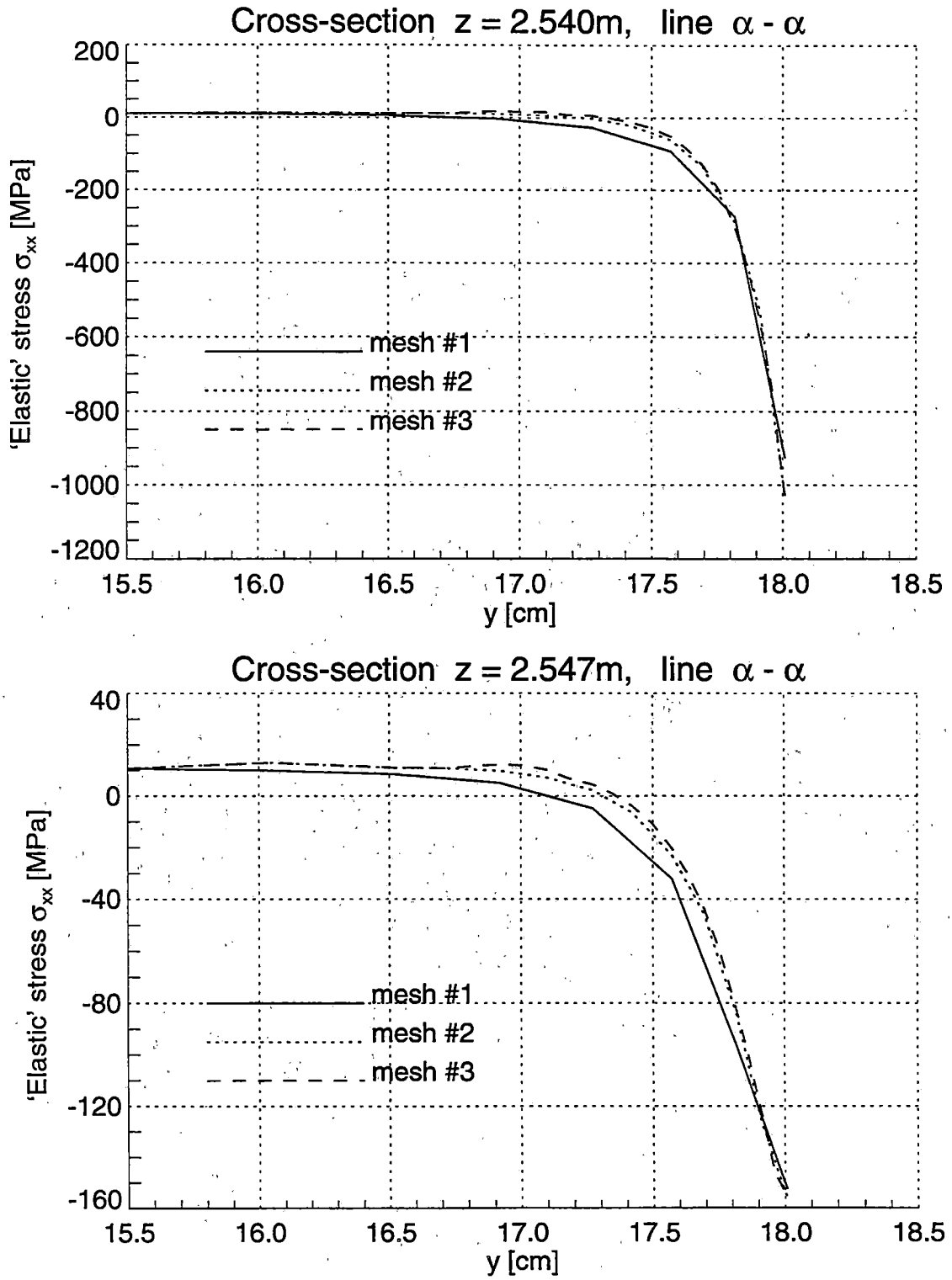

Figure 2.23 Normal 'Elastic' Stresses σ_{xx} in the Railroad Rail under Vertical Loading

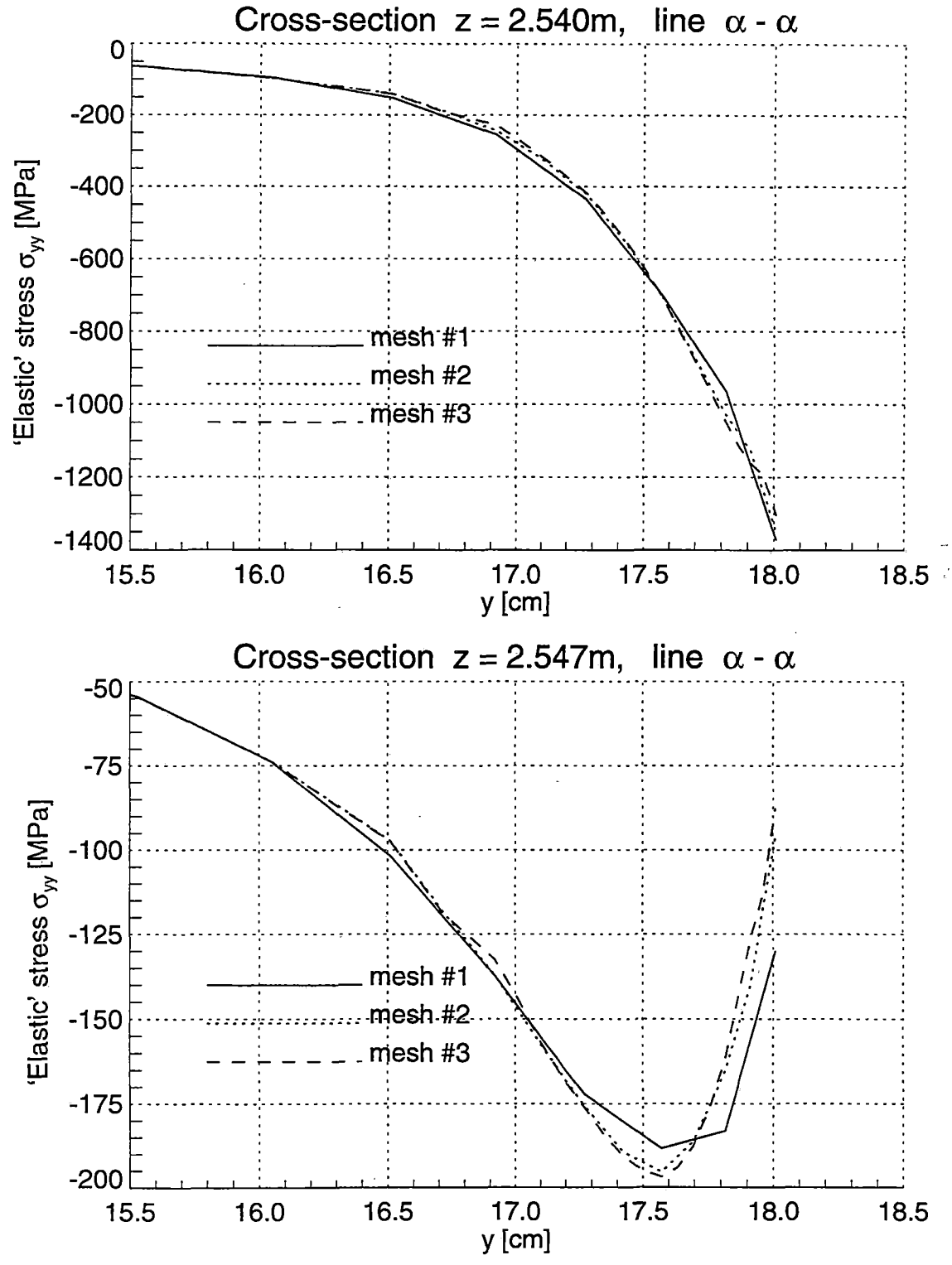

Figure 2.24 Normal 'Elastic' Stresses σ_{yy} in the Railroad Rail under Vertical Loading

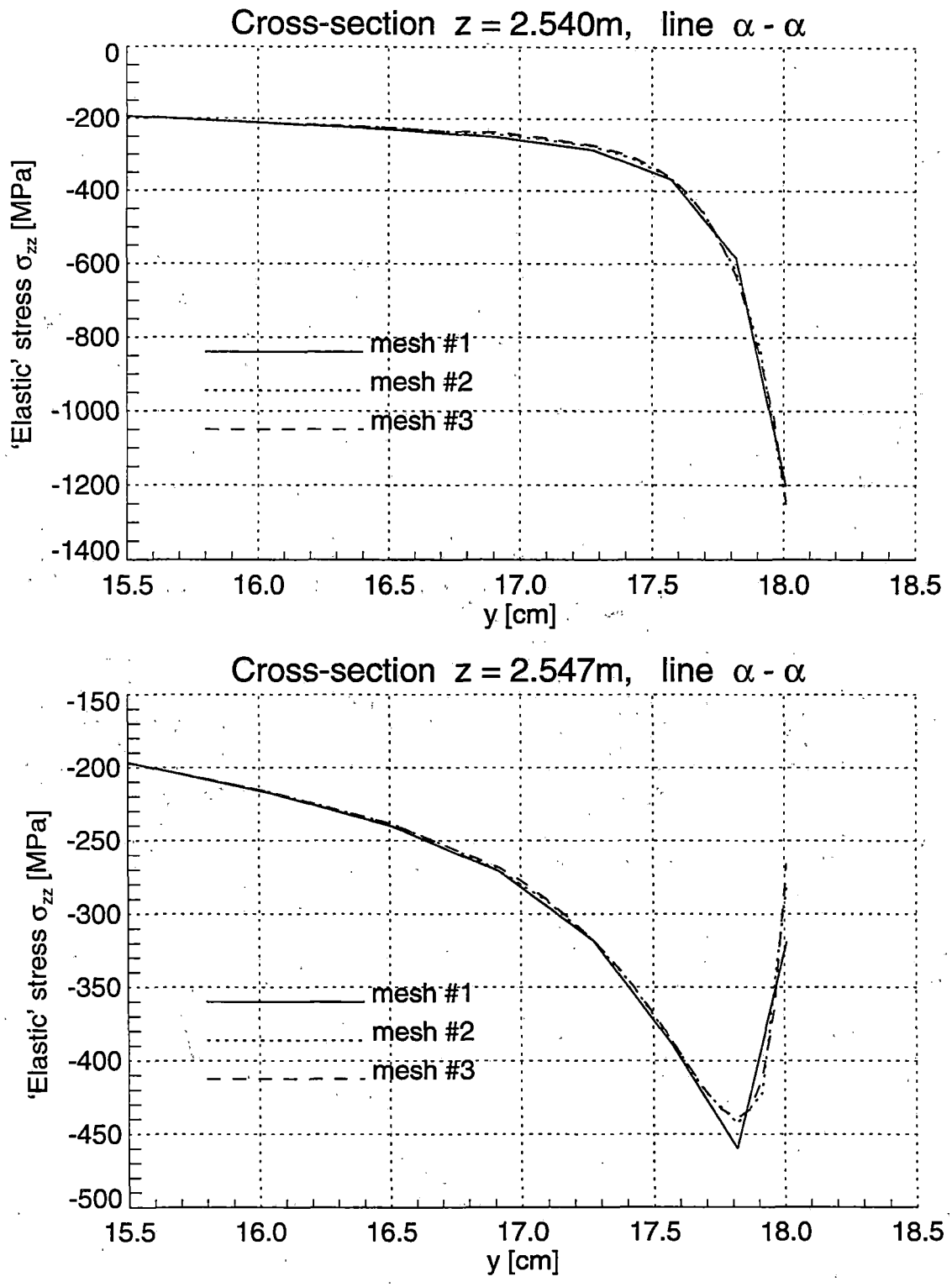

Figure 2.25 Normal 'Elastic' Stresses σ_{zz} in the Railroad Rail under Vertical Loading

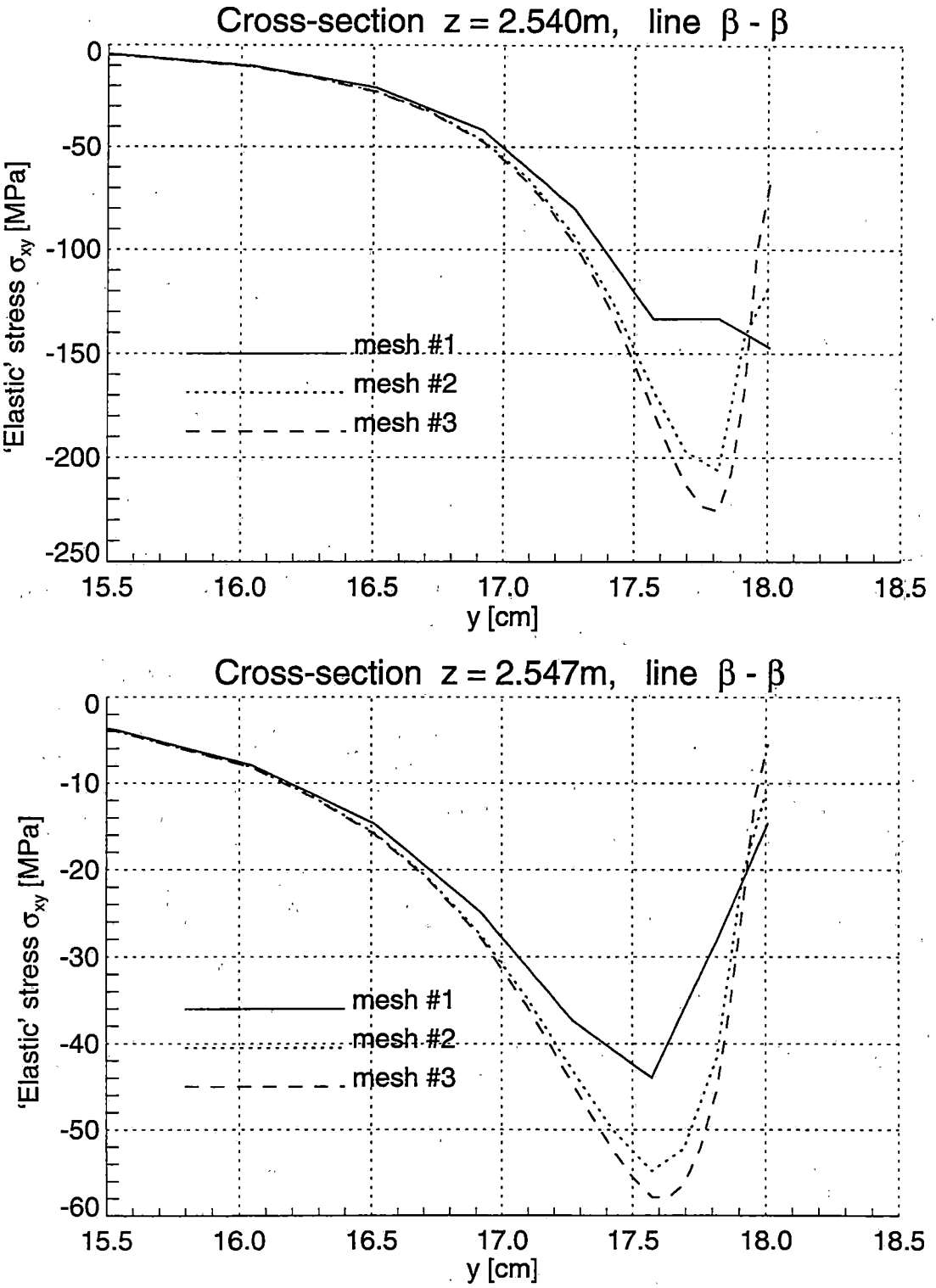

Figure 2.26 Shear 'Elastic' Stresses σ_{xy} in the Railroad Rail under Vertical Loading

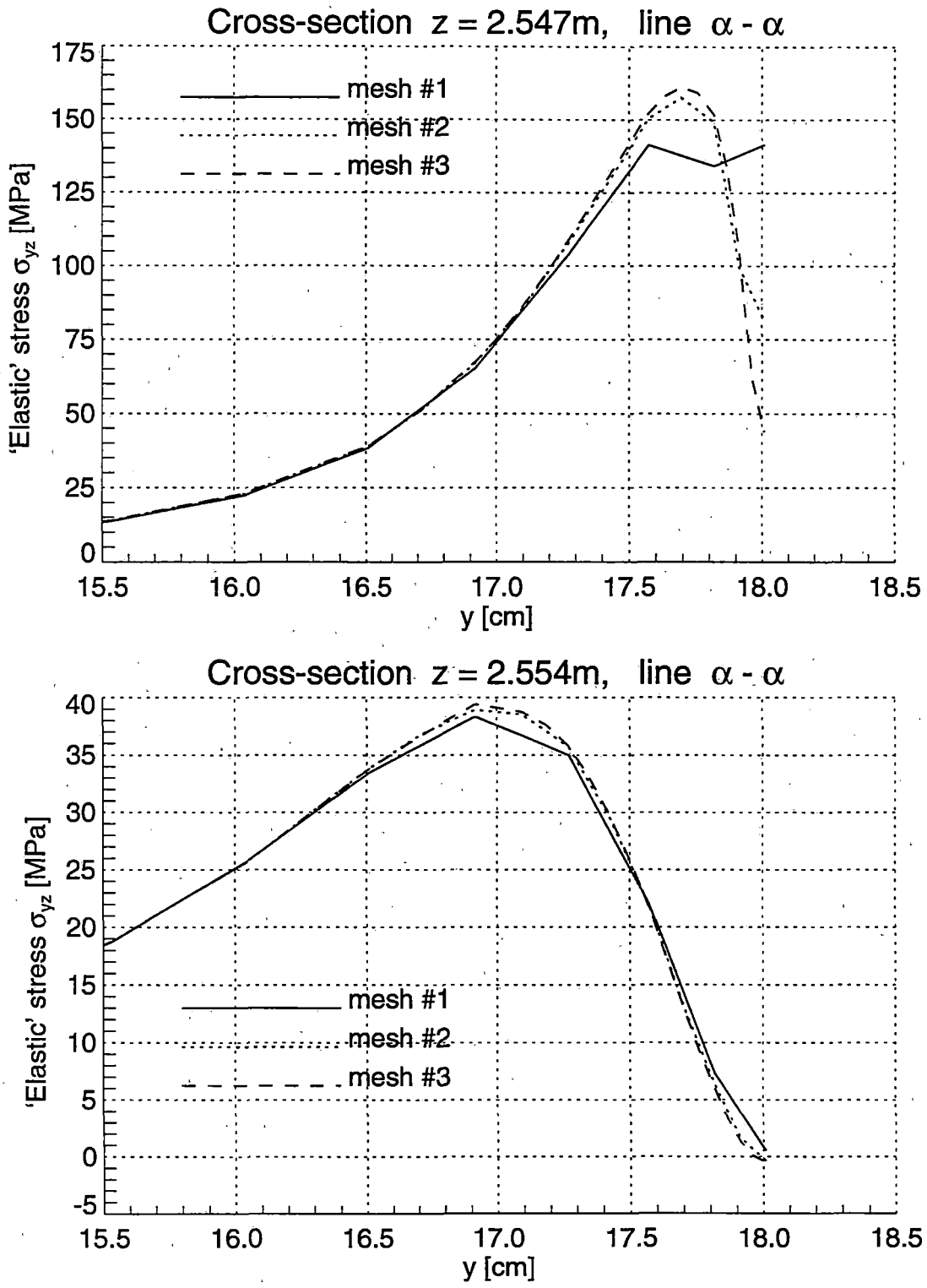

Figure 2.27 Shear 'Elastic' Stresses σ_{yz} in the Railroad Rail under Vertical Loading

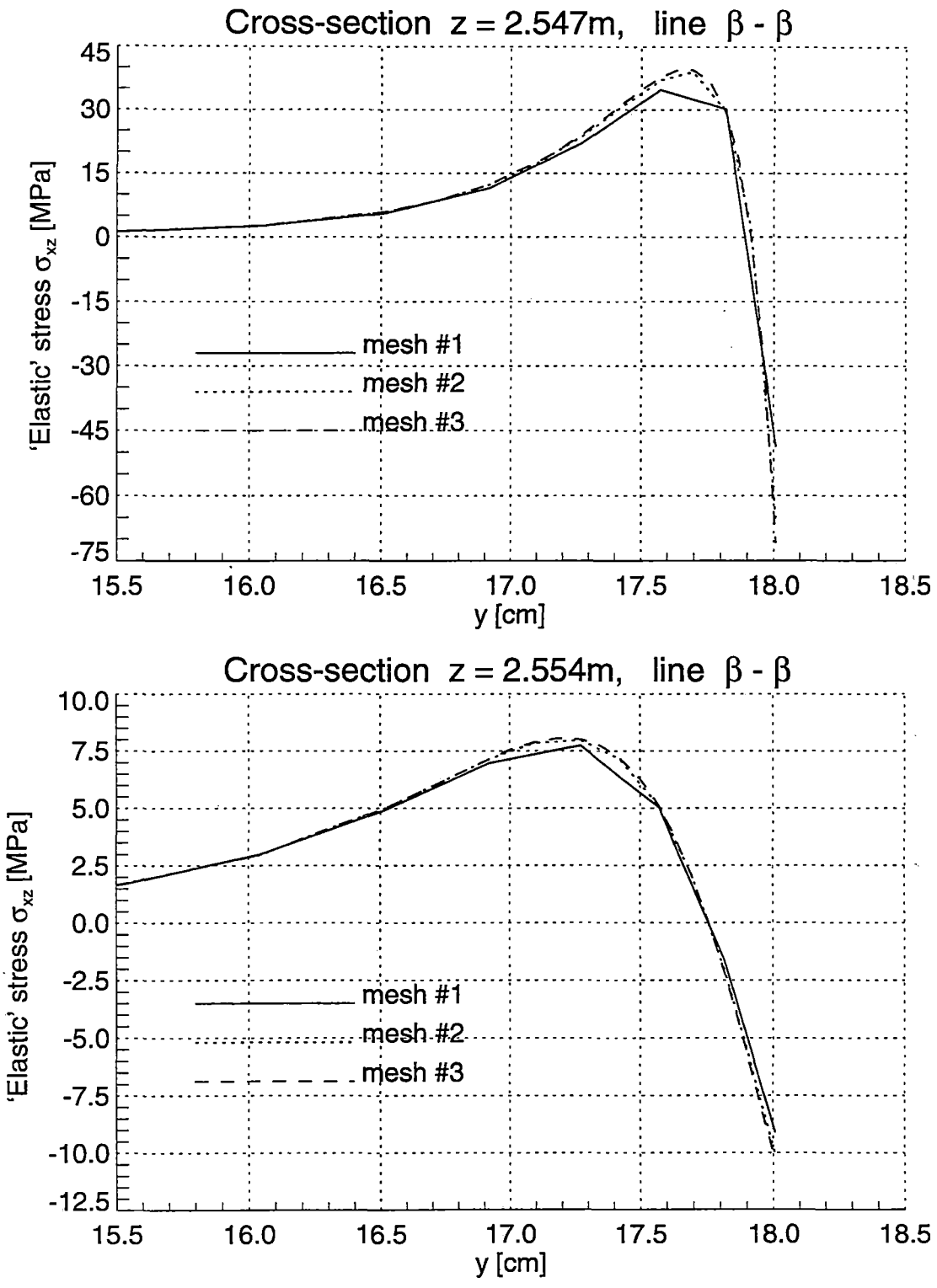

Figure 2.28 Shear 'Elastic' Stresses σ_{xz} in the Railroad Rail under Vertical Loading

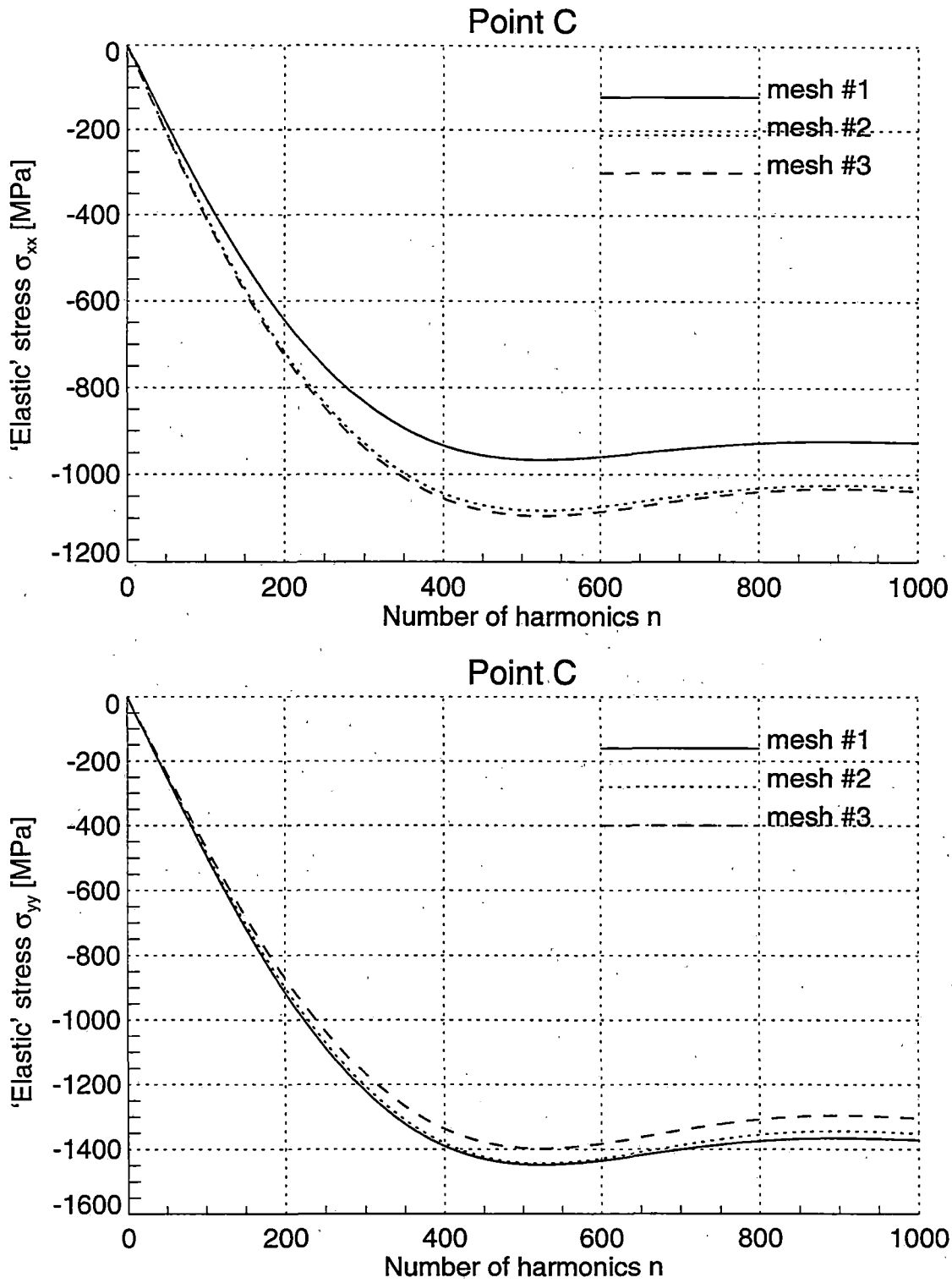

Figure 2.29 Normal 'Elastic' Stresses σ_{xx} and σ_{yy} as a Function of the Number of Fourier Modes in the Railroad Rail under Vertical Loading

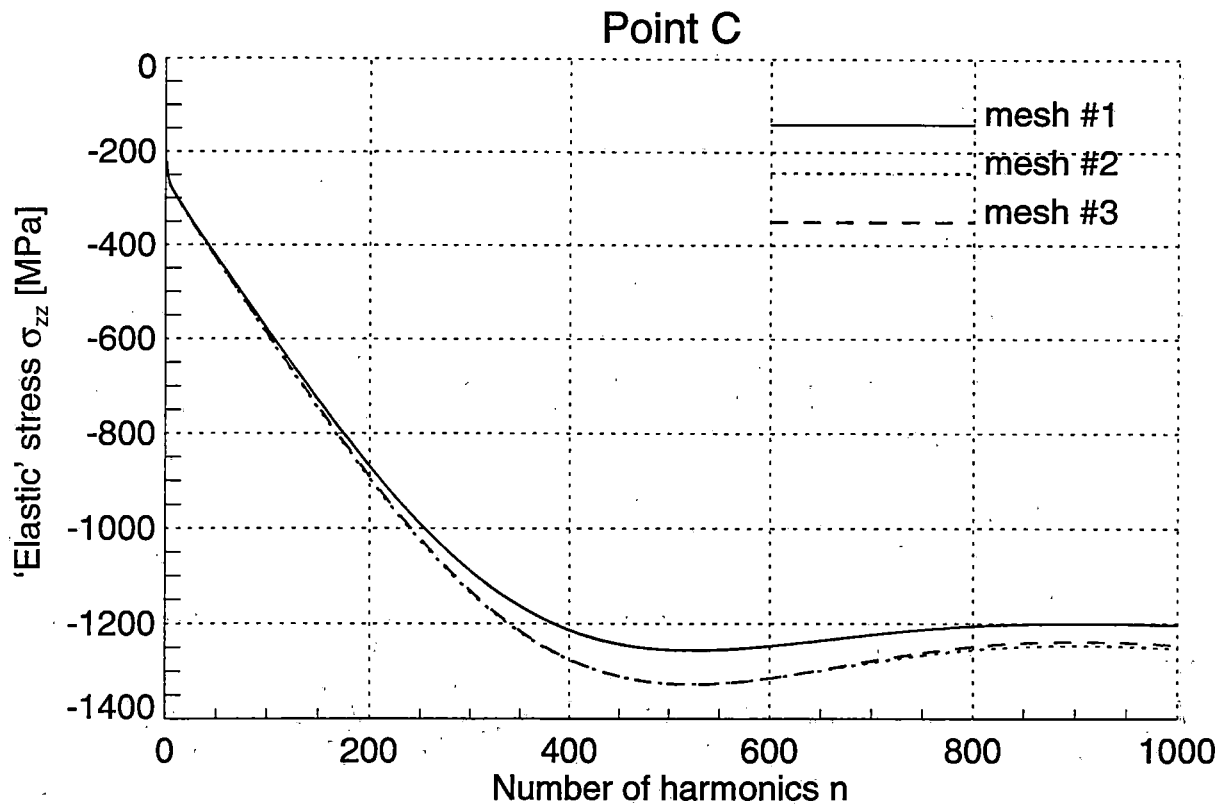

Figure 2.30 Normal 'Elastic' Stresses σ_{zz} as a Function of the Number of Fourier Modes in the Railroad Rail under Vertical Loading

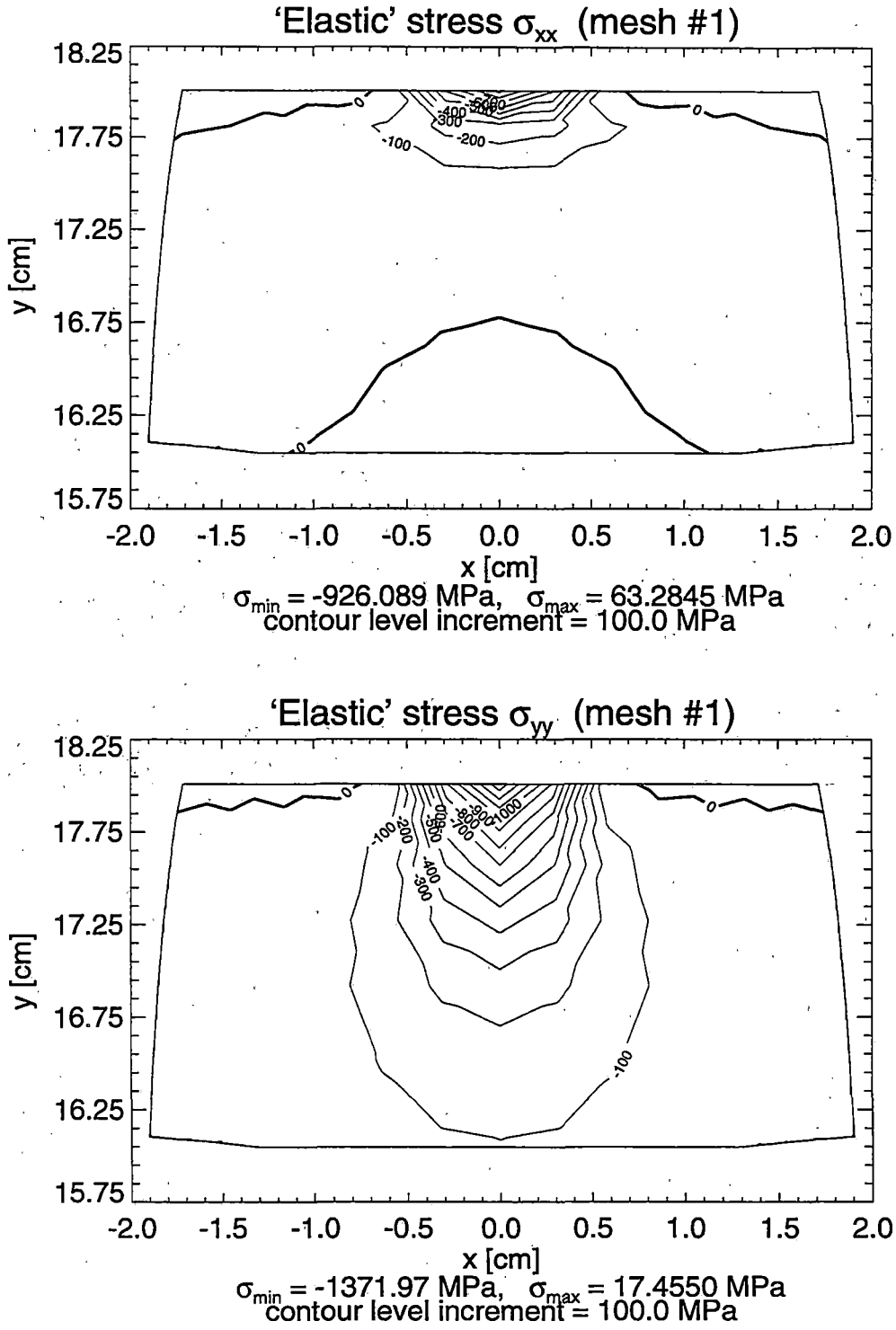

Figure 2.31 Contour Lines of Normal 'Elastic' Stresses σ_{xx} and σ_{yy} in the Railroad Rail under Vertical Loading – Solution for Mesh #1

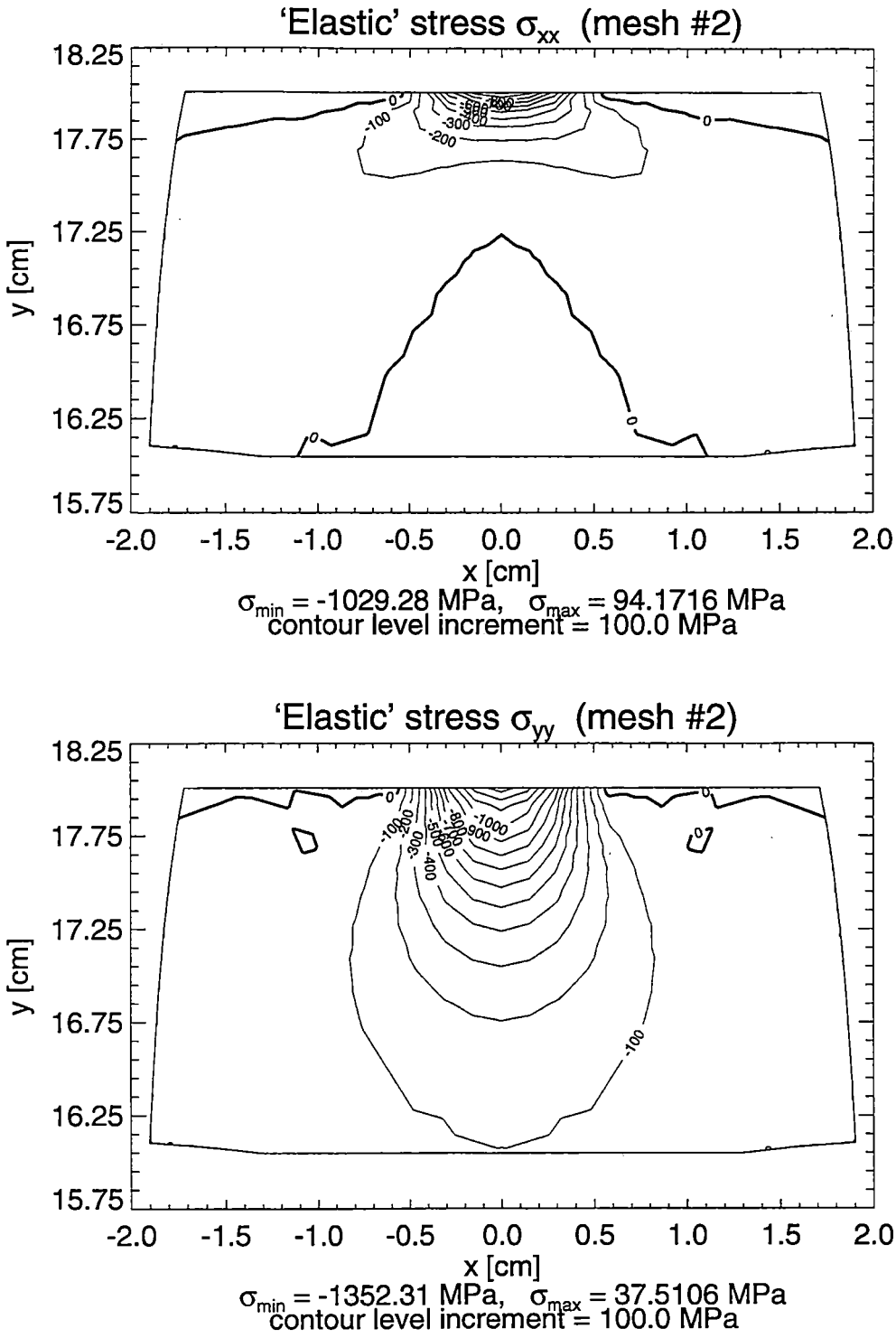

Figure 2.32 Contour Lines of Normal 'Elastic' Stresses σ_{xx} and σ_{yy} in the Railroad Rail under Vertical Loading – Solution for Mesh #2

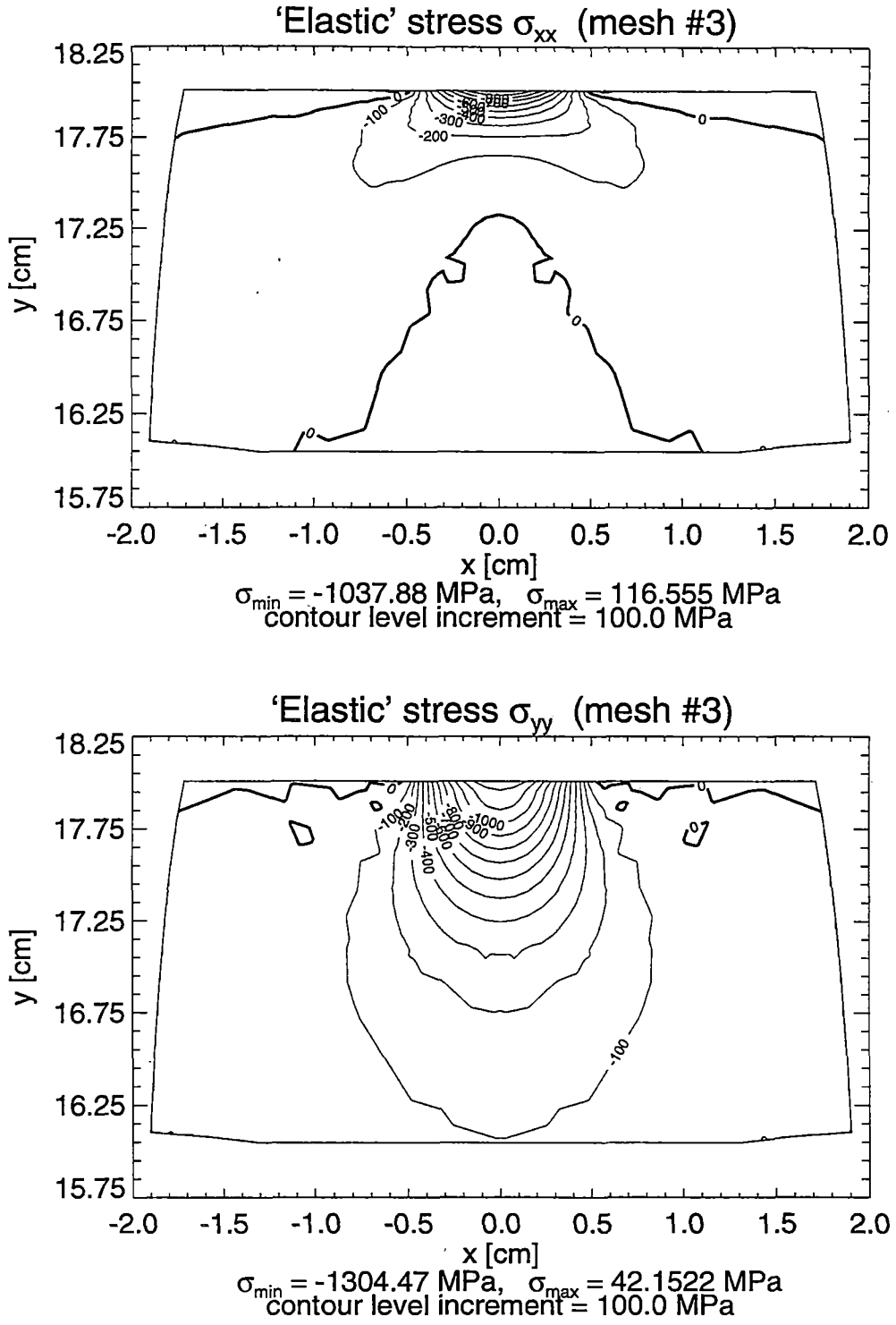

Figure 2.33 Contour Lines of Normal 'Elastic' Stresses σ_{xx} and σ_{yy} in the Railroad Rail under Vertical Loading – Solution for Mesh #3

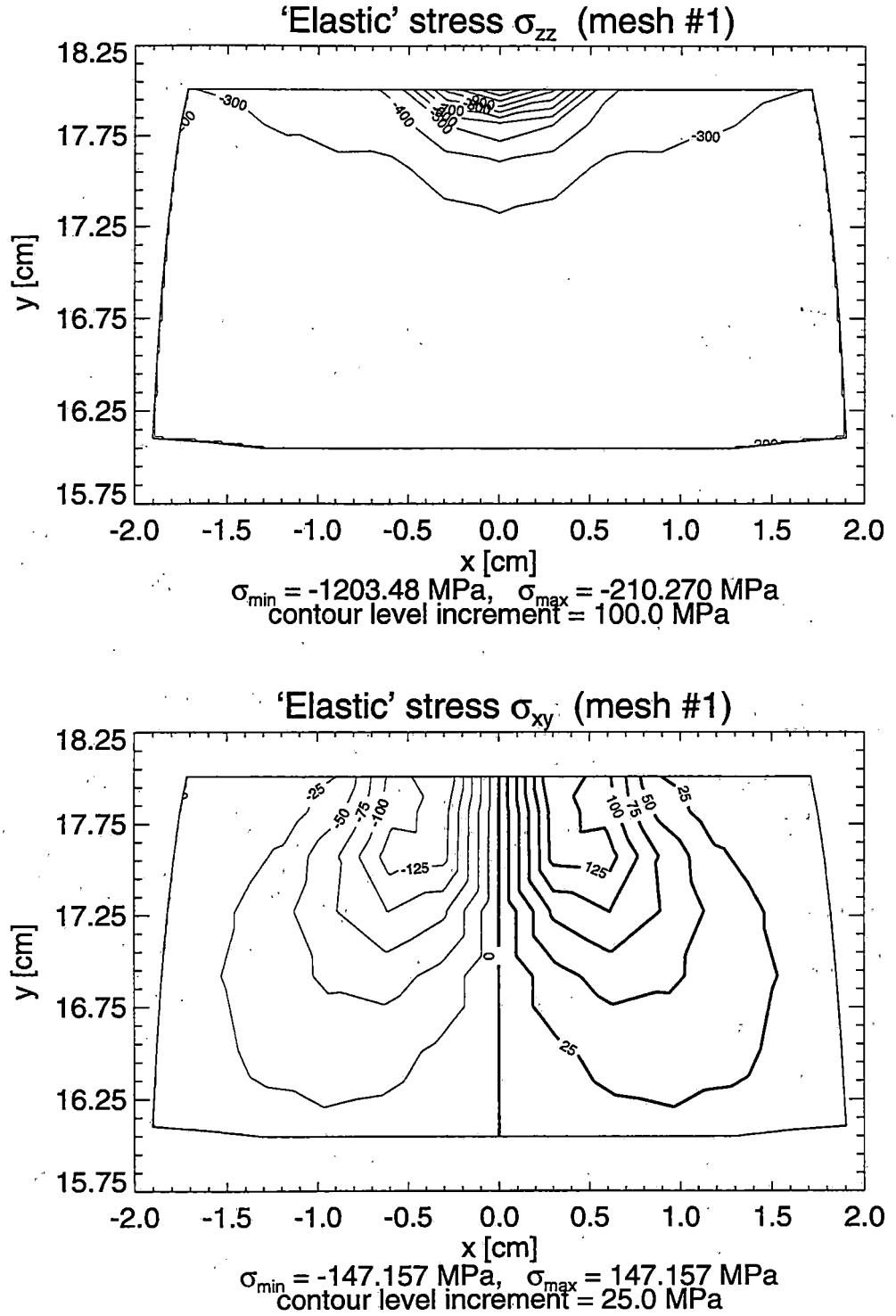

Figure 2.34 Contour Lines of Normal σ_{zz} and Shear σ_{xy} 'Elastic' Stresses in the Railroad Rail under Vertical Loading – Solution for Mesh #1

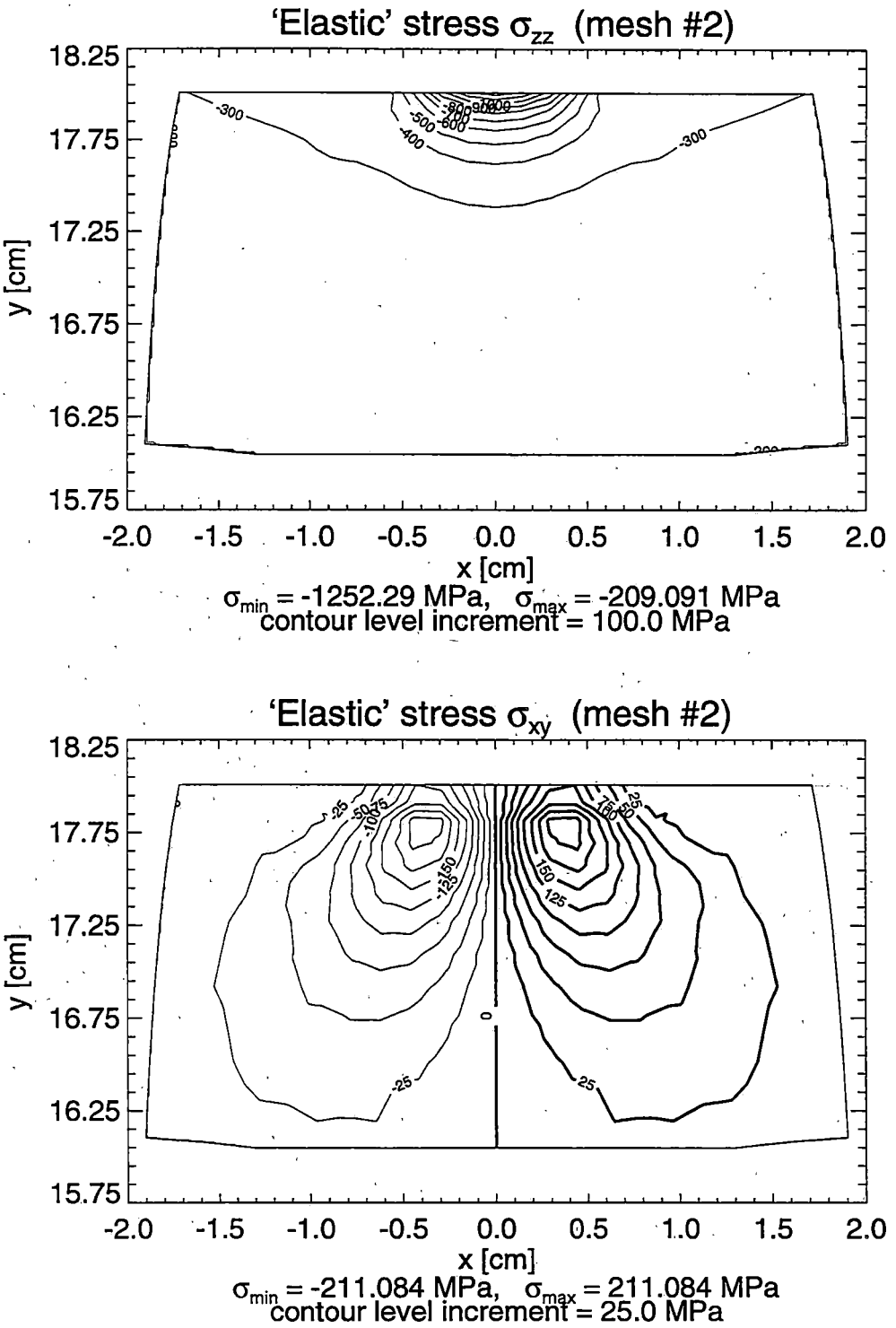

Figure 2.35 Contour Lines of Normal σ_{zz} and Shear σ_{xy} 'Elastic' Stresses in the Railroad Rail under Vertical Loading – Solution for Mesh #2

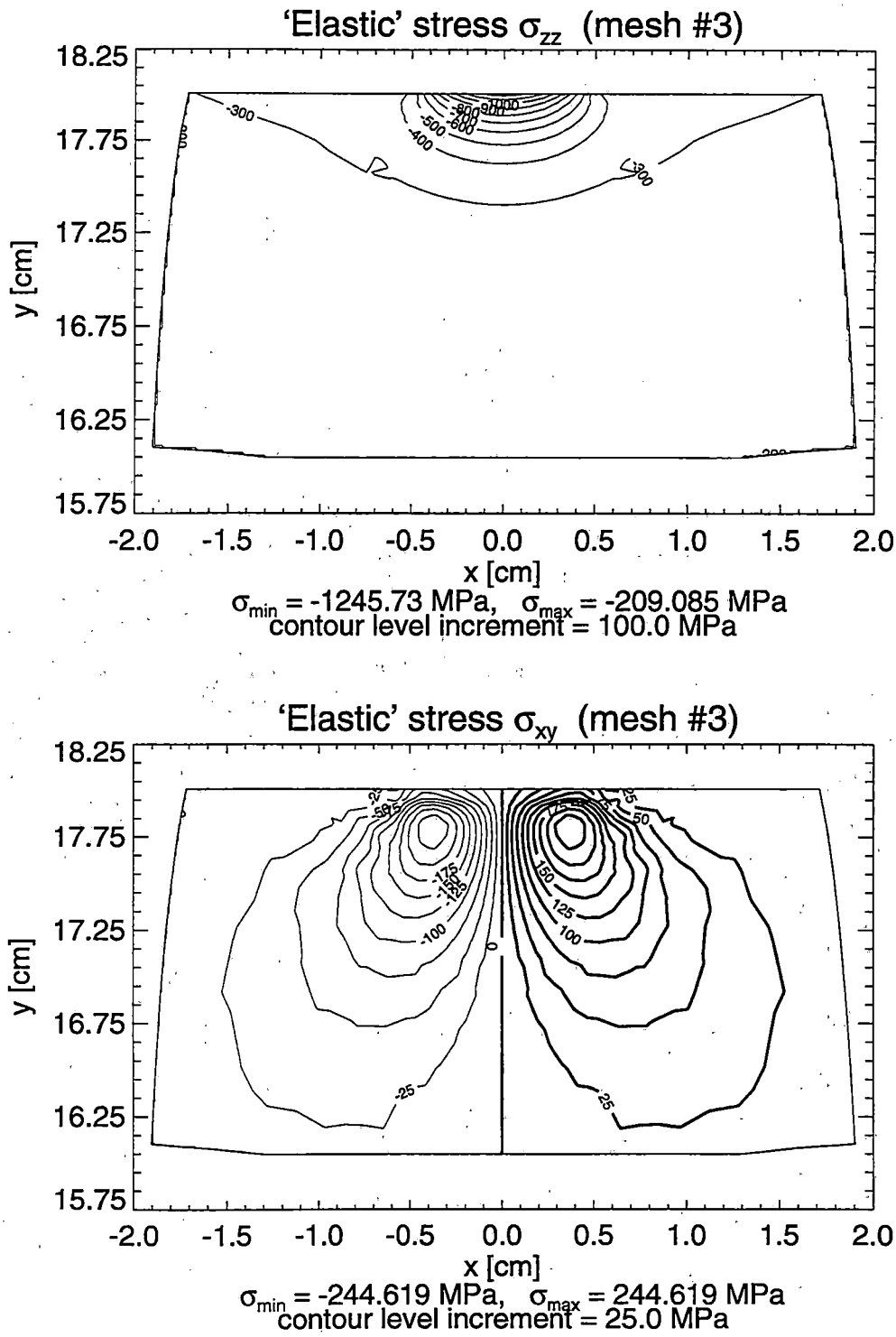

Figure 2.36 Contour Lines of Normal σ_{zz} and Shear σ_{xy} 'Elastic' Stresses in the Railroad Rail under Vertical Loading – Solution for Mesh #3

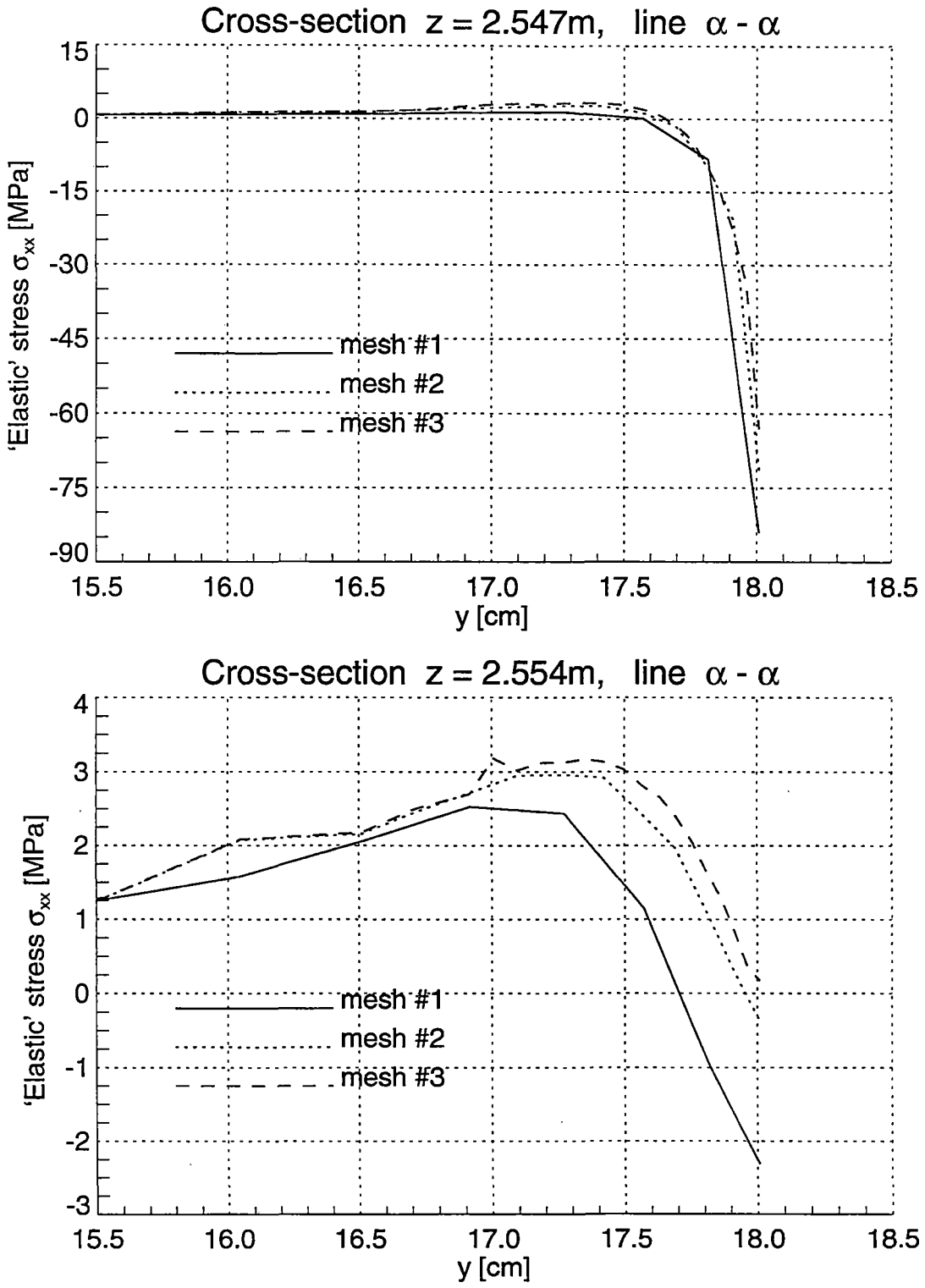

Figure 2.37 Normal 'Elastic' Stresses σ_{xx} in the Railroad Rail under Horizontal Loading

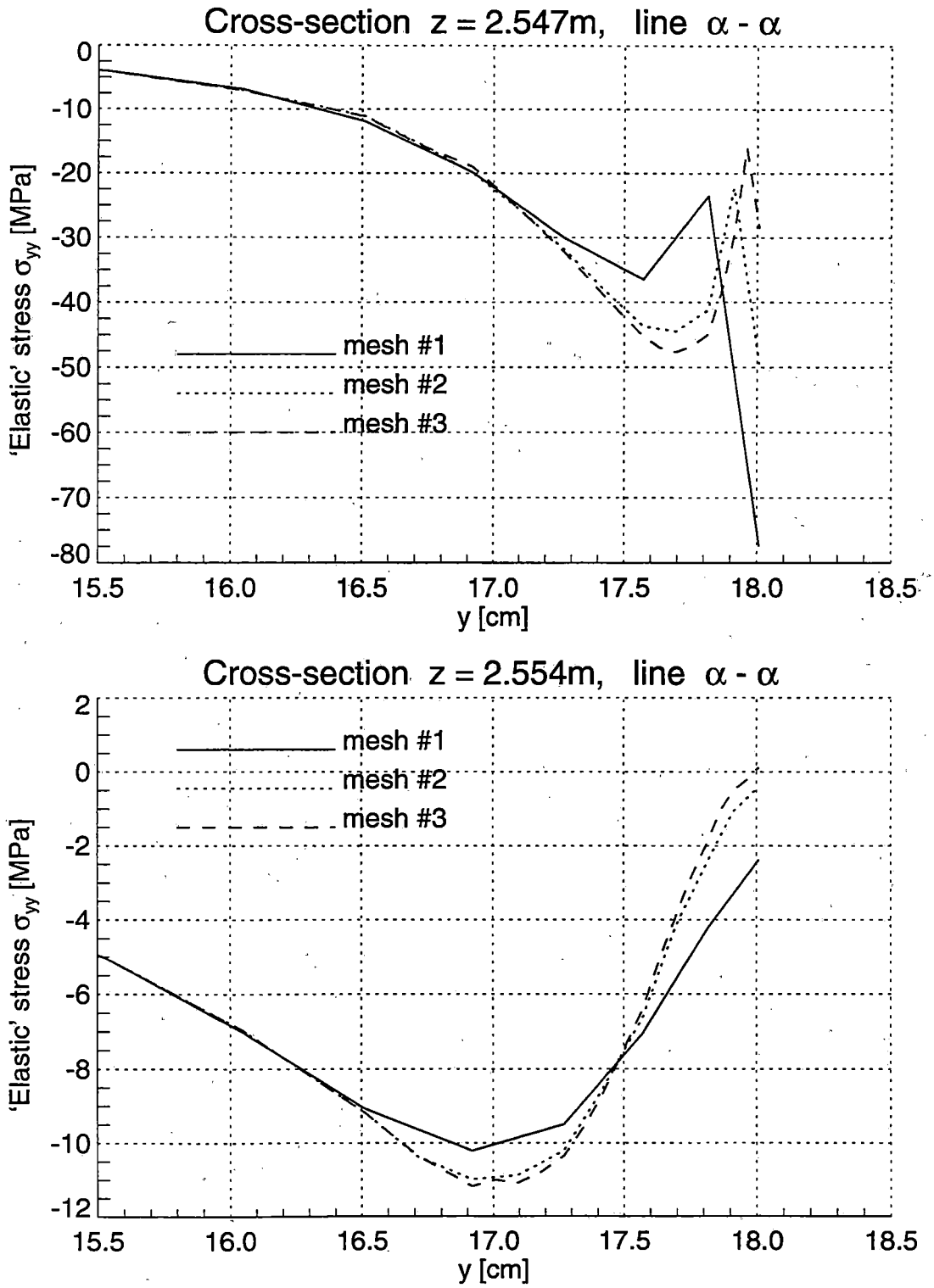

Figure 2.38 Normal 'Elastic' Stresses σ_{yy} in the Railroad Rail under Horizontal Loading

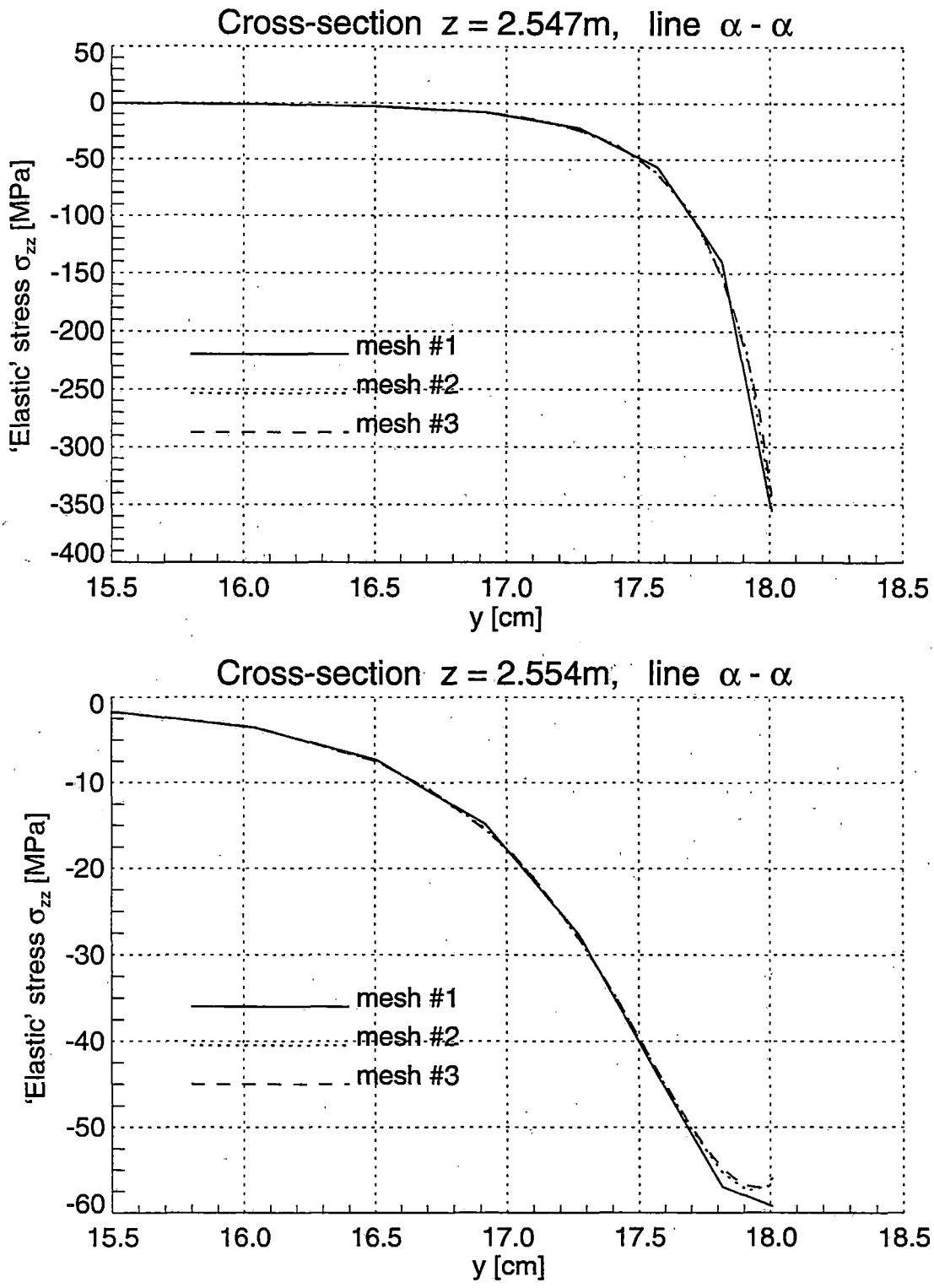

Figure 2.39 Normal 'Elastic' Stresses σ_{zz} in the Railroad Rail under Horizontal Loading

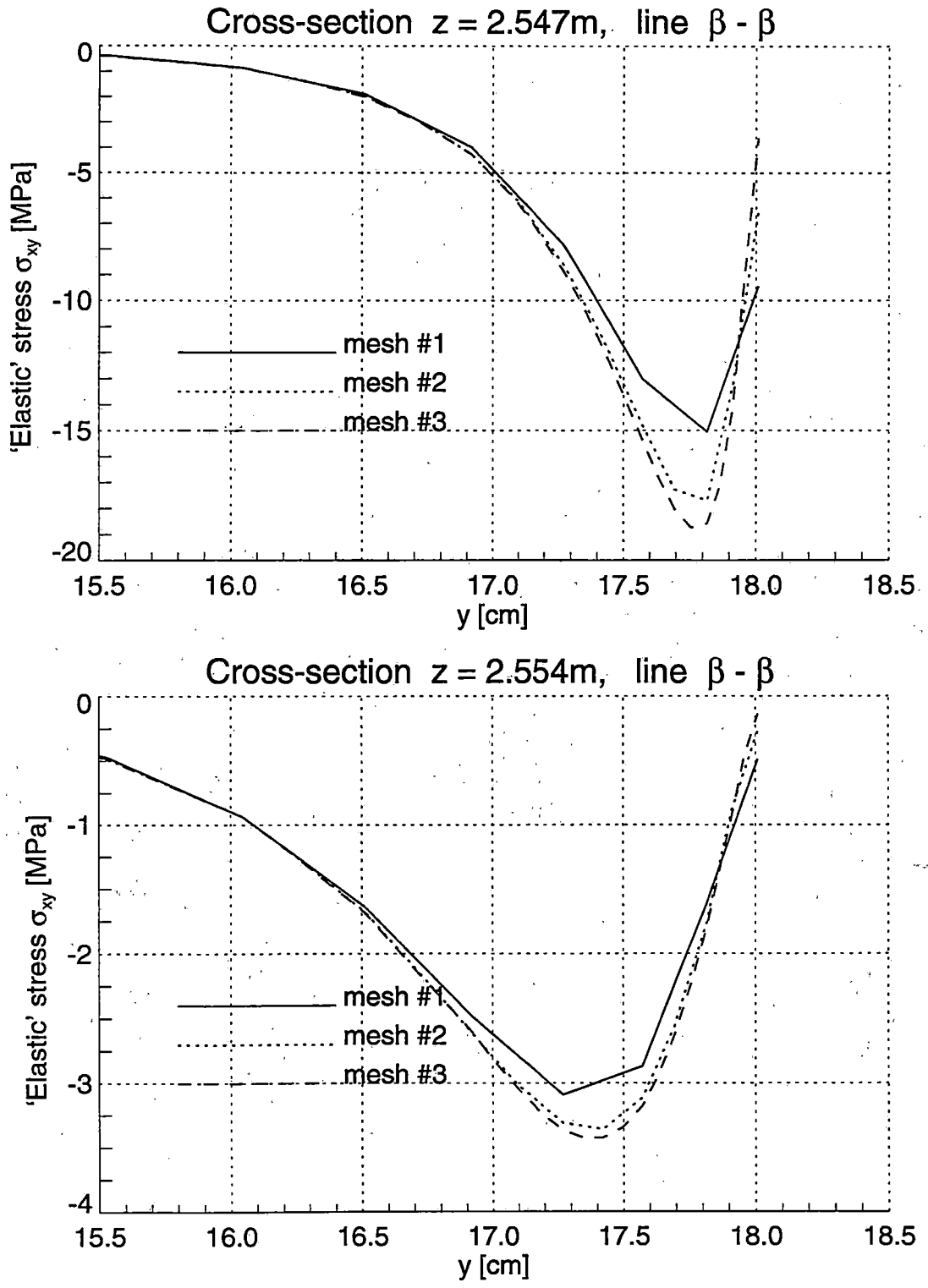

Figure 2.40 Shear 'Elastic' Stresses σ_{xy} in the Railroad Rail under Horizontal Loading

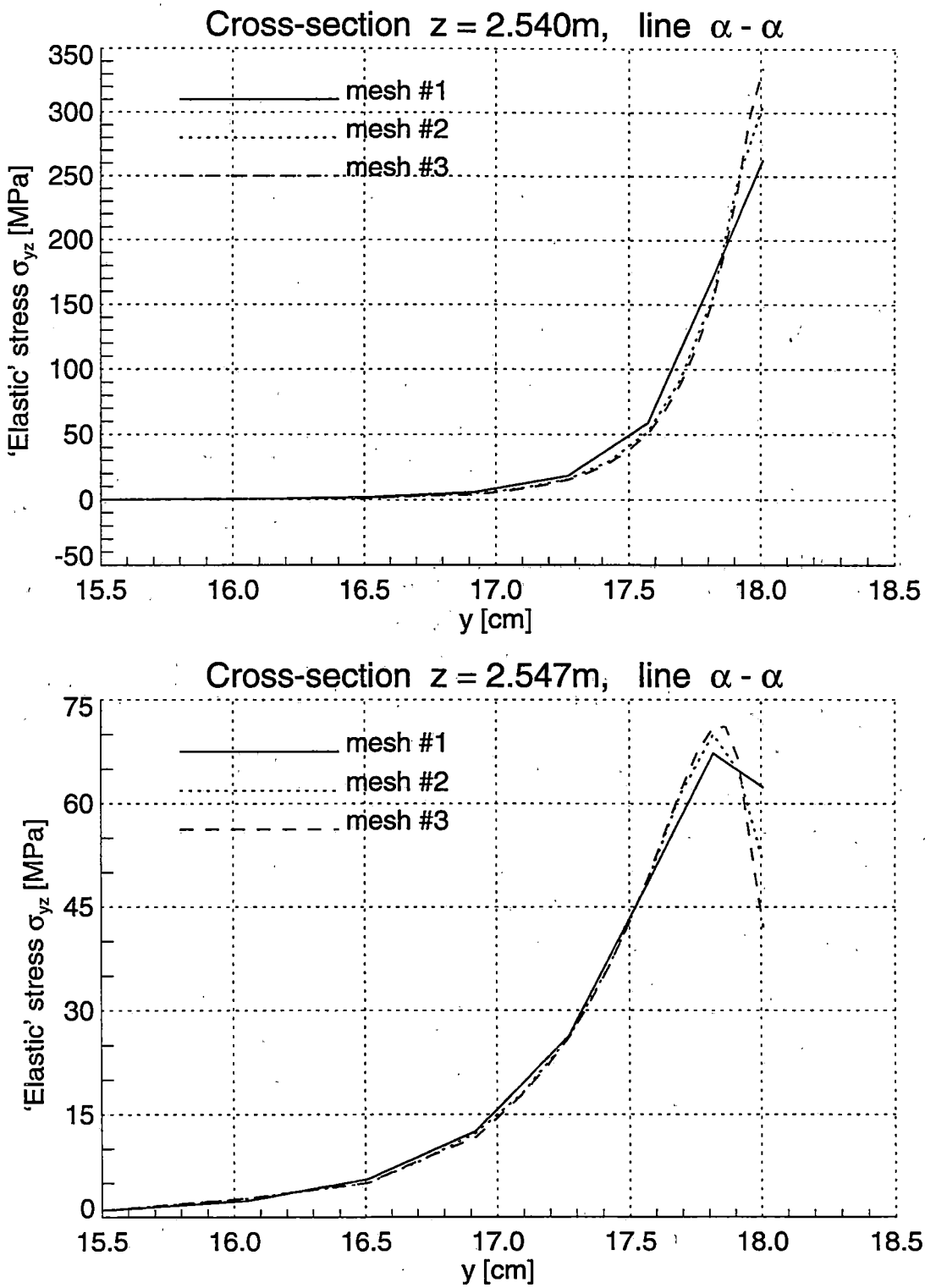

Figure 2.41 Shear 'Elastic' Stresses σ_{yz} in the Railroad Rail under Horizontal Loading

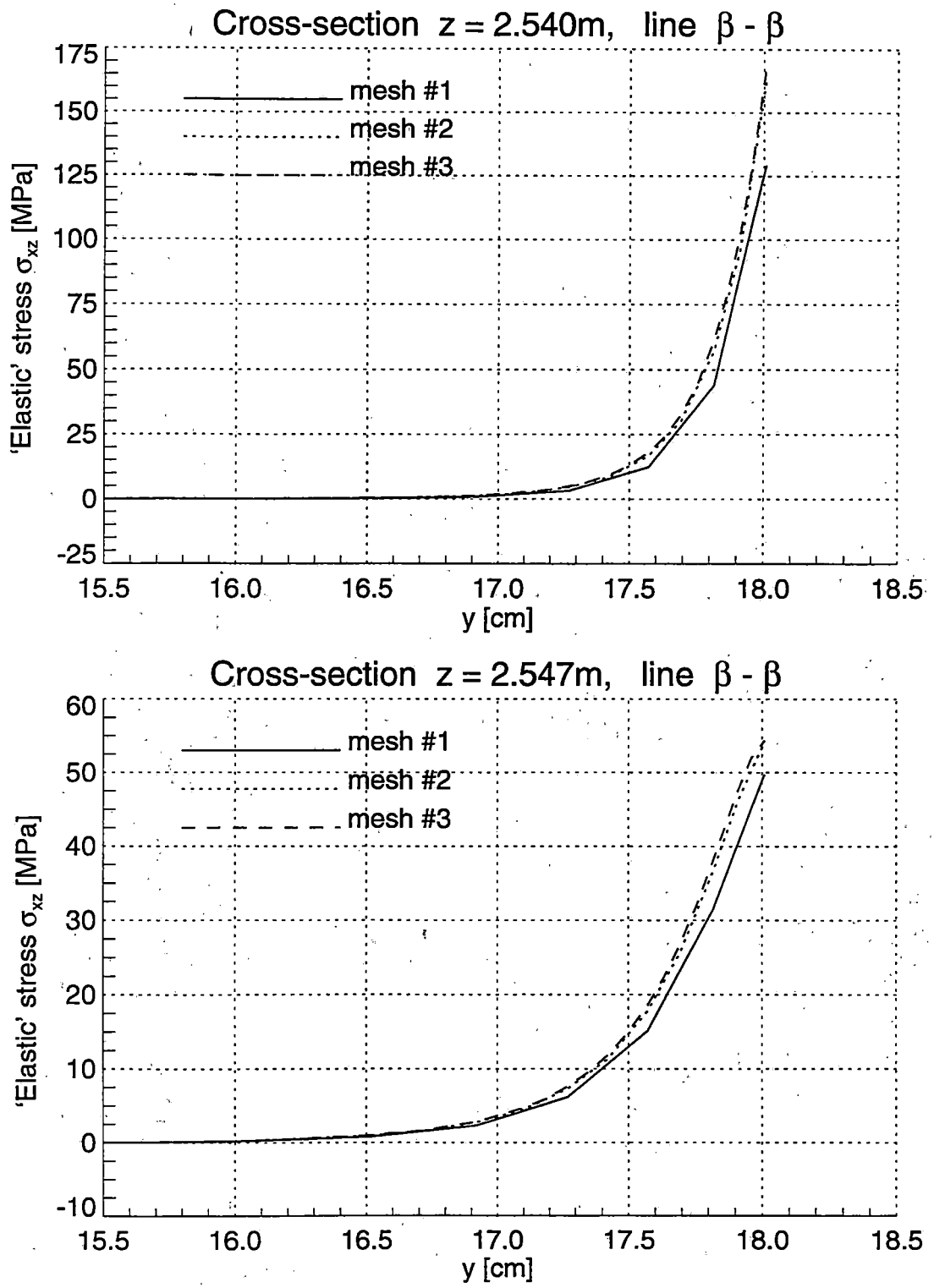

Figure 2.42 Shear 'Elastic' Stresses σ_{xz} in the Railroad Rail under Horizontal Loading

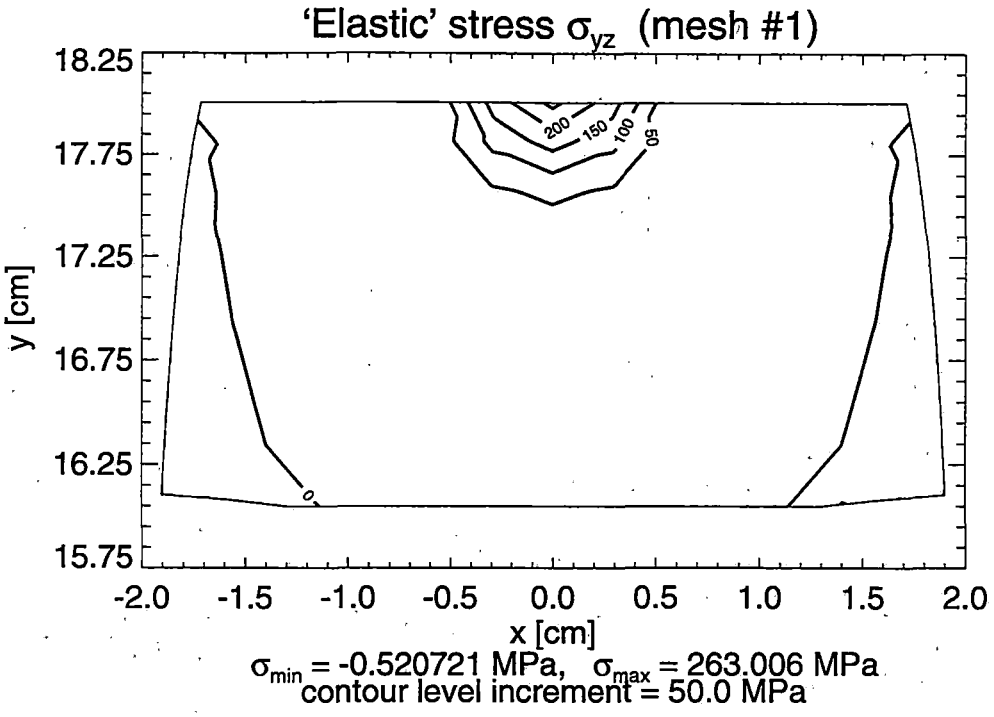

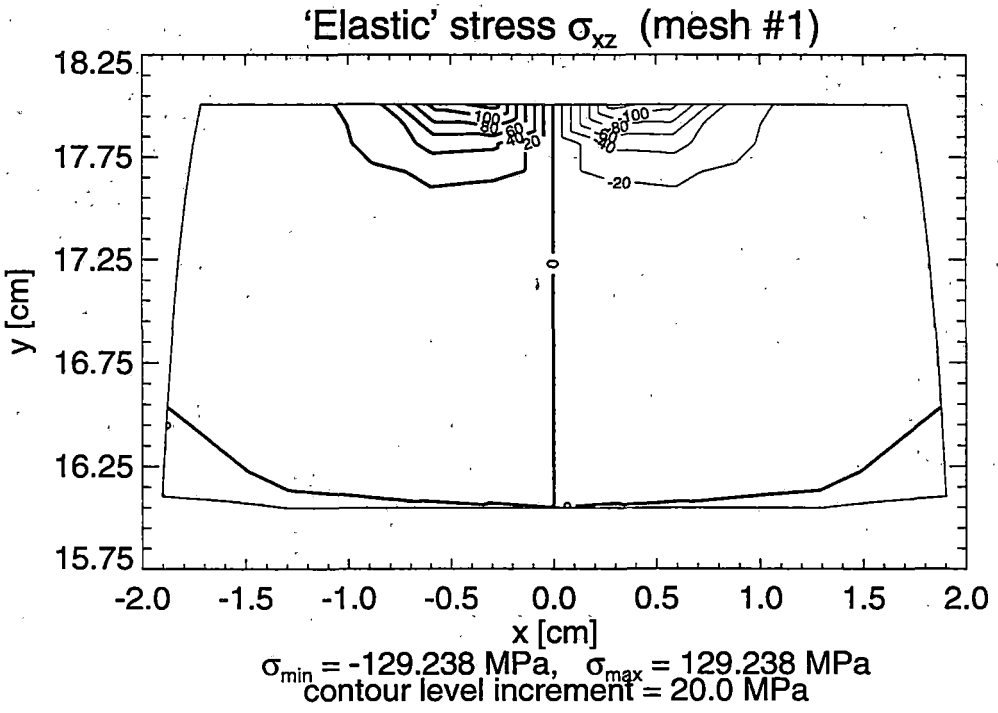

Figure 2.43 Contour Lines of Shear 'Elastic' Stresses σ_{yz} and σ_{xz} in the Railroad Rail under Horizontal Loading – Solution for Mesh #1

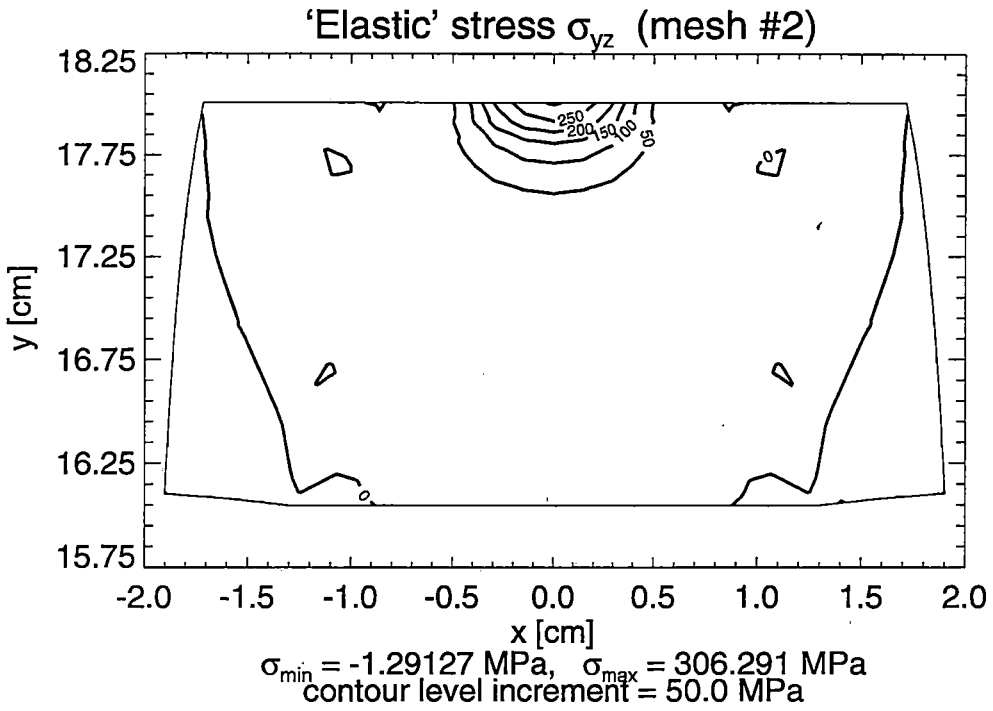

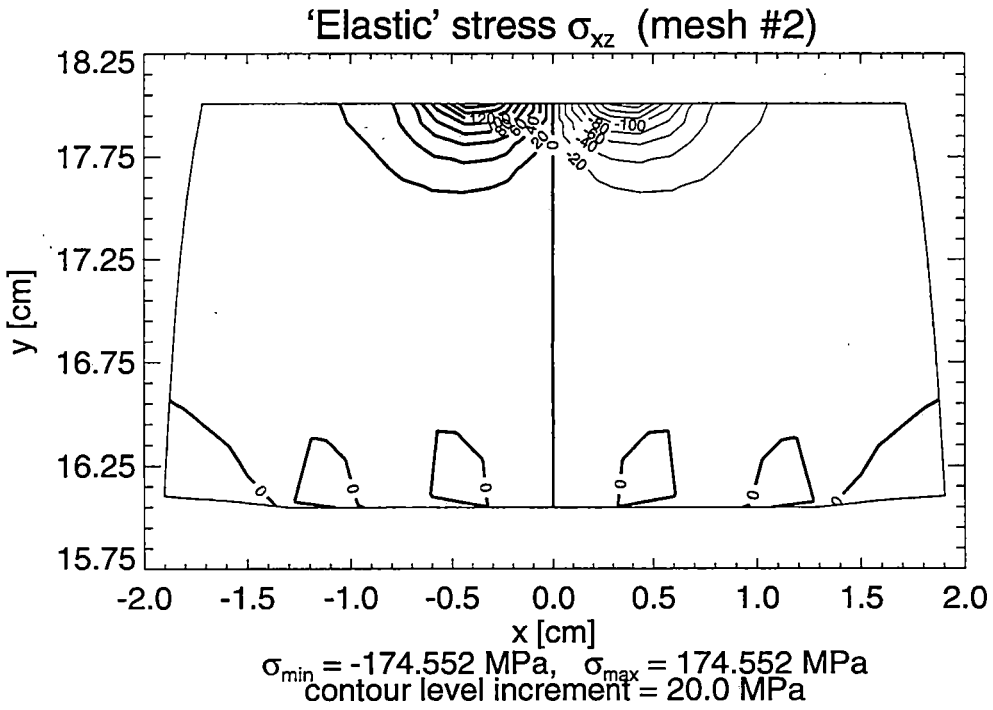

Figure 2.44 Contour Lines of Shear 'Elastic' Stresses σ_{yz} and σ_{xz} in the Railroad Rail under Horizontal Loading Solution for Mesh #2

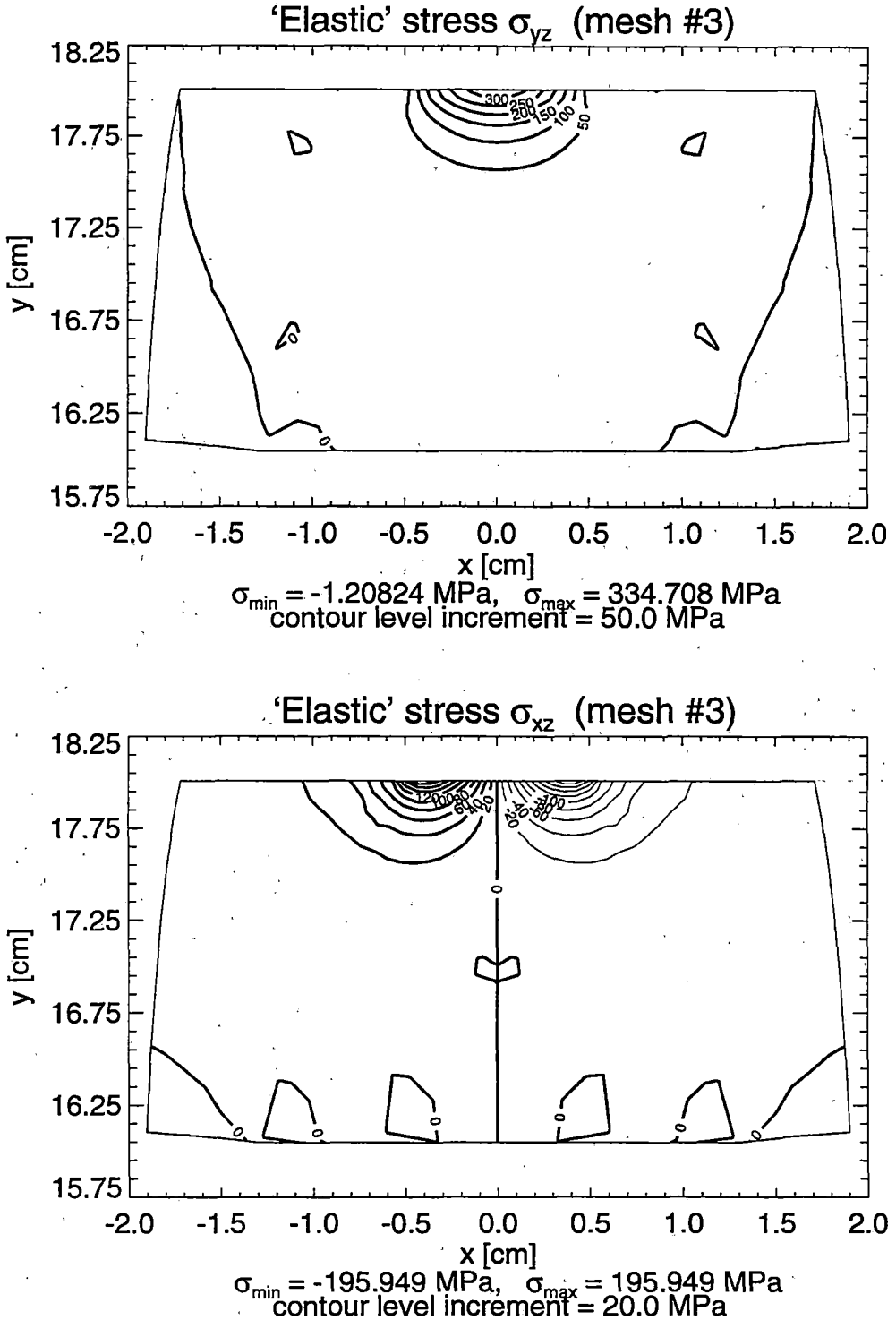

Figure 2.45 Contour Lines of Shear 'Elastic' Stresses σ_{yz} and σ_{xz} in the Railroad Rail under Horizontal Loading Solution for Mesh #3

3. MODEL FOR ANALYSIS OF RESIDUAL STRESSES

This chapter covers all the matters associated with the modification of the existing [17] elastic-plastic model and corresponding computer programs for the analysis of residual stresses in railroad rails. Section 3.1 contains some introductory remarks dealing with possible approaches to residual stress analysis. Sections 3.2 and 3.3 describe the mechanical and numerical models, respectively. The above models have been implemented in a package of computer programs described in section 3.4. Finally, the modified model and computer programs have been extensively validated by means of test problems formulated for a railroad rail subject to contact loading. Some selected results of these tests and their discussion are presented in section 3.5.

3.1 INTRODUCTION

The subject of this chapter is analysis of residual stresses in a selected class of prismatic bodies made of an elastic-perfectly plastic material and subject to both mechanical and thermal cyclic loads. The purpose of the work is to improve the existing model and computer programs for analysis of residual stresses in railroad rails working in service conditions.

In general, there are two methods for analysis of residual stresses in a body under a cyclic load. The first one is the classical incremental analysis [10], [11], oriented towards tracing the full process of loading of the body. It permits the determination of the behavior of the body at each moment of the loading process and the information obtained this way is complete, i.e., both the statical and kinematical quantities are known. The main disadvantage of the incremental analysis is the fact that in case of cyclic loads it is extremely time-consuming. An attempt to trace only one cycle of loading for a real railroad rail would probably require hundreds or thousands of increments. The number of cycles that should be taken into account to reach a state of shakedown may also be quite large. Moreover, the service load-time history required as input data is not known, so, such an analysis should be performed several times assuming the most representative loading paths. Finally, the dimension of a problem that is solved using incremental analysis is determined by the total number of stress or strain states and for a railroad rail must be at least equal to three. Thus, practical applications of this approach to the problem under consideration seem to be out of the question unless very powerful computer equipment is available.

The second method of analysis of residual stresses is the shakedown analysis. It allows one to determine whether the body under consideration is able to adapt to current cyclic loads. If the body shakes down, some additional information of either stress or displacement type may be obtained depending on the method used (either the classical statical Melan theorem or the kinematical Koiter theorem [13]). The main advantage of this approach is the fact that only the final state of the body after adaptation is considered without tracing the whole service load-time history. The analysis requires only the enveloping load states to be known and they can usually be found quite easily. Moreover, the dimension of a problem that is solved using shakedown analysis is determined by the number of residual stress or strain states. For railroad rails, these states can be assumed to be two-dimensional, simplifying the analysis significantly. The main disadvantage of this approach in the classical sense is the fact that only some selected

information may be obtained, and it corresponds to the maximal magnitude of the load for which shakedown is possible.

A novel approach to the problem of evaluation of residual stresses, the constrained energy minimization method [2], [14], [16], has been applied in this work. In contrast to the classical shakedown analysis, it allows one to compute residual stresses not only for the load of maximal magnitude but also for a load of any magnitude for which shakedown is possible (the so-called actual stresses). This approach has been successfully applied to the evaluation of residual stresses in railroad rails [4], [17], [18], and wheels (report 7). It has proven to be powerful and reliable and gives esimates of rail residual stress fields that seem to be in reasonable agreement with available experimental measurements. In this work, significant changes have been made regarding the types of loads. They can be divided into two groups. The first one deals with traction loads. In the rail analyses to date, only normal tractions due to wheel/rail contact have been modelled because this appears to be a reasonable approximation for the unpowered wheels of freight cars, which constitute the major source of rail mechanical loading. In this case, some residual stress tensor components can be assumed to be equal to zero. Additionally, external loads can be represented by only one enveloping elastic stress state that corresponds to the cross section containing the center of the contact zone. However, in some cases such simplifying assumptions seem to be unjustified and not only normal but also tangent surface tractions should be taken into consideration. Consequently, all the residual stress tensor components have to be included in the analysis, and several enveloping elastic stress states should be considered to represent external loads properly (the selection of one enveloping stress state is straightforward only in case of normal loads). The above issues have been taken into account while formulating a new finite element and expanding the constraint flow logic in the computer programs (many enveloping stress states can be defined). The second group of modifications is connected with thermal loads. These loads are usually accompanied by substantial variations in material properties, requiring the application of an appropriate algorithm for the evaluation of residual stresses. Such an algorithm has been proposed in [4] and implemented in the computer programs described in section 3.4.

3.2 MECHANICAL MODEL

The mechanical model applied to the analysis of residual stresses in railroad rails is based on the classical Melan theorem and the Haar-Karman principle [13]. It has been formulated for an elastic-perfectly plastic body that is subject to cyclic loading

– body forces

$$\overline{F}_i(\mathbf{x},t)=\overline{F}_i(\mathbf{x},t+nt_c) \qquad \text{in } V,$$

– surface tractions

$$\overline{T}_i(\mathbf{x},t)=\overline{T}_i(\mathbf{x},t+nt_c) \qquad \text{on } \partial V_\sigma, \tag{3.1}$$

– and displacements

$$\overline{u}_i(\mathbf{x},t)=\overline{u}_i(\mathbf{x},t+nt_c) \qquad \text{in } \partial V_u,$$

where V is the volume occupied by the body, ∂V_σ and ∂V_u are parts of the boundary surface ∂V, $\mathbf{x}$ represents a point of the body, t the time, t_c the period of one cycle, n the number of cycles, and $i = 1, 2, 3$.

The evaluation of residual stresses takes the form of the following optimization problem:

Find the minimum of the total complementary energy functional

$$\Pi_C = \int_V \frac{1}{2}\left(\sigma_{ij}^r - \sigma_{ij}^{R_0}\right) C_{ijkl} \left(\sigma_{kl}^r - \sigma_{kl}^{R_0}\right) dV \tag{3.2}$$

with respect to the residual stress field $\sigma_{ij}^r(\mathbf{x})$ *satisying*

– the equilibrium equations

$$\sigma_{ij,j}^r = 0 \qquad in\, V, \tag{3.3}$$

– the statical boundary conditions

$$v_j \sigma_{ij}^r = 0 \qquad on\, \partial V_\sigma, \tag{3.4}$$

– and the yield conditions

$$\Phi\left(\sigma_{ij}^r + \sigma_{ij}^E\right) \le 0 \qquad in\, V \cup \partial V, \tag{3.5}$$

where $\sigma_{ij}^{R_0} = \sigma_{ij}^{R_0}(\mathbf{x})$ is an initial residual stress field, $\sigma_{ij}^E = \sigma_{ij}^E(\mathbf{x}, t)$ is an elastic stress field, $\Phi\left(\sigma_{ij}\right)$ is a function that represents the yield conditions, v_j is a unit normal vector to the surface ∂V_σ, and C_{ijkl} is the tensor of elastic compliances.

The solution σ_{ij}^r obtained this way is either the exact solution σ_{ij}^R or an upper bound in sense of the total complementary energy of the body, i.e.,

$$\Pi_C\left(\sigma_{ij}^R - \sigma_{ij}^{R_0}\right) \le \Pi_C\left(\sigma_{ij}^r - \sigma_{ij}^{R_0}\right). \tag{3.6}$$

In this work, the above mechanical model has been applied to a selected class of prismatic bodies made of an elastic-perfectly plastic material with temperature-dependent properties. It has been assumed that the residual stress state does not depend on the longitudinal direction. Consequently, the problem may be considered as a two-dimensional one. However, the total stress state is still three-dimensional and the yield conditions should be imposed on enveloping stress states that correspond to different cross sections. The number of such states depends on the type of loading applied to the body and cannot usually be determined in advance.

The elastic stress field $\sigma_{ij}^E(\mathbf{x}, t)$ is the solution to the given boundary value problem under the assumptions of the linear theory of elasticity. It represents both the stresses due to rail-wheel

contact and the stresses associated with thermal effects. The latter stresses are accompanied by substantial variation in material properties, and the optimization problem (3.2–3.5) has to be replaced by a sequence of subproblems corresponding to subsequent time parameter values $t = t_0, t_1, \ldots, t_k$. The ith subproblem is solved by applying the relevant thermal stresses and material properties and assuming that there exist initial residual stresses equal to the residual stresses obtained in the $(i-1)$th step, i.e., $\sigma_{ij}^{R_0}(t_i) = \sigma_{ij}^{r}(t_{i-1})$.

3.3 NUMERICAL MODEL

This section describes the numerical model applied to the analysis of residual stresses in railroad rails. It has been divided into two parts. The first one presents the general formulation of the model, its concepts, and notation. The second part deals with a detailed description of the finite element that has been implemented in the computer programs developed for the problem under consideration.

3.3.1 Finite-Element Formulation

The numerical model applied to the analysis of residual stresses has been derived from the mechanical model presented in the previous section using the assumed stress model of the finite element method [9]. The region of the body V is divided into a finite number N_e of disjoint subregions V_n (finite elements). For each finite element, the following fields are assumed:

(1) a self-equilibrated residual stress field σ_{ij}^{r},

(2) a displacement field u_i that has to be continuous along the common boundary of two adjacent elements, and

(3) the corresponding strain field ε_{ij} related to the displacement field u_i by (2.4).

The stress field approximation in the assumed stress model is discontinuous along the interelement boundaries. In general, this is allowed in solid continuum mechanics provided that the corresponding surface tractions are in equilibrium. To satisfy this requirement, the total complementary energy functional (3.2) has to be modified by an additional term with the strain field playing the role of Lagrange multipliers. Taking into account the division of the region into finite elements, the mechanical model (3.2–3.5) may be written as follows:

Find the minimum of the total complementary energy functional

$$\Pi_C = \sum_{n=1}^{N_e} \left(\int_{V_n} \frac{1}{2} \overline{\sigma}_{ij} C_{ijkl} \overline{\sigma}_{kl} \, dV - \int_{V_n} \overline{\sigma}_{ij} \varepsilon_{ij} \, dV \right) \tag{3.7}$$

with respect to the self-equilibrated residual stress field $\sigma_{ij}^{r}(\mathbf{x})$ *satisfying the yield conditions*

$$\Phi\left(\overline{\sigma}_{ij}+\sigma_{ij}^{R_0}+\sigma_{ij}^{E}\right)\le 0 \qquad in\ V_n\cup(\partial V)_n, \tag{3.8}$$

where

$$\overline{\sigma}_{ij}=\sigma_{ij}^{r}-\sigma_{ij}^{R_0}. \tag{3.9}$$

It should be stressed that the statical boundary conditions (3.4) are satisfied automatically when the modified form (3.7) of the total complementary energy functional is used.

For each finite element, the stresses $\overline{\sigma}_{ij}$ and the displacements u_i are represented (using matrix notation) as follows

$$\overline{\boldsymbol{\sigma}}=\mathbf{Q}\boldsymbol{\beta}_n, \tag{3.10}$$

$$\mathbf{u}=\mathbf{N}\mathbf{q}_n \tag{3.11}$$

where $\mathbf{Q}$ is a stress interpolation matrix, $\boldsymbol{\beta}_n$ is a vector of stress parameters, $\mathbf{N}$ is a displacement interpolation matrix, and $\mathbf{q}_n$ is a vector of generalized displacements defined at a finite number of nodal points of the element. The corresponding strains $\boldsymbol{\varepsilon}$, related to the displacements $\mathbf{u}$ by (2.4), can also be expressed in terms of the generalized displacements $\mathbf{q}_n$, that is

$$\boldsymbol{\varepsilon}=\mathbf{L}\mathbf{u}=\mathbf{L}\mathbf{N}\mathbf{q}_n=\mathbf{B}\mathbf{q}_n \tag{3.12}$$

where $\mathbf{L}$ is the matrix of differential operators and $\mathbf{B}$ is a strain interpolation matrix.

The substitution of (3.10) and (3.12) into (3.7) and (3.8) results in the following numerical model for the evaluation of residual stresses:

Find the minimum of the total complementary energy functional

$$\Pi_C=\sum_{n=1}^{N_e}\left(\frac{1}{2}\boldsymbol{\beta}_n^T\mathbf{H}_n\boldsymbol{\beta}_n-\boldsymbol{\beta}_n^T\mathbf{G}_n\mathbf{q}_n\right) \tag{3.13}$$

with respect to the generalized displacements $\mathbf{q}_n$ *and the stress parameters* $\boldsymbol{\beta}_n$ *satisfying the yield conditions*

$$\frac{1}{2}\boldsymbol{\beta}_n^T\mathbf{Y}_{1n}\boldsymbol{\beta}_n+\boldsymbol{\beta}_n^T\mathbf{Y}_{2n}+Y_{3n}\le 0 \qquad in\ V_n\cup(\partial V)_n, \tag{3.14}$$

in which

$$\mathbf{H}_n=\int_{V_n}\mathbf{Q}^T\mathbf{C}\mathbf{Q}\,dV, \tag{3.15}$$

$$\mathbf{G}_n = \int_{V_n} \mathbf{Q}^T \mathbf{B}\, dV, \tag{3.16}$$

$$\mathbf{Y}_{1n} = \frac{3E}{1+\nu} \mathbf{Q}^T \mathbf{C}_d \mathbf{Q}, \tag{3.17}$$

$$\mathbf{Y}_{2n} = \frac{3E}{1+\nu} \mathbf{Q}^T \mathbf{C}_d \left(\sigma^{R_0} + \sigma^E\right), \tag{3.18}$$

$$Y_{3n} = \frac{3E}{2(1+\nu)} \left(\sigma^{R_0} + \sigma^E\right)^T \mathbf{C}_d \left(\sigma^{R_0} + \sigma^E\right) - \sigma_0^2, \tag{3.19}$$

where E is Young's modulus, ν is Poisson's ratio, $\mathbf{C}_d$ is the deviatoric part of the matrix of elastic compliances, and σ_0 is a flow stress, usually assumed to be 5 or 10% above the specified average 0.2% offset yield strength. The forms of the yield conditions (3.14) and matrices (3.17–3.19) have been derived assuming the Mises-Hencky yield criterion.

The above description of the numerical model applied to the analysis of residual stresses is very concise. Its goal was to present the basics of the model, particularly the notation that is necessary to understand the detailed information about the finite element used in case of railroad rails. For more extensive description of the model and the techniques that are used in real implementations, the reader is referred to [16], [18].

3.3.2 Quadrilateral Finite Element

The finite element applied to the analysis of residual stresses in railroad rails is a four-node element with linear approximation of the stress field and bilinear approximation of the displacement field. In the present case, all elements are described in the global system of rectangular cartesian coordinates (x, y) defined on a selected cross section. In general, they are irregular quadrilateral elements (figure 2.1a) and that is why it is usually convenient first to transform them into squares (figure 2.1b) and then to construct the interpolation functions and basic finite element matrices only for one typical element defined in the local system of rectangular cartesian coordinates (ξ, η). The transformation and the relations between integration and differentiation in both the systems of coordinates are described in section 2.3.3.

The vector of stresses $\overline{\sigma}$, the vector of stress parameters β_n, and the stress interpolation matrix $\mathbf{Q}$ defined in (3.10) can be written in the global system of rectangular cartesian coordinates as follows:

$$\overline{\sigma}^T = \left\{\sigma_{xx} \quad \sigma_{yy} \quad \sigma_{zz} \quad \tau_{xy} \quad \tau_{yz} \quad \tau_{xz}\right\}, \tag{3.20}$$

$$\beta_n^T = \left\{\beta_1 \quad \ldots \quad \beta_{15}\right\}, \tag{3.21}$$

$$\mathbf{Q} = [\mathbf{Q}_1 \quad \mathbf{Q}_2] \tag{3.22}$$

in which

$$\mathbf{Q}_1 = \begin{bmatrix} 1 & x & y & 0 & 0 & 0 & 0 & 0 & 0 & 0 \\ 0 & 0 & 0 & 1 & x & y & 0 & 0 & 0 & 0 \\ 0 & 0 & 0 & 0 & 0 & 0 & 1 & x & y & 0 \\ 0 & -y & 0 & 0 & 0 & -x & 0 & 0 & 0 & 1 \\ 0 & 0 & 0 & 0 & 0 & 0 & 0 & 0 & 0 & 0 \\ 0 & 0 & 0 & 0 & 0 & 0 & 0 & 0 & 0 & 0 \end{bmatrix}, \tag{3.23}$$

$$\mathbf{Q}_2 = \begin{bmatrix} 0 & 0 & 0 & 0 & 0 \\ 0 & 0 & 0 & 0 & 0 \\ 0 & 0 & 0 & 0 & 0 \\ 0 & 0 & 0 & 0 & 0 \\ 1 & x & y & 0 & 0 \\ 0 & 0 & -x & 1 & y \end{bmatrix}, \tag{3.24}$$

where the matrix $\mathbf{Q}$ has been derived assuming the linear approximation of the stress tensor components and then satisfying the equilibrium equations. Additionally, it has been divided into submatrices $\mathbf{Q}_1$ and $\mathbf{Q}_2$ to simplify the derivation of the matrix $\mathbf{H}_n$.

Before the matrix $\mathbf{H}_n$, defined in (3.15), is derived, it is convenient to divide it into two parts that correspond to the deviatoric $\mathbf{C}_d$ and volumetric $\mathbf{C}_v$ parts of the matrix of elastic compliances $\mathbf{C}$, that is

$$\mathbf{H}_n = \mathbf{H}_{dn} + \mathbf{H}_{vn} \tag{3.25}$$

in which

$$\mathbf{H}_{dn} = \int_{V_n} \mathbf{Q}^T \mathbf{C}_d \mathbf{Q} \, dV, \tag{3.26}$$

$$\mathbf{H}_{vn} = \int_{V_n} \mathbf{Q}^T \mathbf{C}_v \mathbf{Q} \, dV, \tag{3.27}$$

where

$$\mathbf{C}_d = \frac{1+\nu}{3E}\begin{bmatrix} 2 & -1 & -1 & 0 & 0 & 0 \\ & 2 & -1 & 0 & 0 & 0 \\ & & 2 & 0 & 0 & 0 \\ & & & 6 & 0 & 0 \\ & \text{sym} & & & 6 & 0 \\ & & & & & 6 \end{bmatrix}, \tag{3.28}$$

$$\mathbf{C}_\nu = \frac{1-2\nu}{3E}\begin{bmatrix} 1 & 1 & 1 & 0 & 0 & 0 \\ & 1 & 1 & 0 & 0 & 0 \\ & & 1 & 0 & 0 & 0 \\ & & & 0 & 0 & 0 \\ & \text{sym} & & & 0 & 0 \\ & & & & & 0 \end{bmatrix}. \tag{3.29}$$

The substitution of (3.22–3.24), (3.28), and (3.29) into (3.26) and (3.27) results in the following form of both the integrands:

$$\mathbf{Q}^T\mathbf{C}_d\mathbf{Q} = \begin{bmatrix} \mathbf{Q}_1^T \\ \mathbf{Q}_2^T \end{bmatrix}\mathbf{C}_d\begin{bmatrix} \mathbf{Q}_1 & \mathbf{Q}_2 \end{bmatrix} = \begin{bmatrix} \mathbf{Q}_1^T\mathbf{C}_d\mathbf{Q}_1 & 0 \\ 0 & \mathbf{Q}_2^T\mathbf{C}_d\mathbf{Q}_2 \end{bmatrix}, \tag{3.30}$$

$$\mathbf{Q}^T\mathbf{C}_\nu\mathbf{Q} = \begin{bmatrix} \mathbf{Q}_1^T \\ \mathbf{Q}_2^T \end{bmatrix}\mathbf{C}_\nu\begin{bmatrix} \mathbf{Q}_1 & \mathbf{Q}_2 \end{bmatrix} = \begin{bmatrix} \mathbf{Q}_1^T\mathbf{C}_\nu\mathbf{Q}_1 & 0 \\ 0 & 0 \end{bmatrix} \tag{3.31}$$

where

$$\mathbf{Q}_1^T\mathbf{C}_d\mathbf{Q}_1 = \frac{1+\nu}{3E}\times$$

$$\begin{bmatrix} 2 & 2x & 2y & -1 & -x & -y & -1 & -x & -y & 0 \\ & 2x^2+6y^2 & 2xy & -x & -x^2 & 5xy & -x & -x^2 & -xy & -6y \\ & & 2y^2 & -y & -xy & -y^2 & -y & -xy & -y^2 & 0 \\ & & & 2 & 2x & 2y & -1 & -x & -y & 0 \\ & & & & 2x^2 & 2xy & -x & -x^2 & -xy & 0 \\ & & & & & 2y^2+6x^2 & -y & -xy & -y^2 & -6x \\ & & & & & & 2 & 2x & 2y & 0 \\ & & & & & & & 2x^2 & 2xy & 0 \\ & \text{sym} & & & & & & & 2y^2 & 0 \\ & & & & & & & & & 6 \end{bmatrix}, \tag{3.32}$$

$$\mathbf{Q}_2^T\mathbf{C}_d\mathbf{Q}_2=\frac{1+\nu}{3E}\begin{bmatrix}6 & 6x & 6y & 0 & 0\\ & 6x^2 & 6xy & 0 & 0\\ & & 6y^2+6x^2 & -6x & -6xy\\ & \text{sym} & & 6 & 6y\\ & & & & 6y^2\end{bmatrix}, \tag{3.33}$$

$$Q_1^TC_vQ_1=\frac{1-2\nu}{3E}\begin{bmatrix}1 & x & y & 1 & x & y & 1 & x & y & 0\\ & x^2 & xy & x & x^2 & xy & x & x^2 & xy & 0\\ & & y^2 & y & xy & y^2 & y & xy & y^2 & 0\\ & & & 1 & x & y & 1 & x & y & 0\\ & & & & x^2 & xy & x & x^2 & xy & 0\\ & & & & & y^2 & y & xy & y^2 & 0\\ & & & & & & 1 & x & y & 0\\ & & & & & & & x^2 & xy & 0\\ & \text{sym} & & & & & & & y^2 & 0\\ & & & & & & & & & 0\end{bmatrix}. \tag{3.34}$$

Finally, to compute the matrices $\mathbf{H}_{dn}$ and $\mathbf{H}_{vn}$, appropriate integration should be performed. Taking into account the fact that the residual stress state does not depend on the longitudinal direction, such integration can be carried out over the area A_n of the nth element, that is

$$\int_{V_n} f(x,y)\,dV = L\int_{A_n} f(x,y)\,dx\,dy \tag{3.35}$$

where L is the length of the element (any non-zero value). Usually, it is much more convenient to use the local system of coordinates (ξ,η) instead of the global system (x,y), thus the formula (2.40) should be additionally applied.

The vector of displacements $\mathbf{u}$, the vector of generalized displacements $\mathbf{q}_n$, and the displacement interpolation matrix $\mathbf{N}$ defined in (3.11) can be written in the local system of coordinates as follows:

$$\mathbf{u}^T(\xi,\eta)=\left\{u_x(\xi,\eta)\quad u_y(\xi,\eta)\quad u_z(\xi,\eta)\right\}, \tag{3.36}$$

$$\mathbf{q}_n^T=\left\{\mathbf{q}_1^T\ \cdots\ \mathbf{q}_4^T\right\}, \tag{3.37}$$

$$\mathbf{N}(\xi,\eta)=\left[\mathbf{N}_1(\xi,\eta)\ \cdots\ \mathbf{N}_4(\xi,\eta)\right] \tag{3.38}$$

in which

$$\mathbf{q}_i^T = \{ q_{xi} \quad q_{yi} \quad q_{zi} \}, \qquad i = 1, \ldots, 4, \tag{3.39}$$

$$\mathbf{N}_i(\xi,\eta) = \begin{bmatrix} \mathbf{N}_i(\xi,\eta) & 0 & 0 \\ 0 & \mathbf{N}_i(\xi,\eta) & 0 \\ 0 & 0 & \mathbf{N}_i(\xi,\eta) \end{bmatrix}, \tag{3.40}$$

where $\mathbf{q}_i$ is the vector of generalized nodal displacements at the ith node of the element, and N_i is the shape function associated with this node, that is

$$N_i(\xi,\eta) = \frac{1}{4}(1+\xi\xi_i)(1+\eta\eta_i). \tag{3.41}$$

Further analysis requires the relation (3.12) also to be specified in the local system of coordinates. The strain vector ε and the matrix of differential operators $\mathbf{L}$ can be written as follows:

$$\varepsilon^T = \{\varepsilon_{xx} \quad \varepsilon_{yy} \quad \varepsilon_{zz} \quad \gamma_{xy} \quad \gamma_{yz} \quad \gamma_{xz}\}, \tag{3.42}$$

$$\mathbf{L} = \begin{bmatrix} \dfrac{\partial}{\partial x} & 0 & 0 \\ 0 & \dfrac{\partial}{\partial y} & 0 \\ 0 & 0 & 0 \\ \dfrac{\partial}{\partial y} & \dfrac{\partial}{\partial x} & 0 \\ 0 & 0 & \dfrac{\partial}{\partial y} \\ 0 & 0 & \dfrac{\partial}{\partial x} \end{bmatrix} \tag{3.43}$$

Before the strain interpolation matrix $\mathbf{B}$ is derived, it is convenient, as was done in (3.37) and (3.38), to divide it into submatrices that are associated with the nodal points of the element

$$\mathbf{B} = [\mathbf{B}_1 \ \ldots \ \mathbf{B}_4]. \tag{3.44}$$

The substitution of (3.44), (3.43), (3.38), and (3.40) into (3.12) results in

$$\mathbf{B}_i = \begin{bmatrix} \dfrac{\partial N_i}{\partial x} & 0 & 0 \\ 0 & \dfrac{\partial N_i}{\partial y} & 0 \\ 0 & 0 & 0 \\ \dfrac{\partial N_i}{\partial y} & \dfrac{\partial N_i}{\partial x} & 0 \\ 0 & 0 & \dfrac{\partial N_i}{\partial y} \\ 0 & 0 & \dfrac{\partial N_i}{\partial x} \end{bmatrix}. \tag{3.45}$$

Consequently, before the matrix $\mathbf{G}_n$ is computed, the integrand in (3.16) should be decomposed, which yields

$$\mathbf{Q}^T\mathbf{B} = \begin{bmatrix} \mathbf{Q}^T\mathbf{B}_1 & \cdots & \mathbf{Q}^T\mathbf{B}_4 \end{bmatrix} \tag{3.46}$$

in which

$$\mathbf{Q}^T\mathbf{B}_i = \begin{bmatrix} \frac{\partial N_i}{\partial x} & 0 & 0 \\ \frac{\partial N_i}{\partial x}x - \frac{\partial N_i}{\partial y}y & -\frac{\partial N_i}{\partial x}y & 0 \\ \frac{\partial N_i}{\partial x}y & 0 & 0 \\ 0 & \frac{\partial N_i}{\partial y} & 0 \\ 0 & \frac{\partial N_i}{\partial y}x & 0 \\ -\frac{\partial N_i}{\partial y}x & \frac{\partial N_i}{\partial y}y - \frac{\partial N_i}{\partial x}x & 0 \\ 0 & 0 & 0 \\ 0 & 0 & 0 \\ 0 & 0 & 0 \\ \frac{\partial N_i}{\partial y} & \frac{\partial N_i}{\partial x} & 0 \\ 0 & 0 & \frac{\partial N_i}{\partial y} \\ 0 & 0 & \frac{\partial N_i}{\partial y}x \\ 0 & 0 & \frac{\partial N_i}{\partial y}y - \frac{\partial N_i}{\partial x}x \\ 0 & 0 & \frac{\partial N_i}{\partial x} \\ 0 & 0 & \frac{\partial N_i}{\partial x}y \end{bmatrix} \tag{3.47}$$

The integration necessary to compute the matrix $\mathbf{G}_n$ should be carried out using the same technique as in the cases of the matrices $\mathbf{H}_{dn}$ and $\mathbf{H}_{vn}$.

With regard to the matrices (3.17–3.19), they can be computed quite easily. The form of the matrix $\mathbf{Y}_{1n}$ has already been derived and can be recognized in (3.30), (3.32), and (3.33). The substitution of (3.22–3.24) and (3.28) into (3.18) and (3.19) results in the following forms of the vector $\mathbf{Y}_{2n}$ and scalar Y_{3n}:

$$\mathbf{Y}_{2n} = \begin{Bmatrix} 2\sigma_{xx} - \sigma_{yy} - \sigma_{zz} \\ (2\sigma_{xx} - \sigma_{yy} - \sigma_{zz})x - 6\tau_{xy}y \\ (2\sigma_{xx} - \sigma_{yy} - \sigma_{zz})y \\ -(\sigma_{xx} - 2\sigma_{yy} + \sigma_{zz}) \\ -(\sigma_{xx} - 2\sigma_{yy} + \sigma_{zz})x \\ -(\sigma_{xx} - 2\sigma_{yy} + \sigma_{zz})y - 6\tau_{xy}x \\ -(\sigma_{xx} + \sigma_{yy} - 2\sigma_{zz}) \\ -(\sigma_{xx} + \sigma_{yy} - 2\sigma_{zz})x \\ -(\sigma_{xx} + \sigma_{yy} - 2\sigma_{zz})y \\ 6\tau_{xy} \\ 6\tau_{yz} \\ 6\tau_{yz}x \\ 6(\tau_{yz}y - \tau_{xz}x) \\ 6\tau_{xz} \\ 6\tau_{xz}y \end{Bmatrix} \tag{3.48}$$

$$Y_{3n} = \frac{1}{2}\left[(\sigma_{xx} - \sigma_{yy})^2 + (\sigma_{yy} - \sigma_{zz})^2 + (\sigma_{xx} - \sigma_{zz})^2 + 6(\tau_{xy}^2 + \tau_{yz}^2 + \tau_{xz}^2)\right] - \sigma_0^2 \tag{3.49}$$

where the vector σ represents the sum $\sigma^{R_0} + \sigma^E$.

3.4 COMPUTER PROGRAMS

The mechanical and numerical models described in the previous sections have been implemented in a package of computer programs. The package consists of six programs that can be divided into two groups.

The first group contains four programs called STRATEGY, STATCOND, OPTIM, and ELASTZON. These programs constitute the most important part of the package. They permit the solution of the problem of the evaluation of residual stresses not only for railroad rails but also for car wheels. Virtually any assumed stress finite element can be used. The second group consists of two auxiliary programs called MATRIX and RESIDUAL. These relatively simple programs are strictly connected with the problem to be solved (rail, wheel), with the type of finite elements (quadrilateral, triangular), and finally with the approximations of the stress and displacement fields.

The structure of the programs and the program flow logic are relatively straightforward, except that the user should be prepared to monitor the progress of the optimization and, if necessary, to adjust certain control parameters. The first program to be executed is MATRIX, which computes the finite-element matrices defined in (3.15–3.19) for given input data. Based on this

information and the current state of residual stresses, the control program STRATEGY examines the yield conditions (3.14) for all enveloping stress states and divides the whole body into two parts — elastic and plastic zones. If all the yield conditions are satisfied, the current residual stress state is the final one and the post-processing program RESIDUAL is executed. If this is not the case, a new residual stress state has to be found and the program STATCOND is called. This program allows one to formulate the optimization problem (3.13–3.14) in terms of the unknown stress parameters associated only with the plastic zone. The influence of the elastic zone on the form of the total complementary functional (3.13) is found using static condensation. The optimization problem is solved by means of the program OPTIM, using the method of feasible directions [19]. It should be stressed that OPTIM is the only program that has to be run interactively. In spite of the fact that a special procedure of automated optimization has been developed, user involvement is usually required, especially in the case of very large optimization problems. After the optimization problem has been solved and the stress parameters in the plastic zone have been found, the program ELASTZON is executed and the solution in the elastic zone is computed. The latter program terminates the basic loop in the program flow logic and STRATEGY is called again.

The input data for the programs consist of seven files of ASCII type. Four of them contain the information about the topology of the finite element mesh and material properties. They have exactly the same format as the input files used in the program RAILE described in section 2.4. The other three files contain the information about elastic, thermal, and initial residual stresses. As for the elastic stresses, the number of enveloping stress states is defined by the user and is limited only by available computer equipment. The thermal stresses have been assumed to be constant in the longitudinal direction. In fact, these stresses are elastic stresses and an additional file has been created for the user's convenience. Finally, the initial residual stresses have also been assumed to be constant in the longitudinal direction (a basic assumption in the numerical model) and self-equilibrated. It should be stressed that, if the initial residual stresses come from experimental data, the latter requirement is usually not satisfied unless the measurements are post-processed.

The output data consist of five ASCII files. Four of them contain the solution to the problem, i.e., the residual and total stresses computed at the centroids and nodes of the finite elements. The fifth file contains some information about the optimization problems, elements in the plastic zone, and active constraints (yield conditions) for all enveloping stress states.

3.5 EXAMPLE ANALYSES FOR A RAILROAD RAIL

The approach applied to the analysis of residual stresses in railroad rails and the corresponding computer programs had been verified thoroughly using various benchmark tests with both known and unknown analytical solutions. The comprehensive description of those tests and their results can be found in [4], [17], and [18]. In this work, significant changes have been made regarding the types of loads. First of all, to be able to deal with normal and tangent loads acting simultaneously, a new finite element has been formulated. In comparison to the finite elements considered previously, it contains all the residual stress tensor components. Additionally, the program flow logic has been expanded so that many enveloping stress states can be defined. The new finite element has been verified using the same tests as in [17], where a thick-walled cylinder subject to either internal pressure (normal load) or torsion (tangent load) was considered.

Unfortunately, to the authors' knowledge, there are no benchmark problems with known analytical solutions that could be used to verify the above modifications thoroughly. However, the quality of the results described below indicates that the computer programs have been modified properly. The second group of modifications is connected with thermal loads. These loads are usually accompanied by substantial changes in material properties, requiring the application of an appropriate algorithm for the evaluation of residual stresses. Such an algorithm has been proposed in [14] and verified in [15], where a railroad car wheel subject to thermal load due to stop-braking was considered. The same algorithm has been implemented in the computer programs described in the previous section. In the authors' opinion, additional tests were not necessary. Moreover, such tests would require the corresponding elastic analyses to be performed first, which could be the subject of a separate study.

The computer programs developed for the evaluation of residual stresses have been applied to estimate rail shakedown stress states in a 132 RE rail section. Two cases of loading have been considered.

In case #1, the rail was subject only to vertical surface tractions $t_Z(X,Y)$ of intensity $t_{0Z} = 1239.98$ MPa acting over a rectangular contact area of dimensions $a = 6.947$ mm and $b = 5.083$ mm, with the center C of coordinates $x = 0.0$ m and $y = 0.180086$ m and the slope $\alpha = 0^\circ$ (for the notation and conventions see section 2.4). The parameters $t_{0Z}, a,$ and b were calculated using the formulae (2.48), where the vertical force T_Z was equal to 77.84 kN, and the dimensions of the elliptical contact area, $A = 6.4$ mm and $B = 4.683$ mm, were obtained by means of the Hertz formulae assuming the following data: radius of the wheel $R_2 = 0.4064$ m, radius of the wheel profile $R_2' = \infty$, and radius of the rail profile $R_1 = 0.254$ m; the rail was assumed to be flat in the longitudinal direction, i.e., $R_1' = \infty$.

As far as the material properties are concerned, Young's modulus E, Poisson's ratio ν, and the flow stress σ_0 were assumed to be temperature-independent and equal to 206.832 GPa, 0.3, and 448.137 MPa, respectively. Additionally, the dimensions of the Hertz ellipse were calculated assuming that both the rail and the wheel were made of material with the same elastic constants.

The problem was solved using the same finite element meshes that were used in the elastic analyses presented in section 2.6. The elastic solution necessary as input data was found by means of the programs described in section 2.4. The contour line plots of elastic stresses for meshes #2 and #3 are shown in section 2.6. The analysis of residual stresses was performed assuming only one enveloping elastic stress state for the cross section that contained the center of the contact zone. In spite of the fact that such selection seemed to be straightforward, after the residual stress state had been found, the yield conditions were additionally examined for neighboring cross sections.

Some selected results for case #1 are shown in figures 3.1 through 3.6. The convergence of the solution with respect to the mesh density is presented in figures 3.1 and 3.2, where the stress tensor components are plotted along the lines $\alpha - \alpha$ and $\beta - \beta$ shown in figures 2.20

through 2.22. The contour line plots of stresses for the meshes #2 and #3 are presented in figures 3.3 through 3.6.

These results indicate that mesh #1 is definitely too coarse. Mesh #2 seems to be acceptable, and mesh #3 may be recognized as appropriate for the problem under consideration. The solutions obtained for meshes #2 and #3 are in quite good agreement. Significant differences can be observed only for normal stresses σ_{yy}, but these stresses are strongly influenced by the fact that the boundary conditions on the contact surface are satisfied in an integral sense.

In case #2, the wheel was subject to the vertical surface tractions $t_Z(X,Y)$ of intensity $t_{0Z} = 1239.98$ MPa and the horizontal surface tractions $t_X(X,Y)$ of intensity $t_{0X} = 0.3t_{0Z} = 371.994$ MPa. The other data were assumed to be exactly the same as for case #1. The elastic solution was found using the programs described in section 2.4. The contour line plots of elastic stresses for meshes #2 and #3 are presented in section 2.6.

The analysis of residual stresses was performed assuming that several enveloping stress states had to be taken into consideration. In the first step, the number of such states was assumed to be equal to 5, corresponding to the division of the contact zone into 4 sectors in the longitudinal direction. In the second step, the number of sectors was doubled, resulting in 9 enveloping stress states. The differences between the corresponding solutions were very small and further division was not considered.

The results in the form of contour line plots of residual stresses for meshes #2 and #3 are shown in figures 3.7 through 3.12. In spite of the fact that the horizontal loading constitutes only 30% of the vertical loading, it has relatively significant influence on the quality of the results, which is lower than in #1. Unfortunately, available computer equipment did not permit the solution of this problem for denser meshes. It should be stressed that the quality of the solution is influenced not only by the mesh density but also by the quality of the elastic solution, which is used as input data. Comparative tests carried out for problems with known analytical solutions indicate that even small differences in the latter solution may result in different residual stress states, and that is why appropriate mesh refinement must not be neglected.

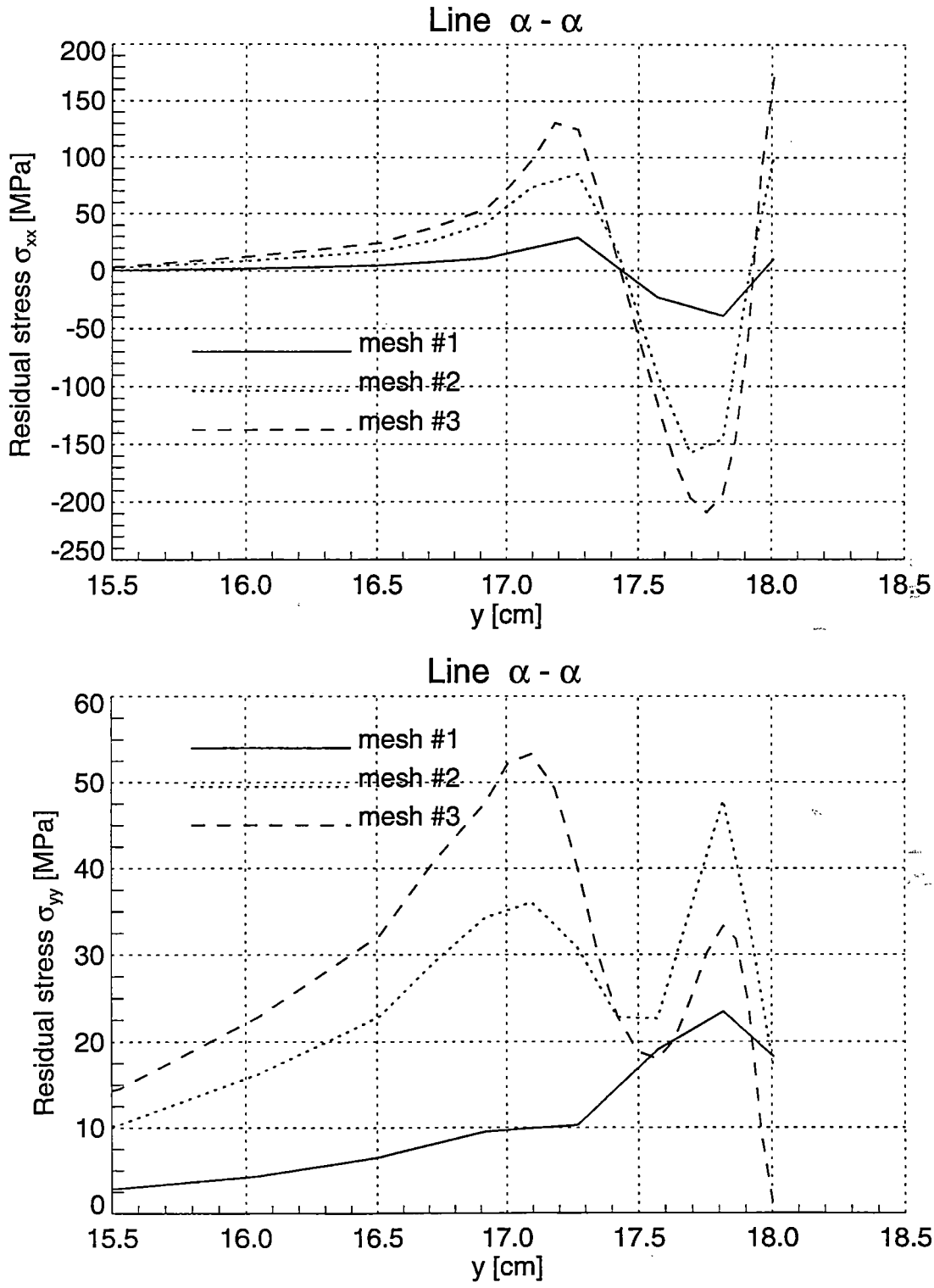

Figure 3.1 Normal Residual Stresses σ_{xx} and σ_{yy} in the Railroad Rail under Vertical Loading (Loading Case #1)

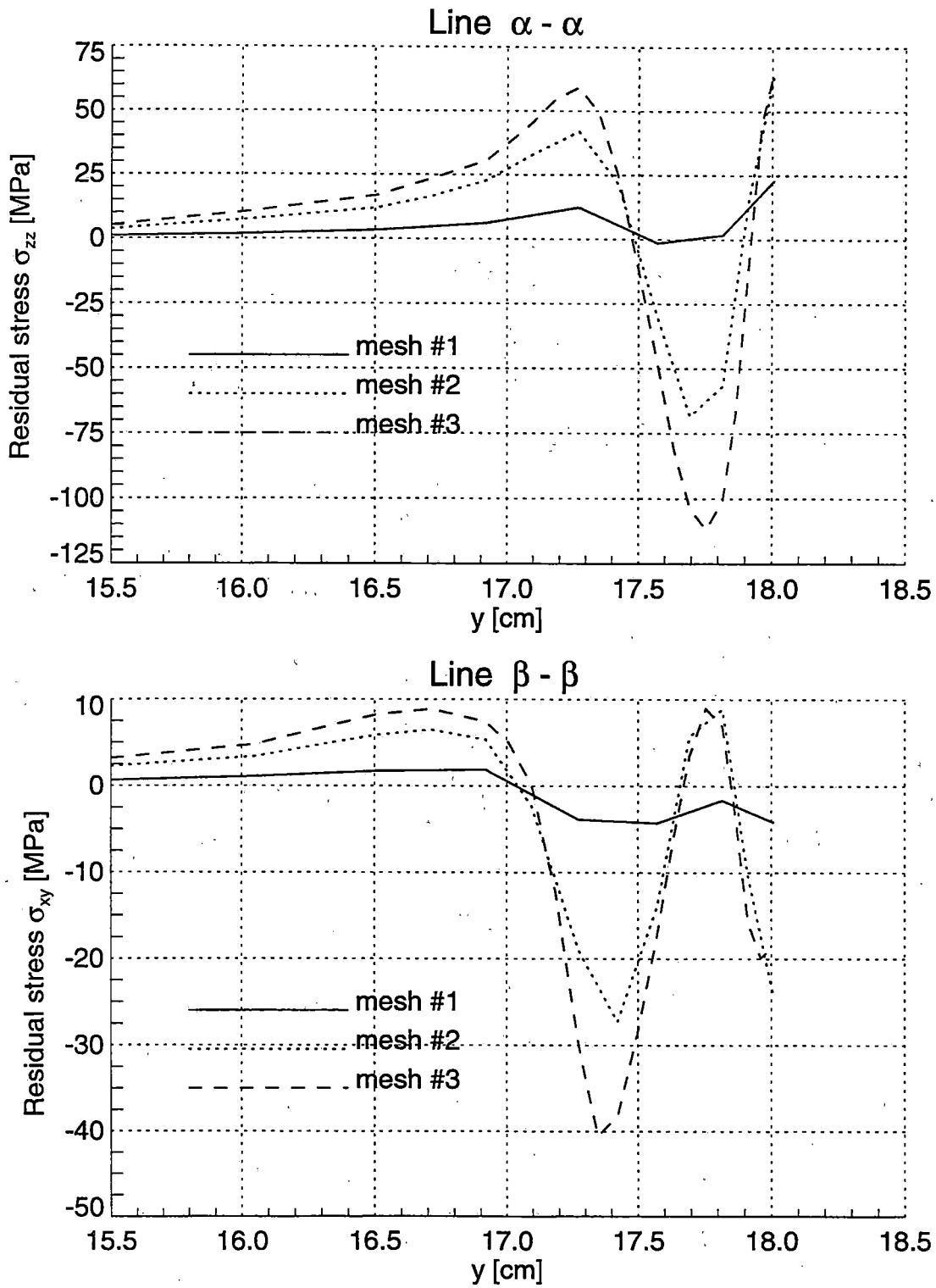

Figure 3.2 Normal σ_{zz} and Shear σ_{xy} Residual Stresses in the Railroad Rail under Vertical Loading (Loading Case #1)

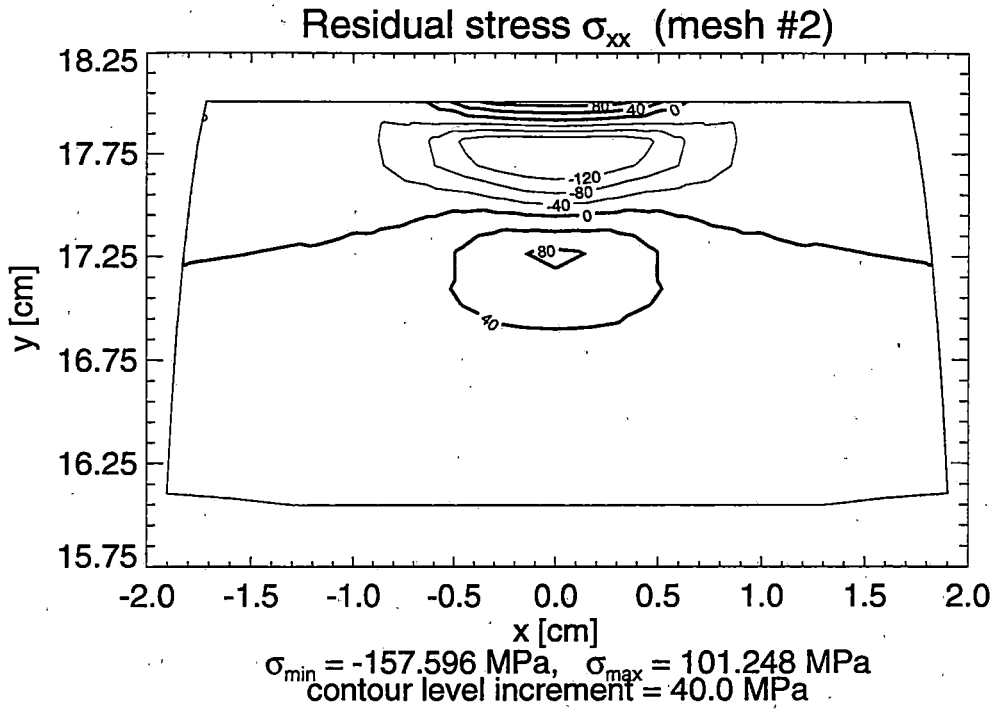

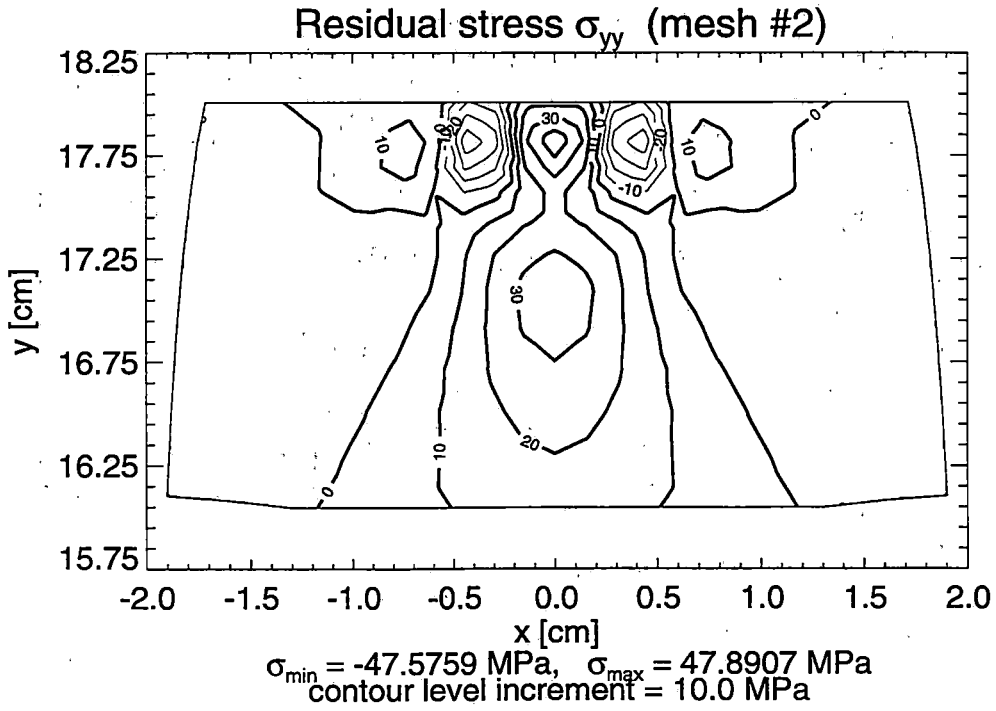

Figure 3.3 Contour Lines of Normal Residual Stresses σ_{xx} and σ_{yy} in the Railroad Rail under Vertical Loading (Loading Case #1) – Solution for Mesh #2

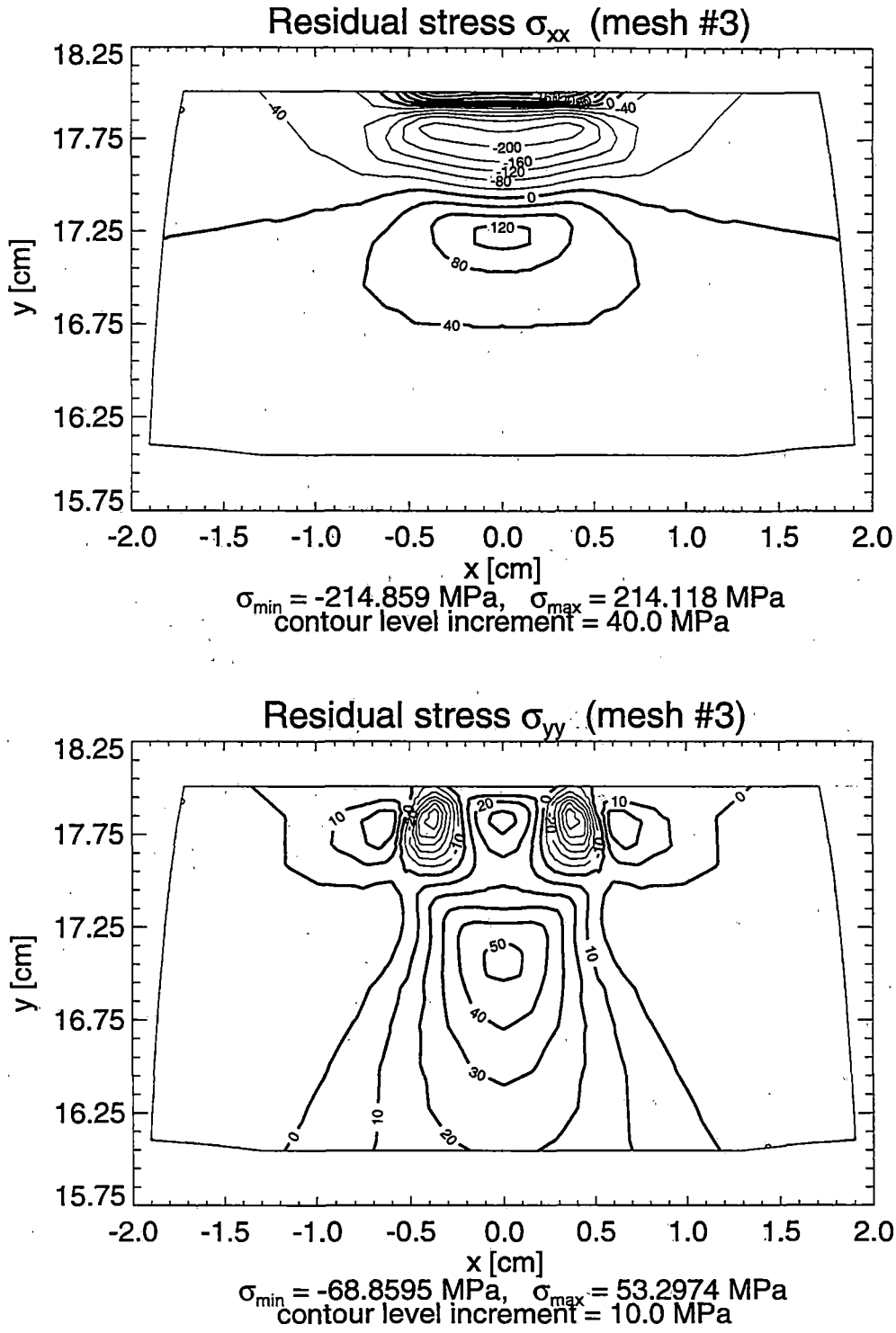

Figure 3.4 Contour Lines of Normal Residual Stresses σ_{xx} and σ_{yy} in the Railroad Rail under Vertical Loading (Loading Case #1) – Solution for Mesh #3

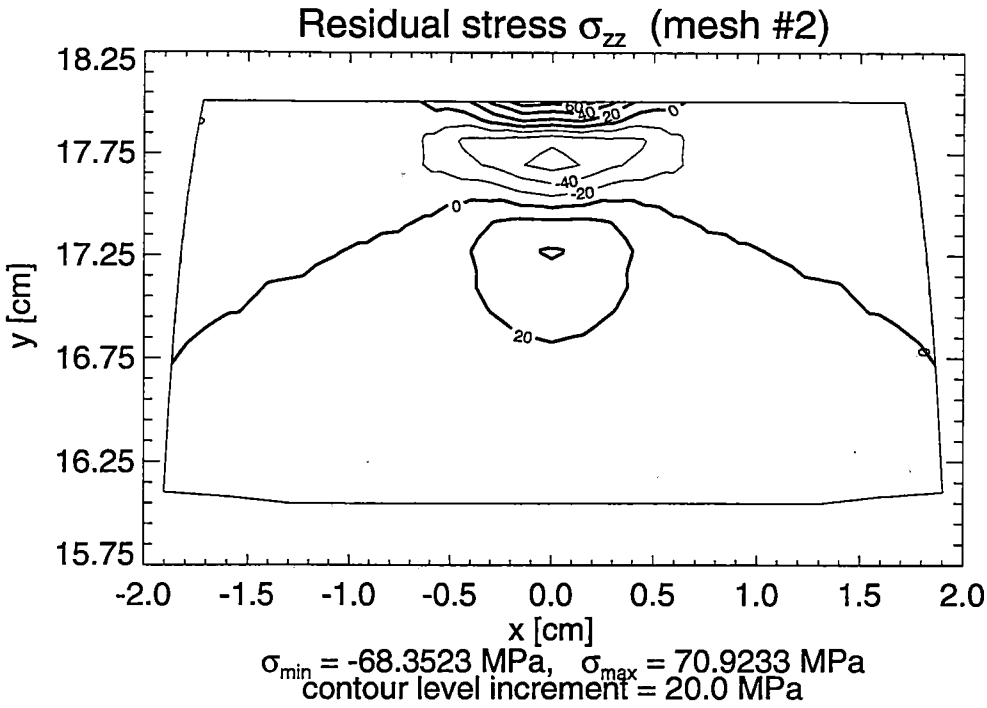

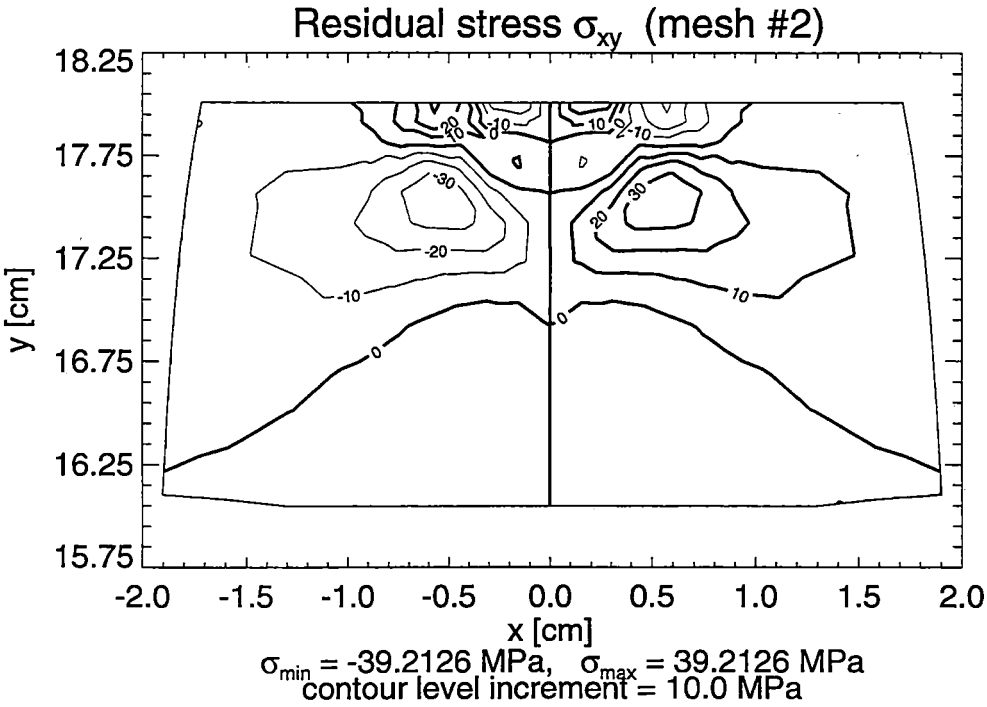

Figure 3.5 Contour Lines of Normal σ_{zz} and Shear σ_{xy} Residual Stresses in the Railroad Rail under Vertical Loading (Loading Case #1) – Solution for Mesh #2

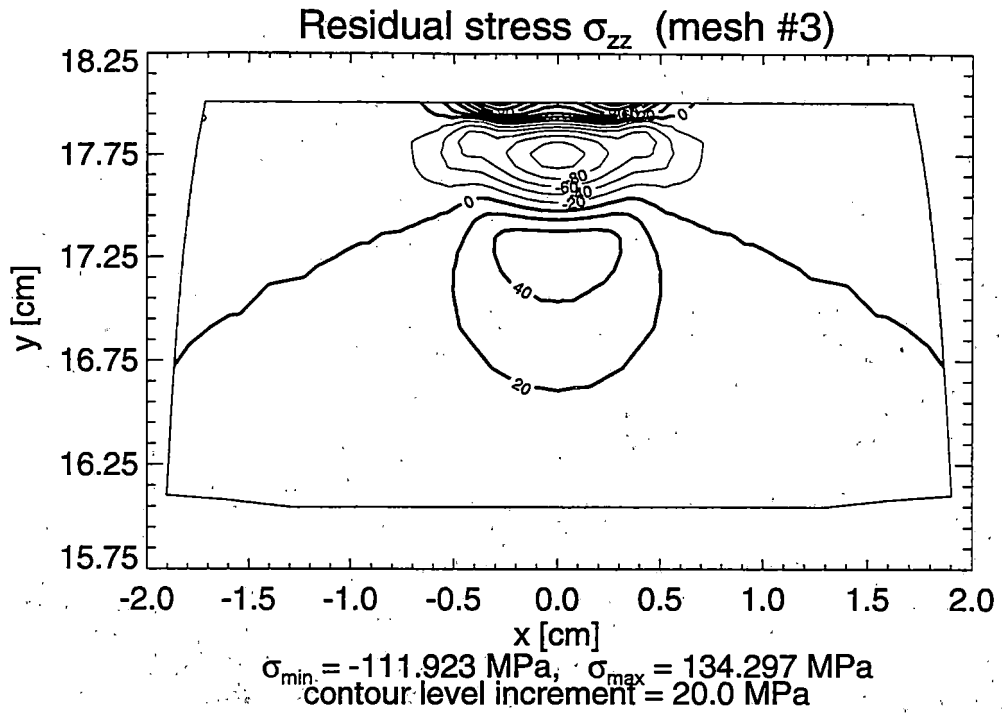

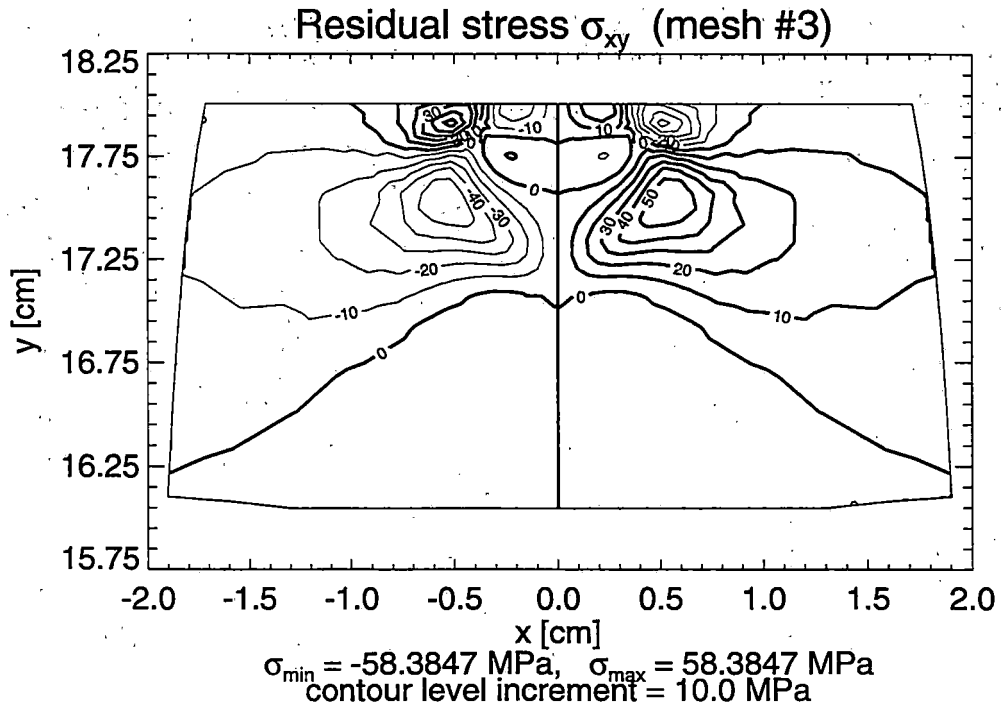

Figure 3.6 Contour Lines of Normal σ_{zz} and Shear σ_{xy} Residual Stresses in the Railroad Rail under Vertical Loading (Loading Case #1) – Solution for Mesh #3

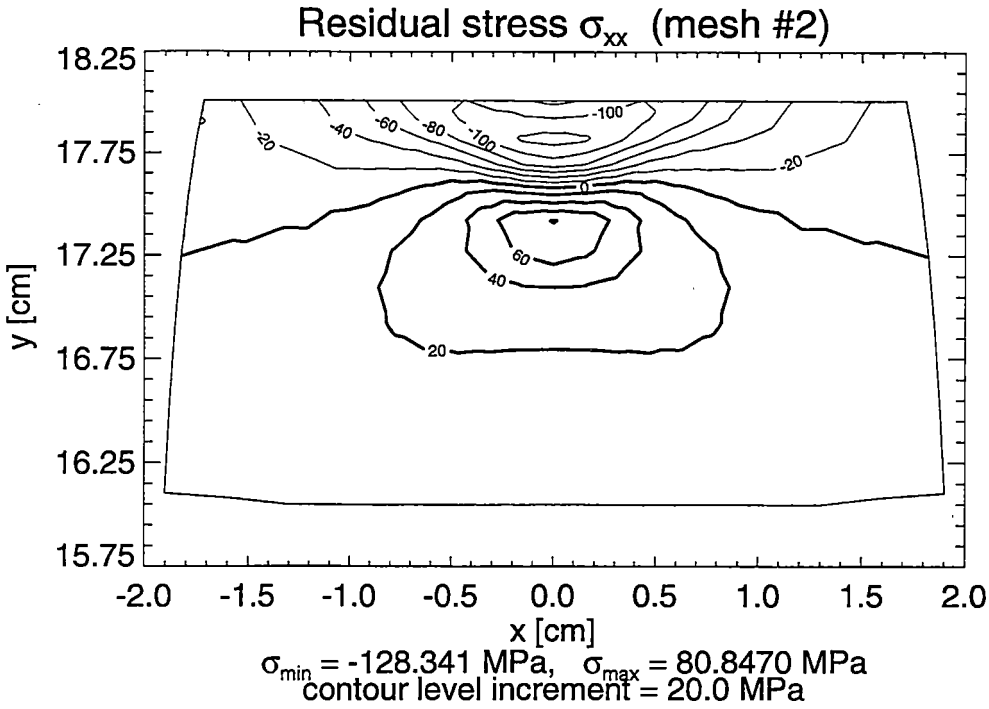

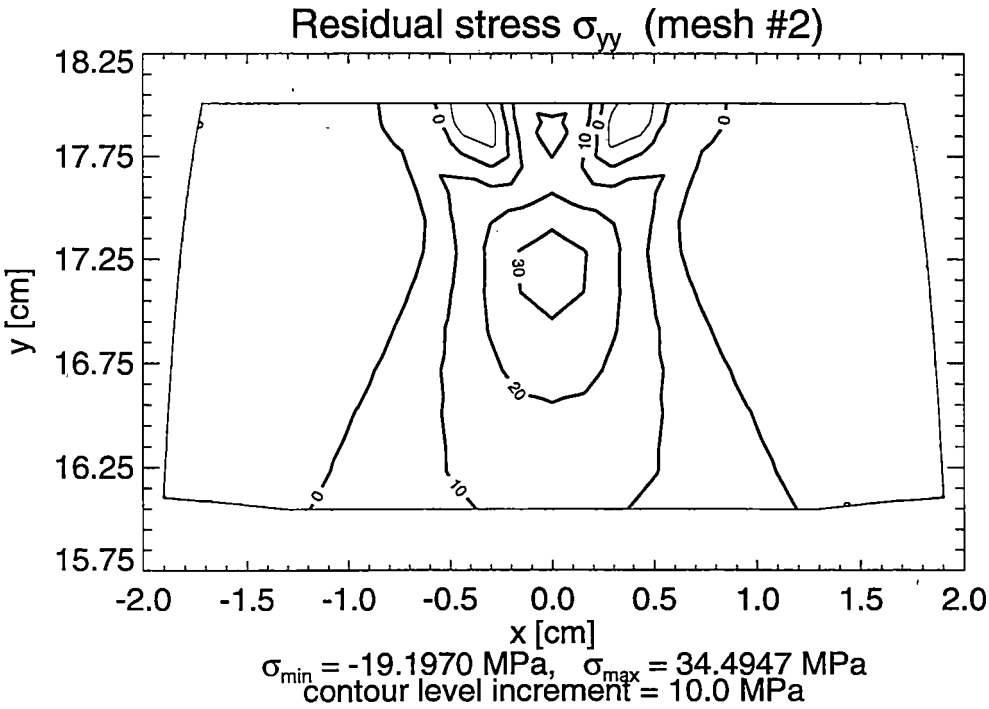

Figure 3.7 Contour Lines of Normal Residual Stresses σ_{xx} and σ_{yy} in the Railroad Rail under Vertical and Horizontal Loading (Loading Case #2) – Solution for Mesh #2

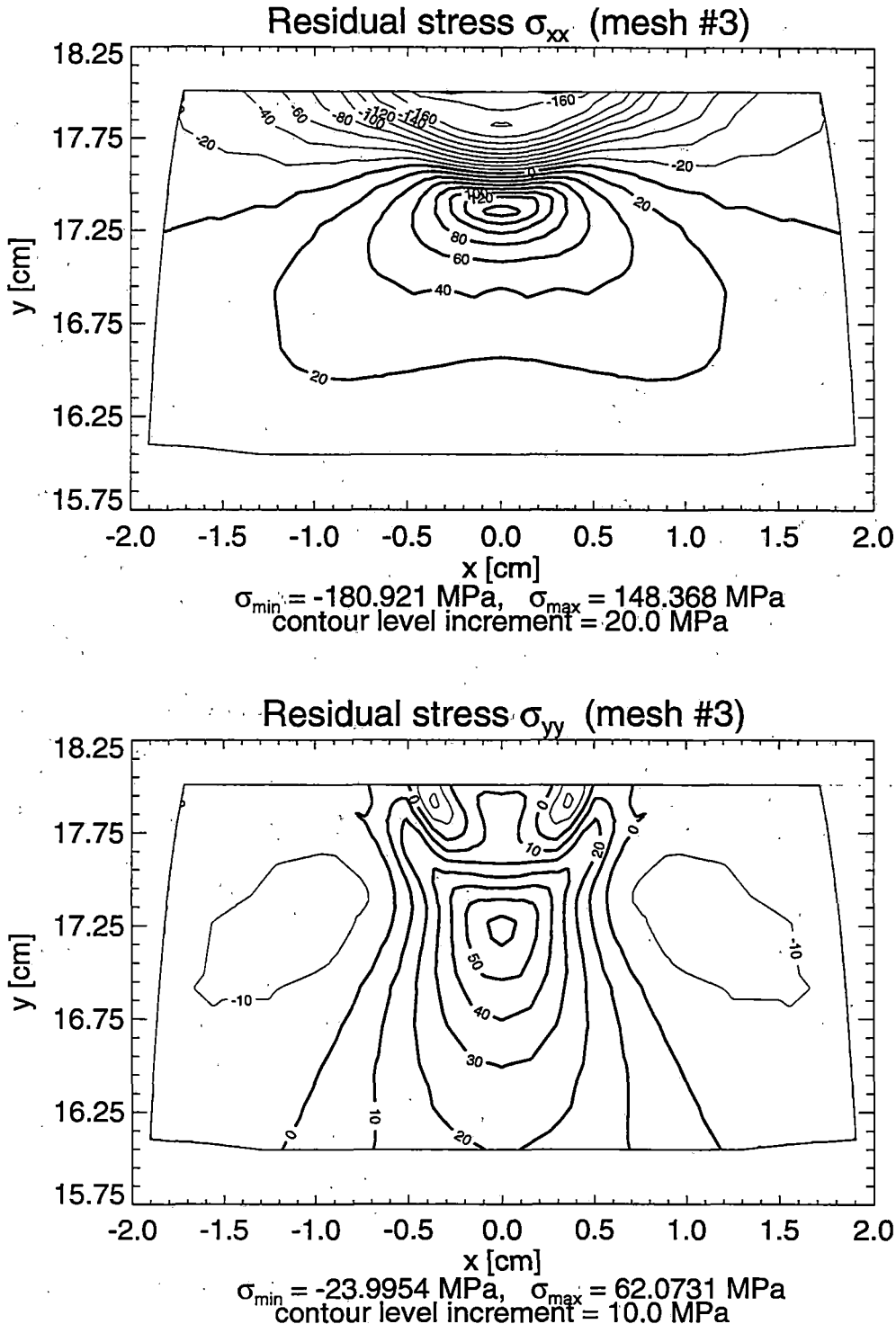

Figure 3.8 Contour Lines of Normal Residual Stresses σ_{xx} and σ_{yy} in the Railroad Rail under Vertical and Horizontal Loading (Loading Case #2) – Solution for Mesh #3

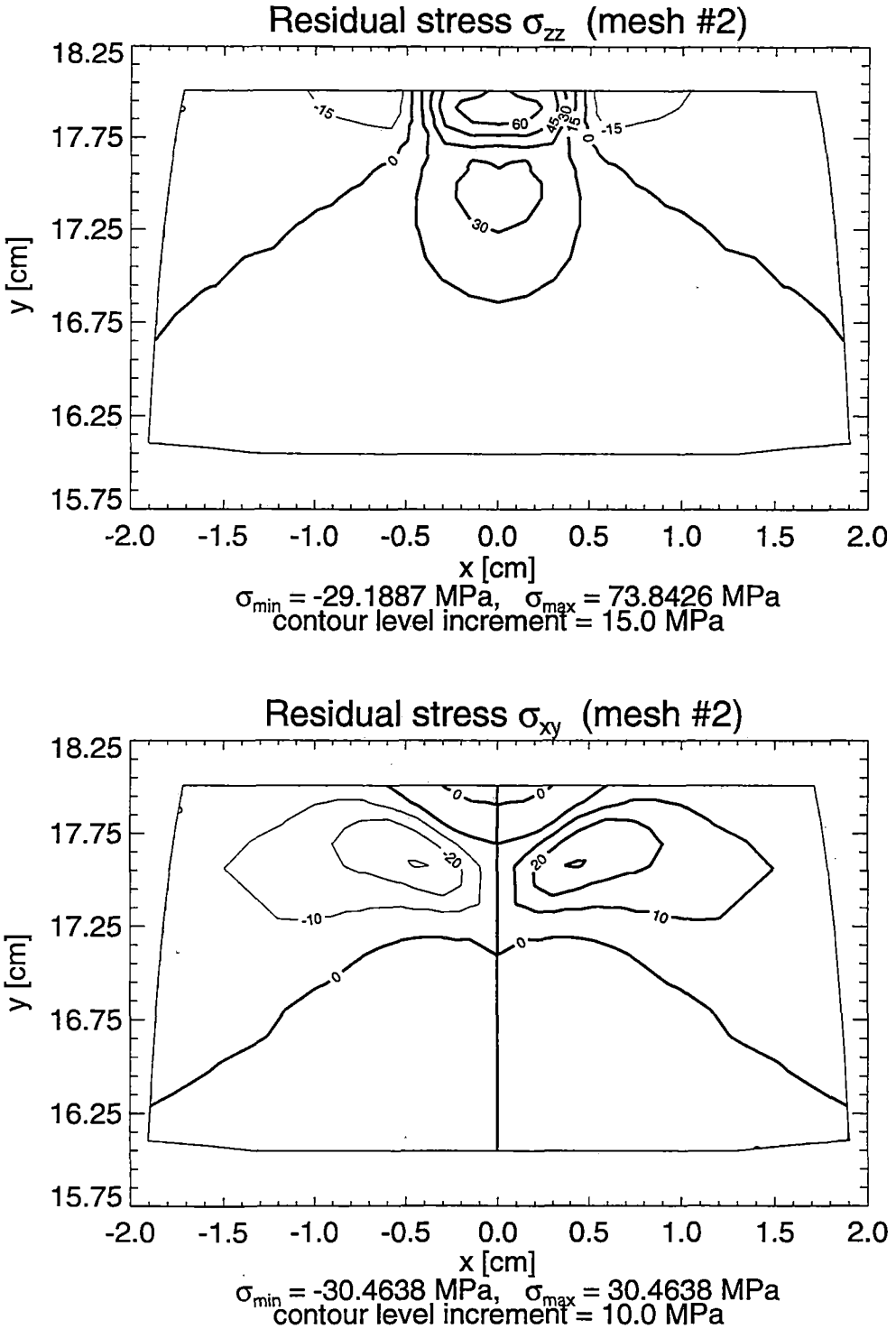

Figure 3.9 Contour Lines of Normal σ_{zz} and Shear σ_{xy} Residual Stresses in the Railroad Rail under Vertical and Horizontal Loading (Loading Case #2) – Solution for Mesh #2

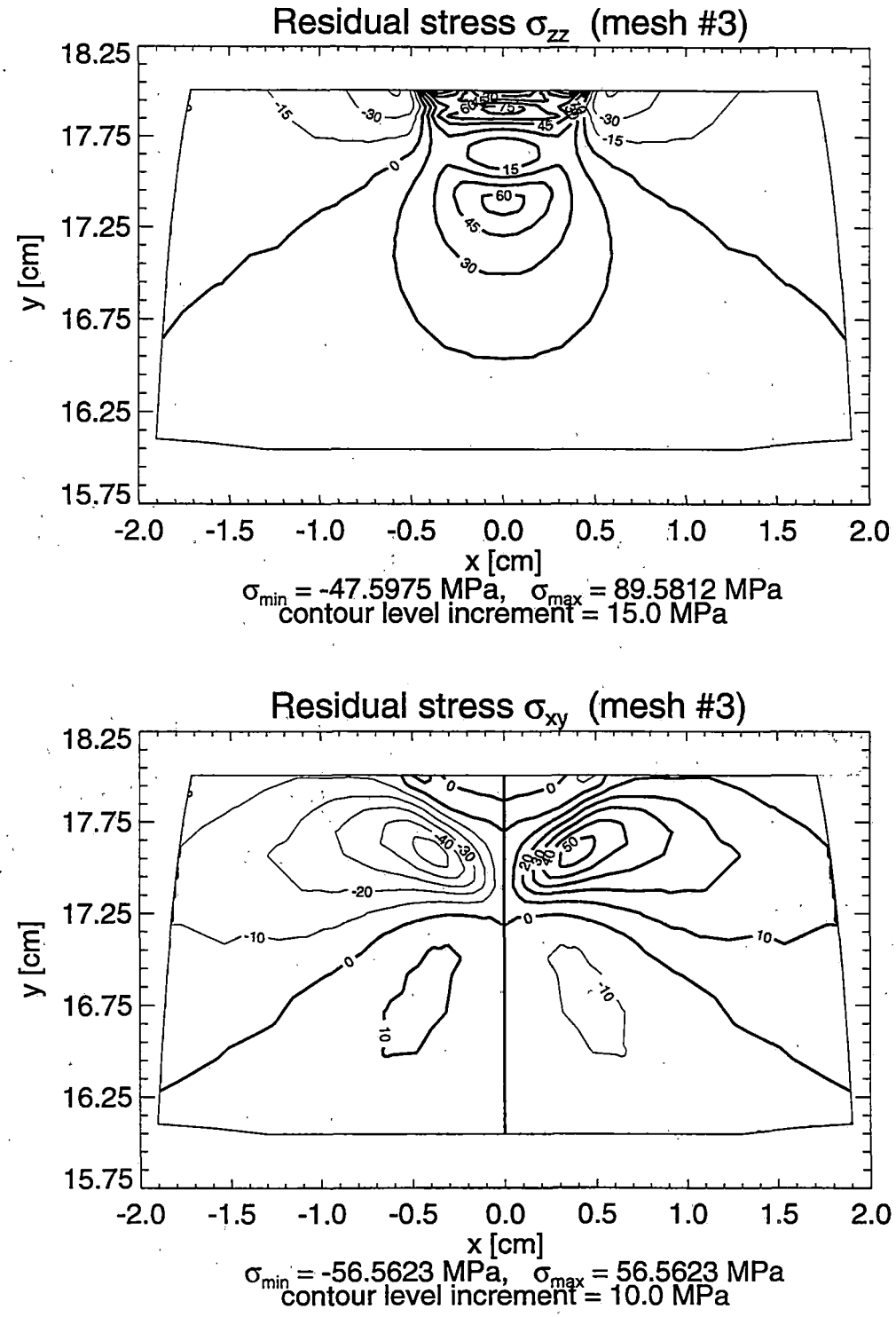

Figure 3.10 Contour Lines of Normal σ_{zz} and Shear σ_{xy} Residual Stresses in the Railroad Rail under Vertical and Horizontal Loading (Loading Case #2) – Solution for Mesh #3

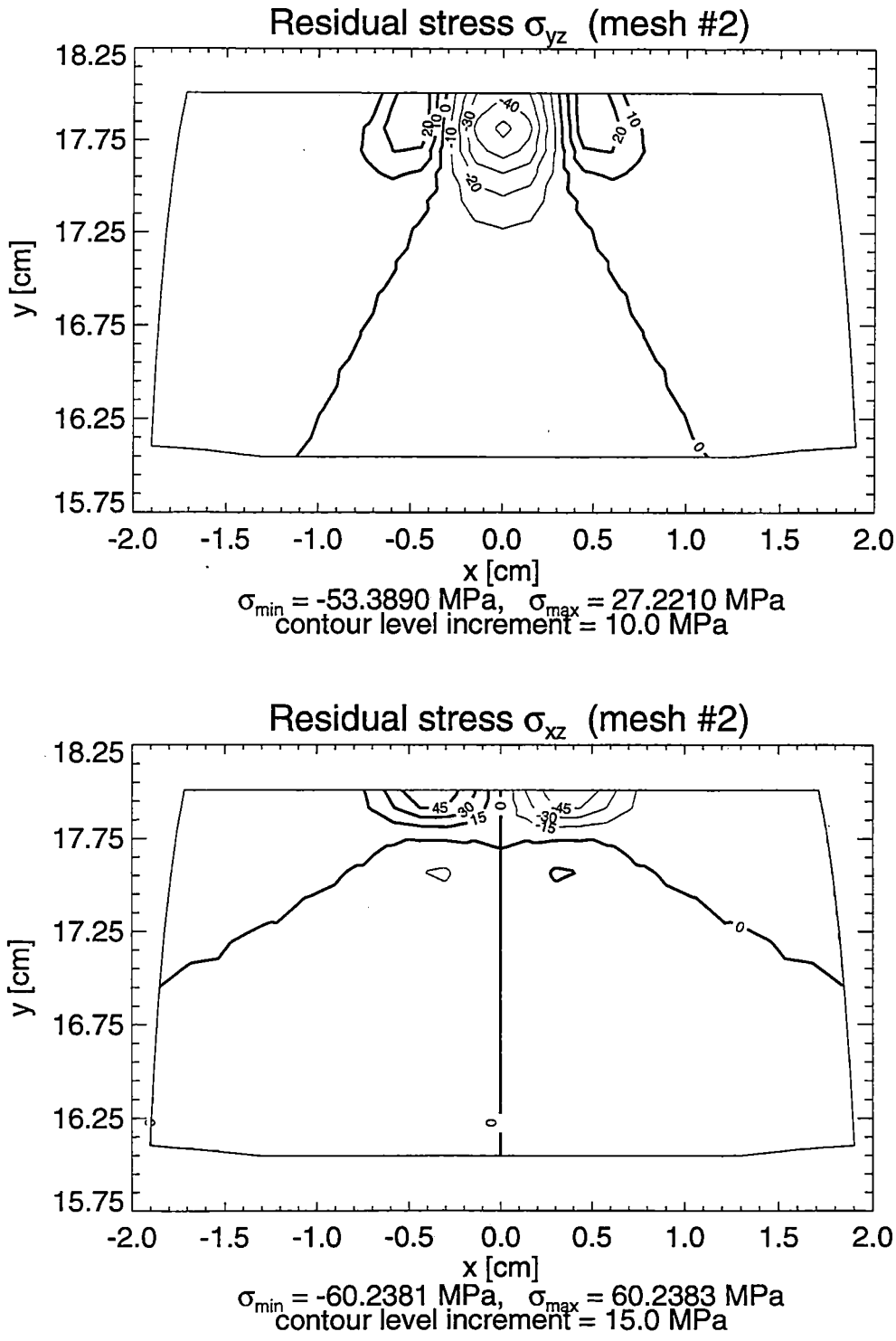

Figure 3.11 Contour Lines of Shear Residual Stresses σ_{yz} and σ_{xz} in the Railroad Rail under Vertical and Horizontal Loading (Loading Case #2) – Solution for Mesh #2

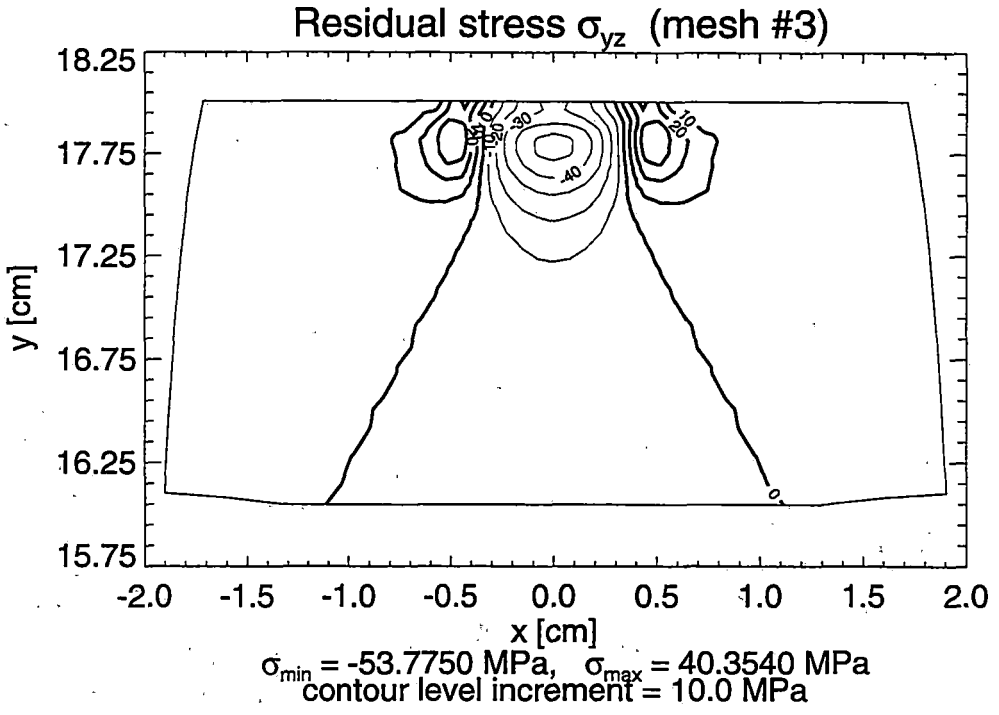

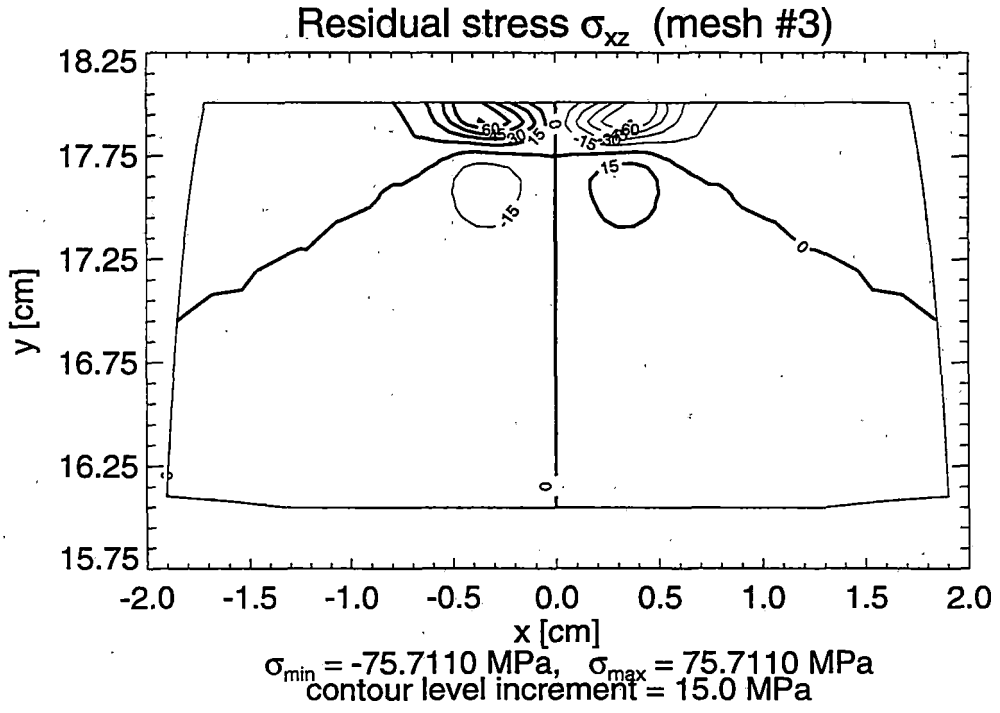

Figure 3.12 Contour Lines of Shear Residual Stresses σ_{yz} and σ_{xz} in the Railroad Rail under Vertical and Horizontal Loading (Loading Case #2) – Solution for Mesh #3

REFERENCES

[1] Orringer, O. and D. E. Gray, in press. Thermal cracking in railroad vehicle wheels subjected to high performance stop braking. In *Theoretical and Applied Fracture Mechanics.*

[2] Orkisz, J., O. Orringer, M. Holowinski, M. Pazdanowski, and W. Cecot. 1990. Discrete analysis of actual residual stresses resulting from cyclic loadings. In *Computers & Structures 35(4).*

[3] Orringer, O., J. Orkisz, and Z. Swiderski (ed.). 1992. *Residual Stress in Rails: Effects on Rail Integrity and Railroad Economics.* Kluwer Academic Publishers, Dordrecht, The Netherlands.

[4] Orkisz, J. and M. Holowinski. 1992. Prediction of residual stresses in rails: practical benefits from theoretical approach. In *Rail Quality and Maintenance for Modern Railway Operation.* Edited by J. J. Kalker, D. F. Cannon, and O. Orringer. Kluwer Academic Publishers, Dordrecht, The Netherlands.

[5] Perlman, A. B., J. E. Gordon, and O. Orringer. 1992. Effect of grinding strategy on residual stress in the rail head. In *Rail Quality and Maintenance for Modern Railway Operation (op.cit).*

[6] Gordon, J. E., in press. Simulation of the quenching process of railroad wheels. In *Proc. 11th International Wheelset Congress.*

[7] Johnson, K. L. 1985. *Contact Mechanics.* Cambridge University Press.

[8] Maugin, G. A. 1992. *The Thermomechanics of Plasticity and Fracture.* Cambridge University Press.

[9] Tong, P. and J. N. Rossetos. 1977. *Finite Element Method: Basic Technique and Implementation.* MIT Press.

[10] Bathe, K. J. 1982. *Finite Element Procedures in Engineering Analysis.* Prentice-Hall.

[11] Zienkiewicz, O. C. and R. L. Taylor. 1991. *The Finite Element Method.* McGraw-Hill.

[12] *ABAQUS User's Manual, version 5.3-2.* Hibbitt, Karlsson & Sorenson, Inc.

[13] Martin, J. B. 1975. *Plasticity: Fundamentals and General Results.* MIT Press.

[14] Orkisz, J. 1990. Residual stress analysis in railroad car wheels working in service conditions. In *Mechanika Teoretyczna i Stosowana 1-2(28).*

[15] Holowinski, M. and E. S. Bobrov. 1996. *Estimation of Actual Residual Stresses Due to Braking and Contact Loading of Rail Vehicle Wheels.* Volpe National Transportation Systems Center. Report no. DOT/FRA/ORD-96/02.

[16] Orkisz, J. 1992. Prediction of actual residual stresses by constrained minimization of energy. In *Residual Stress in Rails Effects on Rail Integrity and Railroad Economics (op.cit.).*

[17] Holowinski, M. 1992. *Hybrid FEM Analysis of Residual Stresses under Cyclic Loading.* Ph.D. thesis, Cracow University of Technology, Poland (in Polish).

[18] Holowinski, M. and J. Orkisz. 1992. Hybrid finite element method for estimation of actual residual stresses. In *Residual Stress in Rails (op.cit.).*

[19] Vanderplaats, G. N. 1984. *Numerical Optimization Techniques for Engineering Design: with Applications.* McGraw-Hill.

REPORTS IN THIS SERIES

1. Orringer, O., D. E. Gray, and R. J. McCown. 1993. *Evaluation of Immediate Actions Taken to Deal with Cracking Problems in Wheels of Rail Commuter Cars.* Volpe National Transportation Systems Center. Report no. DOT/FRA/ORD-93/15.

2. Tang, Y. H., J. E. Gordon, A. B. Perlman, and O. Orringer. 1993. *Finite Element Models, Validation, and Results for Wheel Temperature and Elastic Thermal Stress Distributions.* Volpe National Transportation Systems Center. Report no. DOT/FRA/ORD-93/17.

3. Tang, Y. H., J. E. Gordon, O. Orringer, and A. B. Perlman. 1993. *Stress Reconstruction Analysis of Wheel Saw Cut Tests and Evaluation of Reconstruction Procedure.* Volpe National Transportation Systems Center. Report no. DOT/FRA/ORD-93/18.

4. Stuart, C. 1993. *Thermal Measurements of Commuter Rail Wheels under Revenue Service Conditions.* ENSCO, Inc. Report no. DOT/FRA/ORD-93/19.

5. Pelloux, R. M. and D. C. Grundy. 1994. *Thermomechanical Testing and Microstructural Development of Class L Steel Wheel Alloy.* Department of Materials Science and Engineering, MIT. Report no. DOT/FRA/ORD-94/01.

6. Gordon, J. E. and O. Orringer. 1996. *Investigation of the Effects of Braking System Configurations on Thermal Input to Commuter Car Wheels.* Volpe National Transportation Systems Center. Report no. DOT/FRA/ORD-96/01.

7. Bobrov, E. S. and M. Holowinski. 1995. *Estimation of Actual Residual Stresses Due to Braking and Contact Loading of Rail Vehicle Wheels.* Volpe National Transportation Systems Center. Report no. DOT/FRA/ORD-95/13.